Alma Mater Studiorum – Università di Bologna

DOTTORATO DI RICERCA IN SCIENZE CHIMICHE
Ciclo XXVI

Settore Concorsuale di afferenza: 03 / B1

Settore Scientifico disciplinare: CHIM / 03

Novel two photon absorbers: evaluation of photophysical properties in view of biomedical applications

Presentata da: ADINA IULIANA CIUCIU

Coordinatore Dottorato:	**Relatore:**
Prof. ALDO RODA	Prof.ssa PAOLA CERONI
	Correlatore:
	Dott.ssa LUCIA FLAMIGNI

Esame finale anno 2014

Table of contents

Presentazione della tesi

Dottorando   **Adina Iuliana Ciuciu**

Tutor   **Prof.ssa Paola Ceroni**   *Co-tutor*   **Dott.ssa Lucia Flamigni**

Curriculum, indirizzo **Scienze Chimiche: Nanoscienze e Nanotecnologie**

Titolo tesi   **NOVEL TWO PHOTON ABSORBERS: EVALUATION OF PHOTOPHYSICAL PROPERTIES IN VIEW OF BIOMEDICAL APPLICATIONS**

Scientific report

The PhD studies were financed by the Marie Curie ITN project TOPBIO (TwO Photon absorbers for BIOmedical applications). The research activity was focused on the investigation of the linear optical properties of novel two photon absorbers provided by various partners of the network.

Most of the activity was devoted to the characterization of the photophysical properties of compounds designed for two photon bioimaging. Various substituted imidazole and imidazopyridine derivatives and organic dendrimers made the object of the study. The results obtained showed superior luminescence properties for sulphonamido imidazole derivatives with respect to other substituted imidazoles. Imidazo[1,2-*a*]pyridines exhibited an important dependence on the substitution pattern of their luminescence properties. Substitution at imidazole ring led to a higher fluorescence yield than the substitution at the pyridine one. Furthermore, bis-imidazo[1,2-*a*]pyridines of the Donor-Acceptor-Donor type were examined. Bis-imidazo[1,2-*a*]pyridines dimerized at C3 position had better luminescence properties than those dimerized at C5, displaying emission quantum yields close to unity and important 2PA cross sections.

Phosphazene-based dendrimers with fluorene branches and cationic charges on the periphery were also examined as potential 2PA fluorofores. Due to aggregation phenomena in polar solvents, the dendrimers registered a significant loss of luminescence with respect to fluorene chromophore model. An improved design of more rigid chromophores yields enhanced luminescence properties which, connected to a large 2PA cross-section, make this compounds valuable as fluorophores in bioimaging.

The candidate also examined 2PA absorbers for applications in photopolymerization. The photophysical study of several ketocoumarine photoinitiators, designed for the fabrication of small dimension prostheses by two photon polymerization (2PP), was carried out. The compounds showed low emission quantum yields, indicative of a high population of the triplet excited state,

which is the active state in producing the reactive species. Their efficiency in 2PP was proved by the fabrication of 3D structures in one of the collaborator's laboratory.

In the frame of the 2PA photorelease of drugs, three fluorene-based dyads have been investigated. They were designed to release the neurotransmitter γ-aminobutyric acid (GABA) *via* two photon induced electron transfer. The experimental data in polar solvents showed a fast electron transfer followed by an almost equally fast back electron transfer process, which indicate a poor optimization of the system.

Giudizio del tutor e co-tutor

Adina Ciuciu ha lavorato con impegno e dedizione, applicandosi per raggiungere buoni risultati testimoniati da 7 pubblicazioni su riviste internazionali, 2 pubblicazioni sottomesse e 2 in preparazione. Ha mostrato una enorme serieta' ed il desiderio di apprendere sia nuove tecniche che nuovi concetti. Nel corso degli anni è notevolmente maturata acquistando competenza, sicurezza ed autonomia nella conduzione ed interpretazione degli esperimenti. Ha anche acquistato una certa autonomia nella preparazione di articoli scientifici. La candidata ha dimostrato un'elevata attitudine al lavoro di gruppo e alle comunicazioni interpersonali.

Nei tre anni del dottorato ha regolarmente partecipato ai meeting semestrali del progetto europeo TOPBIO, dove ha presentato relazioni orali sulla propria attivita', mostrando ottime capacita' comunicative. Ha inoltre partecipato ad un congresso nazionale e due congressi internazionali in cui ha presentato rispettivamente un contributo orale e due poster. Ha seguito due scuole internazionali ed una nazionale di fotochimica e due seminari internazionali sui processi e le applicazioni della eccitazione a 2 fotoni nonche' un seminario sul trasferimento tecnologico. Ha partecipato alle attività scientifiche ed organizzative del Progetto TOPBIO, contribuendo alla organizzazione del Mid-Term Review tenuto a Bologna. Ha interagito proficuamente con i colleghi italiani e stranieri, assistendo ed addestrando tre studenti provenienti da altri gruppi nell'ambito dei "secondments" previsti dal progetto EU. Inoltre ha svolto due "secondments" di un mese ciascuno nel corso dei quali ha avuto un training di base in chimica organica sintetica (Faculty of Chemistry, Warsaw University of Technology) ed in misure di 2PA mediante "two photon excited fluorescence (TPEF)" presso Universite de Bordeaux.

TOPBIO project

The present thesis is the result of my research activity over the last three years as early stage researcher (ESR) within Marie Curie FP7 project '**TOPBIO** – **T**w**O** **P**hoton absorbers for **BIO**medical applications'. I have worked at Istituto per la Sintesi Organica e Fotoreattivita' (ISOF), Consiglio Nazionalle delle Ricerche (CNR), under the supervision of Dr. Lucia Flamigni.

It is well-known that two-photon (2PA) technologies may have a strong impact in cell biology, physiology, neurobiology and medicine. Within this context, **TOPBIO** aims at developing new two photon absorbers in view of biomedical applications. The project includes the development and the use of two-photon chromophores for (a) fluorescence microscopy and other luminescence methods to image dynamical events, (b) the photo-initiated release, and concomitant activation, of covalently-bound physiological probes and/or drugs, (c) elucidating mechanisms of photoinduced cell death which will ultimately contribute to the design of better "drugs" for use in photodynamic therapy and (d) photoinitiated polymerization reactions used to produce microscale devices.

Between many groups involved in **TOPBIO**, Bologna node had the role of studying the excited state properties of the new 2PA systems, project that can be pursued in the majority of cases by using simple one photon excitation. This makes the subject of the thesis.

List of publications

Referred in the thesis

Chapter 2

1) K. Skonieczny, A. I.Ciuciu, E. M. Nichols, V. Hugues, M. Blanchard-Desce, L. Flamigni, D. T. Gryko, Bright, emission tunable fluorescent dyes based on imidazole and π-expanded imidazole. *J. Mater. Chem.* **2012,** *22* (38), 20649-20664.

2) A. I. Ciuciu, K. Skonieczny, D. Koszelewski, D. T. Gryko, L. Flamigni, Dynamics of Intramolecular Excited State Proton Transfer in Emission Tunable, Highly Luminescent Imidazole Derivatives. *J. Phys. Chem. C* **2013,** *117* (2), 791-803.

3) A. I. Ciuciu, L. Flamigni, K. Skonieczny, D. T. Gryko, Blue-green emitting sulphonamido-imidazole derivatives: ESIPT based excited state dynamics. *Phys. Chem. Chem. Phys.* **2013,** *15,* 16907-16916.

Chapter 3

1) D. Firmansyah, A. I. Ciuciu, V. Hugues, M. Blanchard-Desce, L. Flamigni, D. T. Gryko, Bright, Fluorescent Dyes Based on Imidazo[1,2-*a*]pyridines that are Capable of Two-Photon Absorption. *Chem. Asian J.* **2013,** *8* (6), 1279-1294.

2) A. I. Ciuciu, D. Firmansyah, V. Hugues, M. Blanchard-Desce, D. T. Gryko, L. Flamigni, Non-classical donor-acceptor-donor chromophores. A strategy for high two-photon brightness. *J. Mater. Chem. C* **2014**, DOI:10.1039/C4TC00234B.

Chapter 4

1) E. J. Cueto-Diaz, A. I. Ciuciu, B. Ventura, L. Flamigni, M. Blanchard-Desce,...., Soft organic dendrimers for fluorescence imaging. **2014** *–manuscript in preparation.*

Chapter 5

1) R. Nazir, P. Danilevicius, A. I. Ciuciu, M. Chatzinikolaidou, D. Gray, L. Flamigni, M. Farsari, D. T. Gryko, π-Expanded ketocoumarins as efficient, biocompatible initiators for two-photon induced polymerization. *Chem. Mater.* **2014** *– submitted.*

2) K. Korzycka, A. I. Ciuciu, L. Flamigni, H. Anderson,..., Light-driven processes in fluorene-based dyads designed for GABA uncaging via PeT, **2014** –*work in progress.*

Other publications

1) A. I. Ciuciu, L. Flamigni, R. Voloshchuk, D. T. Gryko, Light Energy Collection in a Porphyrin-Imide-Corrole Ensemble. *Chem. Asian J.* **2013,** *8* (5), 1004-1014.

2) R. Voloshchuk, D. T. Gryko, M. Chotkowski, A. I. Ciuciu, L. Flamigni, Photoinduced Electron Transfer in an Amine-Corrole-Perylene Bisimide Assembly: Charge Separation over Terminal Components Favoured by Solvent Polarity. *Chem. Eur. J.* **2012,** *18* (46), 14845-14859.

3) L. Flamigni, A. I. Ciuciu, H. Langhals, B. Böck, D. T. Gryko, Improving the Photoinduced Charge Separation Parameters in Corrole-Perylene Carboximide Dyads by Tuning the Redox and Spectroscopic Properties of the Components. *Chem. Asian J.* **2012,** *7* (3), 582-592.

Conference presentations

1) A. I. Ciuciu, R. Voloshchuk, B. Böck, H. Langhals, D. T. Gryko, L. Flamigni, Photoinduced energy and electron transfer processes in multichromophoric corrole-based arrays. *ICP*, **21 - 26 July 2013**, Leuven, Belgium – **poster presentation**.

2) A. I. Ciuciu, L. Flamigni, R. Voloshchuk, M. Chotkowski, D. T. Gryko, D.T., Effect of solvent polarity on electron transfer processes in a corrole based triad. *Italian Photochemistry Meeting*, **11 - 12 October 2012**, Bologna, Italy – **oral presentation**.

3) A. I. Ciuciu, L. Flamigni, Enhancing the luminescence properties of novel imidazo[1,2-*a*]pyridine systems**.** *Photonics meets biology*, **30 September - 3 October 2013**, Crete, Greece – **poster presentation.**

1. Introduction

1.1. Linear and nonlinear optical methods

1.1.1. Two photon absorption: theoretical aspects

Nonlinear optics (NLO) represents the behavior of light at the interaction with matter when the dielectric polarization P responds nonlinearly to the electric field E of the light (nonlinear medium).[1] In general, the polarization P induced by a high intensity light is related to the electric field E by equation (1.1):

$$P = \alpha E + \beta E^2 + \gamma E^3 + \ldots \tag{1.1}$$

Where α is the molecule polarisability, β is the first hyperpolarisability and γ is the second hyperpolarisability.[2]

Though, the nonlinearity of a bulk medium can be expressed by using the average of all molecules in that medium, as given in the formula:

$$P = \varepsilon_0 \left(\chi^1 E + \chi^2 E^2 + \chi^3 E^3 + \ldots \right) \tag{1.2}$$

Where ε_0 is the permittivity of free space and χ is the susceptibility of the medium to the corresponding power (1, 2, 3,…).
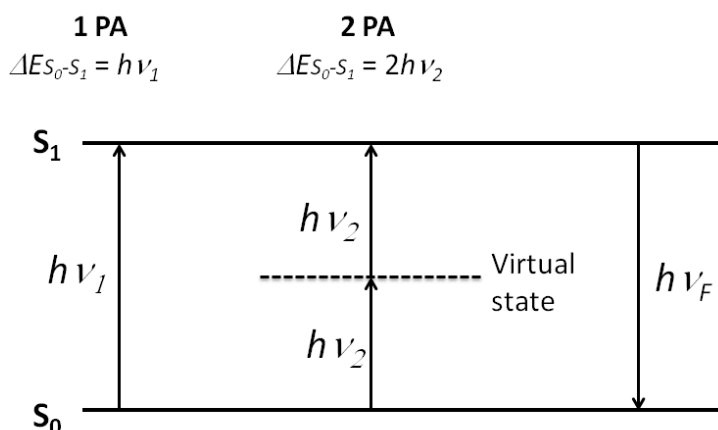
Figure 1.1. Schematic energy level diagram for 1PA and 2PA processes.

In simple words, the two photon absorption (2PA) process represents the electronic excitation of a molecule by near-simultaneous absorption of two photons having the same energy, whereas in one photon absorption (1PA) the excitation occurs by absorption of a single photon with higher energy (Figure 1.1). The prerequisite for almost simultaneous absorption and the very short timescale of light absorption (femtoseconds (fs)) is given by the use of particular excitation sources. These are represented by the mode-locked Ti-Sapphire lasers delivering light pulses of fs duration

at high repetition rates in the infrared (IR) spectral range. The excitation of the chromophore by absorption of two photons occurs through a 'virtual' excited state, as depicted in Figure 1.1.[3] Though the selection rules differ for one- and two-photon excitation and the vertical excited state is different, most often relaxation occurs to the same, lowest excited state.
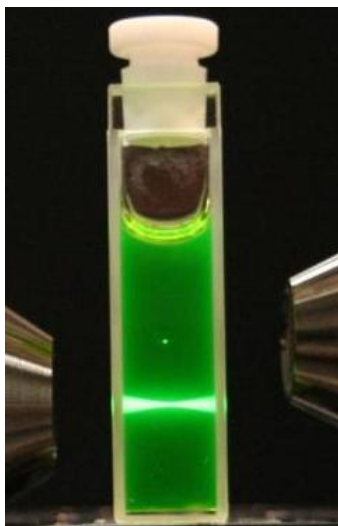
Figure 1.2. Fluorescence emission obtained by one photon excitation at 400 nm (double cone, bottom) and two photon excitation at 800 nm (point, above).

The two photon absorption process was theoretically predicted for the first time by Maria Göppert-Mayer in 1930s[4] and verified experimentally only in 1963 by Kaiser and Garret, with detection of the fluorescence of Eu^{3+} in a doped crystal induced by 2PA excitation.[5] With the advent of sub-picosecond pulsed lasers (i.e. Ti: sapphire laser) in 1990s, 2PA processes became easier to investigate. Within the same period, Denk et al.[6] demonstrated the use of two photon excitation in fluorescence microscopy, by showing images with excellent optical sectioning obtained without killing cells.

The efficiency of 2PA process is known to be dependent on both the spatial and temporal distribution of photons. High spatial photon density can be achieved inexpensively by focusing a laser beam. A high temporal density is more difficult to achieve with current technology since it requires the expensive, ultrafast pulsed light sources. For 2PA process the beam intensity decreases quadratically with distance above and below the diffraction-limited focal plane, and as result, the excitation is effectively restricted to the focal volume of the beam.

The motivation of preferring two photon excitation instead of commonly used one photon excitation lies on the followings. The most important advantage of using 2PA techniques is the restricted excitation to a very tiny volume of the sample (a femtoliter), as depicted in Figure 1.2. Due to the fact that the laser intensity in the focal volume is so high, each fluorescent molecule (provided that it is a good two photon absorber) absorbs concomitantly two photons. The

probability of simultaneous absorption of two photons is proportional to the square of the intensity applied, and this generates an intensity decrease outside the focal volume so steep, that virtually nothing outside the volume is excited.

An important feature for biomedical applications is the higher penetration of the tissues. The normal one photon excitation attained in the UV-Vis range by conventional lasers cannot ensure a reasonable penetration of the living organisms without dealing with large scattering and bleaching and absorption given by biological chromophores. 2PA can be induced at half of the frequency of the actual energy gap, expanding the accessible range (longer wavelengths at 700–1300 nm, the so-called 'biological window') and ensuring a deep penetration into scattering media.

All together, these properties make the 2PA technique a powerful tool in biomedicine field, not only for diagnosis but also for treatments.

1.1.2. Two photon absorption cross-sections

The Lambert-Beer law for 1PA states that the transmission (T) of the light through the substance depends logarithmically on the on the absorption coefficient of the substance, α, and the path length, l, on which the light travels through the material:

$$T = \frac{I}{I_0} = e^{-\alpha l} = e^{-\varepsilon c l} \qquad (1.3)$$

Where I_0 and I are the intensities of the incident and transmitted light, respectively; ε is the molar absorption coefficient and c is the concentration of the sample.

In 2PA the coefficient α turns into the 2PA cross-section σ_2. By using assumptions similar to simple Lambert Beer law for one photon absorption process, for 2PA the beam light attenuation is given by the equation (1.4):

$$\delta I / \delta z = -N\,\alpha_2\,I^2 = -N\,\sigma_2 F\,I \qquad (1.4)$$

Where I represents the intensity, z the distance into the medium, N the number of molecules per unit volume and α_2 is a molecular coefficient for 2PA.[7]

The intensity I can be expressed also as a photon flux (F) (quantified in photons s^{-1} cm^{-2}):

$$F = I/h\nu \qquad (1.5)$$

and $h\nu$ is the photon energy. By replacing the intensity (I) derived from expression 1.5. in the former equation 1.4, the coefficient σ_2 introduced in the last replaces the product of the photon energy and the molecular coefficient for 2PA.

The 2PA activity is usually expressed in two photon absorption cross-sections (σ_2), quantified in Göppert-Mayer (1 GM = 10^{-50} cm^4 s photons^{-1} molecule^{-1}) units. By taking into account the fact that it is measured in cm^4s, it can be deduced that it is derived from the product of the two areas (each photon in cm^2) and the time (in seconds) when the two photons are near-simultaneous absorbed by the molecule.

1.1.3. Two photon absorbers

The distinct properties of 2PA broaden its application field, making this technique favored not only in biomedical, but also in non-medical domain. It is increasingly applied in spectroscopy,[8] optoelectronics,[9] microfabrication,[10] high resolution fluorescence microscopy,[6, 11] data storage,[10b, 12] photodynamic therapy (PDT),[13] different nanobiophotonic applications[14] and the list can go on.

The characteristics of the two photon absorbers may vary as function of the application field. For example, the fluorophores used in two photon excited fluorescence microscopy (TPEM), besides large 2PA cross-section values, should have high luminescence quantum yields (ϕ_{fl}). For imaging purposes, in fact, the parameter to be maximized is the so called two-photon brightness, i.e. $\sigma_2 \times \phi_{fl}$. In PDT, the photosensitizer (PS) should possess long lived triplet excited state allowing the generation of singlet oxygen ($^1O_2$) by energy transfer to molecular oxygen. In two photon polymerization the initiator should have a high quantum yield of the generation of active species (radicals or cations) and large 2PA cross-sections.

As the 2PA technique was rather recently applied and particularly in bioimaging, most of the initial tests were carried out with many of the standard dyes developed for one photon excitation. The first step in the characterization of the 2PA properties of some commonly used fluorophores was made by Xu et al. in 1996,[11a] when over 20 compounds were examined. The results were modest, varying between several to tens of GM units, reducing somehow their attainment in TPEM.

Consequently, a constant effort was dedicated to the development of new systems exhibiting strong TPA while maintaining a high fluorescence quantum yield and possessing suitable properties for the desired use. Between other features, the biocompatibility, solubility and photostability, as

well as the ease of processing of the chromophore had to be taken into account. Later, it was observed a strict dependence of the 2PA properties on the structure of the chromophores. It was shown that enhanced 2PA cross-section values could be measured in π conjugated molecules.[15] It was demonstrated that a more rigid π-bridge can enhance σ_2 values, while maintaining high fluorescence yields, due to the fact that electronic coupling is optimized when a π system has a planar geometry. Another approach was the design of molecules with extended conjugation and containing electron donor and/ or electron acceptor groups. As terminal donors, the alkyl and diaryl amino groups are generally used, whereas the most widely utilized electron acceptors are cyano, nitro, sulfonyl, aldehyde and π-deficient heterocycles. Recent publications showed that the structures that have electron donating groups show comparatively higher σ_2 values than the molecules with electron withdrawing groups at the extremities.[16] In fact, a rigorous choice of donor/acceptor groups and of π conjugated connectors, along with the symmetry can tune the optical properties of the system.

Thus, the attention was moved from simple structures (as amino acids and flavins)[17] to more complex push-pull dipolar[18] or even quadrupolar[15, 19] arrangements. The quadrupolar systems proved to act more efficiently as two photon absorbers than dipolar ones, due to their extended conjugation.[20] The same strategies were applied on systems involving porphyrins,[21] oligomers and polymers.[22] For example, a simple porphyrin monomer possesses a 2PA response of about 8000 GM, whereas a fused tetramer reaches 100 000 GM, due to optimized conjugation and planarity. Successful results were obtained particularly in bioimaging, by using more complex architectures, as conjugated[23] or multichromophoric[24] dendrimers and nanodots.[19, 25]

Herein are described several biomedical applications for which the new 2PA systems described in this thesis are designed for.

1.2. Two photon absorbers applications

1.2.1. Two photon bioimaging

The biological imaging refers to the observation of images of living organisms by making use of a microscope. In the medical field, the technique is widely used for the detection and characterization of pathologies, whose biomarkers can be sensed by fluorescent probes (Figure 1.3). The method is strictly based on the ability of a probe molecule (fluorophore) to fluoresce, requiring

a high luminescence quantum yield, independent of the method used (either common confocal microscopy or two photon bioimaging).
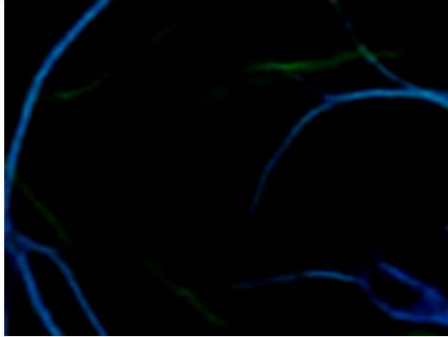
Figure 1.3. Example of a TPEM image of a blood vessels in a living organism.

The first step into bioimaging field was made about one century ago, when experiments using UV light were performed in order to achieve high resolutions. All these tests were initially limited to specimens capable to autofluoresce, but soon after, the necessity for development of new fluorescent dyes emerged. From this point, the interest in imaging cells and tissues enlarged rapidly, but only after 1990 the fluorescence microscopy became a popular technique. The availability, and mainly the efficiency of the use of fluorescent dyes, are highly dependent on factors as photobleaching, autofluorescence and scattering of the media etc.[26] Since these limitations are not always negligible in case of living organisms, the use of the appropriate technique together with the right fluorophores can reduce them to some extent.

Due to its non-invasive characteristics and high penetration of the tissues, the concept of two photon absorption was considered for bioimaging. It was approached not only in the development of new methods as alternative to conventional single-photon confocal microscopy (i.e. novel two-photon excited fluorescence microscopy), but also for design of new fluorophores. Imaging with high resolution of a living animal and extracting quantitative information, became possible only recently with the development of TPEM methods, capable of resolving up to the activity of a single neuron. Thus, the method has gained increased popularity in the biology community. Though TPEM can be carried out with most of the chromophores developed for one-photon excitation, there is a major importance in achieving higher sensitivity using dyes with large 2PA cross sections. Achieving very large σ_2 is particularly important for early diagnostics or for dynamic imaging of fast processes with biological importance (i.e. propagation of action potential in neurons). Moreover, it makes possible the sensitive detection of more dilute species, not accessible to ordinary one photon microscopy.

Imaging based on two-photon excited fluorescence gained an increased consideration when Denk at al.[6] revolutionized three dimensional (3D) in vivo imaging of cells and tissues. Since the use of two lower energy photons can lead to deeper tissue penetration and to a reduction of photodamage of the cells (as already stressed above), the method became particularly important in case of prolonged exposition.[11a] In imaging by 2PA excitation, the most important parameter describing the efficiency of 2PA fluorophores is the two photon brightness, given by the product $\phi_{fl} \times \sigma_2$, and quantified in GM units.

From the fluorophores measured by Xu and Webb,[11a] Rhodamine reached the highest σ_2 value of about 200 GM, but its photostability raised problems. Various reports from later literature described compounds with 2PA cross-sections varying from 10^{-2} GM (for NAD(P)H)[11a] up to 50 000 GM for water soluble quantum dots.[11c] The quantum dots made the object of intense studies, since these semiconductor nanoparticles possess unique photophysical properties, becoming a particular class of fluorophores with special interest for applications *in vitro* and *in vivo*. They are superior to other nanoparticles, being capable of absorbing light on a wide spectrum, having size-tunable emission, large Stokes shift, resistance to photobleaching, and improved brightness. Bruchez and Nie[27] reported for the first time in 1998 the use of QDs in detection of biological targets. After that, various QDs examined by 2PA microscopy and used for brain microvasculature imaging[28], *in vivo* cell tracking[29] and intracellular Förster resonance energy transfer (FRET) studies[30] were reported.

As a better alternative to QDs are the organic metal-free nanodots (or dendrimers), which emerged as non-toxic and biocompatible fluorophores for bioimaging. Though these systems were known from 1978,[31] the first dendrimeric systems with 2PA fluorophores were reported by Frechet only in 2000.[24, 32] Later, the groups of Caminade and Blanchard-Desce[19, 25, 33] made the highest effort in developing new materials exhibiting increased 2PA response. In particular, they described various phosphorous based dendrimers with use in bioimaging. Their photophysical properties, bioavailability and potential applications (imaging, transfection experiments, and carriers of active substances) were investigated by the same groups.[34] More important, their 2PA cross-sections can reach values close to 60 000 GM[19, 25, 33b], while maintaining relatively high fluorescence quantum yields in organic solvents. Very recently, another work of Blanchard-Desce, describing the use in cellular imaging of new octupolar systems with a triphenylamine core was reported.[35] It was shown that strong electron withdrawing end groups coupled to double bonds produced an enhancement of σ_2 up to 2000 GM at peak and larger than 1000 GM over the whole range (700 – 900 nm). The fluorophores retained their fluorescence (ϕ_{fl} up to 0.9) and two photon absorption

properties not only in low polarity media, but also in biological conditions, proving their compatibility in cell imaging.

Other types of fluorophores used in two photon bioimaging, but with modest σ_2 values compared to the ones already stated, were mentioned below. Fluorene chromophore, known for its 2PA activity, was used in the construction of other fluorescent dyes for multiphoton imaging.[36] It was shown that according to the substitution pattern, fluorene derivatives can possess elevated fluorescence (close to unity) and high 2PA absorptivity (from 100 GM to over 2000 GM). Following the basic principles for the design of efficient 2PA chromophores (described above), novel systems based on a tetraketo derivative and with symmetric structure D-A-D (where D and A are electron donor and acceptor, respectively) proved to have important 2PA cross-sections, close to 1000 GM. They were further used to trap metal ions, as calcium.[37] Later, the work of Wong et al.[38] reported a series of novel biocompatible cyanines. They showed not only large two-photon cross-sections (5130 GM at 910 nm), but also a high efficiency in localization of mitochondria and lysosomes. Far better, the 2PA cross-sections (ca. 20 000 GM) and cytotoxicity of NIR emitting squaraine dyes were also measured.[39] Their one photon and two photon fluorescence microscopy imaging were realized after incubation of squaraine probes into various cells, demonstrating their potential in multiphoton fluorescence imaging.

Though only a limited number of fluorophores were mentioned here as used in bioimaging by means of 2PA microscopy, the scientists are confronting new challenges in developing others. Our groups have also reported the linear and non-linear optical properties of novel imidazole and imidazopyridine derivatives, pioneering the 2PA work on these types of systems. The results obtained are discussed in the following sections (Chapters 2 and 3). The photophysical properties of several organic nanodots designed for bioimaging and investigated by our groups are detailed in Chapter 4.

1.2.2. Two photon polymerization

Photopolymerization is defined as a chemical process triggered by light which transforms molecules of low molecular weight (i.e. monomers, *M*) into macromolecules of repeating units (i.e. polymers). In this case, the use of a light-sensitive photoinitiator (*I*) that produces an active species upon irradiation with UV, Vis or IR light is actively involved. The photoinitiators that have been

most extensively used so far are divided according to the nature of the generated active species (free radicals, cations or anions).

Figure 1.4. Microstructure fabricated by 2PP. Scale bar represents 10 μm. Readapted from reference [40].

Free-radical polymerizations are chain reactions in which the addition of a monomer molecule to an active chain-end regenerates the active site at the chain-end:

Initiation: $\qquad$ $I \rightarrow I^* \rightarrow R^\bullet$ $\qquad$ (1.5.)

Propagation: $\qquad$ $R^\bullet + M \rightarrow RM^\bullet \rightarrow RM^\bullet$ $\qquad$ (1.6)

Termination: $\qquad$ $RM^\bullet_n + RM^\bullet_m \rightarrow RM^\bullet_{n+m}R$ $\qquad$ (1.7)
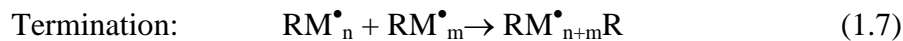
An effective photoinitiator has a high quantum yield in generation of active species, high thermal stability, it is highly soluble in the polymerization medium and displays stability in the darkness. Reactions can occur via singlet excited state, or more often via triplet excited state.

There are many studies referring to 1PP, where the radicals are formed upon excitation with a continuous light source. In 1PP it is essential to have an absorption path length comparable to or larger than the thickness of the object to be polymerized. In this way, the absorption does not prevent the polymerization of the object's area farthest from the light source. It reduces to some extent the concentration of the photoinitiator used for 1PP. Other problems in this method are given by a series of limitations, such as multistep procedures or long fabrication times.

To overcome this, two photon polymerization method (2PP) has emerged in 1997.[10a] In 2PP, nearly simultaneous absorption of two photons within a small volume in a photosensitive compound induces chemical reactions between photoinitiator molecules and monomers. A laser with femtosecond pulses (titanium:sapphire laser operating at 800 nm) is used to generate high energy intensity in the focal volume. Moreover, in 2PP the sample is transparent at the laser wavelength, and polymerization occurs only in the focal region, making possible the use of a photoinitiator with a higher concentration. As in 2PP the number of photons absorbed per unit time is proportional to the concentration (c) of the initiator, implicitly the number of radicals generated is dependent on c. [41]

In case of biomedical applications increased efforts have been made for the fabrication of new biocompatible and biodegradable structures, in particular for drug delivery (i.e. microneddles)[42] or scaffolds for tissue engineering.[43] Microneedles with complex shapes (i.e. rocket type geometry) were fabricated by 2PP in view of transdermal delivery.[42] They are characterized mainly by a very small tip angle, associated with lower microneedle penetration forces.[44] The method demonstrated the ease of duplicating the microneedles by 2PP, which may facilitate their use in clinical applications.

2PP was also used for creating sensors for medical applications. 3D grid structures were obtained from organically modified ceramics and biotin was immobilized on them by ultraviolet-activated cross-linking.[45] Recently, a glucose sensing electrode was created by Kim et al.[46] by 2PP and the electrochemical detection of glucose was demonstrated by using a single-walled carbon nanotube (which facilitates the ferrocene activity) containing electrode. The results presented here demonstrate the ease of fabrication of sensors by 2PP technique and also point to their successful use in combination with biologically active compounds.

The fabrication of structures that guide cell development and provide them mechanical support is imperative for replacing damaged tissues.[47] A series of studies involving different types of cells grown on polymeric scaffolds with results on their migration and morphology were reported.[43a, 48] Besides the fabrication of structures from different materials followed by tests to prove their biocompatibility, a more viable route involving living cells containing materials was approached. Therefore, scaffolds were prepared by 2PP from organically modified ceramics seeded with B35-neuroblast cells[49] or endothelial and Chinese hamster ovary cells, without harming the living cells.[50] This might eliminate the biocompatibility problem often raised in first scaffolds mentioned above (not containing cells).

Only a limited part of the achievements by means of 2PP technique were reported here. Since only a limited number of photosensitive polymers were processed by using this method, there is still room for expanding the class of materials to be used. Our groups have studied the photophysical properties of a number of ketocoumarins, as well as their involvement in the fabrication of microstructures (as photoinitiators) and the biocompatibility of these 3D grids. The results are explained in Chapter 5 of the thesis.

1.2.3. Two photon uncaging of biologically active molecules

The 'caged' compounds are light sensitive probes that encapsulate a biologically active molecule, modified to remain inactive while caged. The irradiation with light allows the fragmentation and the subsequent release of the molecule, which becomes afterwards active. Ideally, the caged molecules are water soluble, but the 'cage' compound is stable under hydrolysis. Moreover, the release of the trapped molecule should should occur with high quantum yield and upon high wavelengths excitation (two photon excitation). Additionally, the photodeprotection is a very fast process. The process of uncaging (or photolysis) plays an important role in photomanipulation of the cellular chemistry and some examples of released compounds are: protons[51], neurotransmitters[52], nucleotides[53], enzymes[54], mRNA[55] etc.

In the past decade, a considerable progress has been made in developing new families of photolabile protecting groups and exploring their efficiency by various methods. The release of the caged molecules was done via Norrish reactions (type I or II), photosolvolysis, photoisomerization *trans-cis* or photoinduced electron transfer. All these procedures were limited to one photon excitation technique.

By taking advantage of two-photon excitation, one can further gain spatial control, deeper penetration into tissues and reduced scattering, as already mentioned. In this case, the uncaging rate is dependent on the application and its efficiency is quantified by the uncaging quantum yield (ϕ_u) (the number of uncaging events per absorbed photon). Another important parameter for two photon uncaging groups is the product of $\sigma_2 \phi_u$, known as two-photon uncaging cross-section.

Unfortunately, only few data are available so far for the two photon uncaging systems. Since the 2PA cross-sections (σ_2) of the systems used to date in uncaging is rather low, the development of new chromophores with excellent 2PA properties is a rather emerging process. Initially, several chromophores commonly used in one photon uncaging (as *o*-nitrobenzyl group and all its derivatives, coumarin derivatives…) were probed for two photon release and their 2PA uncaging yields were measured. For example, the *o*-nitrobenzyl-based photoprotecting groups have uncaging yields between 0.01 to 0.035 GM, as function of the substitution pattern.[56] Later, an improvement of the uncaging yield and 2PA cross-sections of uncaging was reported for the same photoprotecting groups, due to an energy transfer process from the dye to the caging chromophore. Other compounds, as coumarin derivatives ($\sigma_2 \phi_u$ = 2 GM at 700 nm) [57] or ruthenium complexes releasing glutamine or 4- aminopyridine ($\sigma_2 \phi_u$ ~ 0.1 GM) [58] were tested, but they displayed modest results.

A rather new methodology involved in two photon uncaging is the release of the caged molecules *via* photoinduced electron transfer process. The electron donor group (two photon absorption dye) is excited by the incident light and transfers one electron to the electron acceptor (caging group). Consequently, the formed charge separated state rearranges and the caged molecule is released (Figure 1.5).
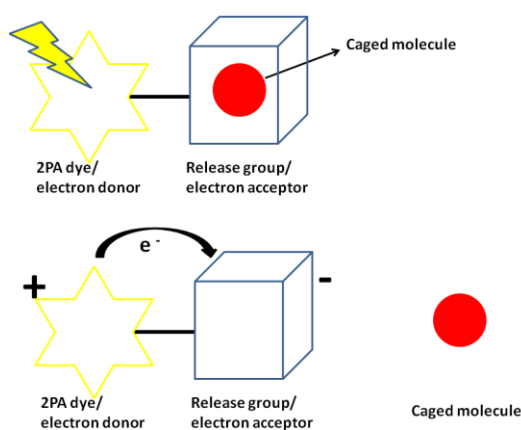
Figure 1.5. Schematic representation of 2PA uncaging process by means of electron transfer from 2PA absorbing dye/ electron donor to the release group/ electron acceptor. The process is followed by the immediate release of the caged molecule.

Falvey et al. pioneered the release of the molecules via photoinduced electron transfer, but using one photon excitation.[59] They have showed that the acetic acid could be released of from *N,N*- dimethylaniline [60] and that 4-pyridylmethyl (picolyl) group could be reduced in the presence of *N,N,N',N'*-tetramethylbenzidine.[61]

Dore et al. have measured the two-photon uncaging cross-sections of (quinoline-4-yl)methyl PPGs via electron transfer process.[62] From this, the most efficient two photon uncaging quantum yields values were up to 1 GM at 740 nm.[63] Further, a decrease of the two photon uncaging value was registered upon replacement of *bromo* substituent with *cyano*[64] and *chloro*.[65]

Substantial improvements were made in the past years on the synthesis, stability, solubility, as well as rate and efficiency of release for one photon absorbing dyes. Though, extending the excitation wavelengths in the NIR-IR region (by two photon excitation) and combination with the natural features of the systems used in uncaging applications, are challenges still to be solved. The data obtained by our group on the investigation of the electron transfer dynamics in three fluorene-based arrays, synthesized for photorelease of neurotransmitters *via* PeT, are detailed in Chapter 5.

1.3. References

[1]   R. W. Boyd, *Nonlinear Optics, 3rd Edition*, **2008**.

[2]   D. J. Williams, *Angew. Chem. Int. Ed. Eng.* **1984**, *23*, 690-703.

[3]   R. R. Birge, *An introduction to two-photon spectroscopy, Vol. 139*, NATO ASI Ser., Ser. C,, **1984**.

[4]   M. Goppert-Mayer, *Ann. Phys.* **1931**, *9*, 273-295.

[5]   W. Kaiser, C. G. B. Garret, *Phys. Rev. Lett.* **1961**, *7*, 229–231.

[6]   W. Denk, J. H. Strickler, W. W. Webb, *Science* **1990**, *248*, 73-76.

[7]   M. Pawlicki, H. A. Collins, R. G. Denning, H. L. Anderson, *Angew. Chem. Int. Ed.* **2009**, *48*, 3244 – 3266.

[8]   a) R. R. Birge, *Acc. Chem. Res.* **1986**, *19*, 138-146; b) S. Shima, R. P. Ilagan, N. Gillespie, B. J. Sommer, R. G. Hiller, F. P. Sharples, H. A. Frank, R. R. Birge, *J. Phys. Chem. A* **2003**, *107*, 8052-8066.

[9]   M. P. Joshi, H. E. Pudavar, J. Swiatkiewicz, P. N. Prasad, B. A. Reianhardt, *Appl. Phys. Lett.* **1999**, *74*, 170-172.

[10]   a) S. Maruo, O. Nakamura, S. Kawata, *Opt. Lett.* **1997**, *22*, 132-134; b) B. H. Cumpston, S. P. Ananthavel, S. Barlow, D. L. Dyer, J. E. Ehrlich, L. L. Erskine, A. A. Heikal, S. M. Kuebler, I. Y. S. Lee, D. McCord-Maughon, J. Q. Qin, H. Rockel, M. Rumi, X. L. Wu, S. R. Marder, J. W. Perry, *Nature* **1999**, *398*, 51-54; c) S. Kawata, H. B. Sun, T. Tanaka, K. Takada, *Nature* **2001**, *412*, 697-698; d) W. H. Zhou, S. M. Kuebler, K. L. Braun, T. Y. Yu, J. K. Cammack, C. K. Ober, J. W. Perry, S. R. Marder, *Science* **2002**, *296*, 1106-1109.

[11]   a) C. Xu, W. Zipfel, J. B. Shear, R. M. Williams, W. W. Webb, *Proc. Natl. Acad. Sci. U. S. A.* **1996**, *93*, 10763-10768; b) W. Denk, P. B. Detwiler, *Proc. Natl. Acad. Sci. U. S. A.* **1999**, *96*, 7035-7040; c) D. R. Larson, W. R. Zipfel, R. M. Williams, S. W. Clark, M. P. Bruchez, F. W. Wise, W. W. Webb, *Science* **2003**, *300*, 1434-1436; d) G. C. Cianci, J. R. Wu, K. M. Berland, *Microsc. Res. Tech.* **2004**, *64*, 135-141; e) A. N. Kuzmin, A. V. Kachynski, T. Y. Ohulchanskyy, I. Roy, P. N. Prasad, S. Bruckenstein, *Appl. Phys. Lett.* **2004**, *84*, 2454-2456; f) F. Helmchen, W. Denk, *Nat. Met.* **2005**, *2*, 932-940.

[12]   a) H. E. Pudavar, M. P. Joshi, P. N. Prasad, B. A. Reinhardt, *Appl. Phys. Lett.* **1999**, *74*, 1338-1340; b) K. D. Belfield, Y. Liu, R. A. Negres, M. Fan, G. Pan, D. J. Hagan, F. E. Hernandez, *Chem. Mater.* **2002**, *14*, 3663-3667; c) K. D. Belfield, K. J. Schafer, *Chem. Mater.* **2002**, *14*, 3656-3662.

[13]   a) A. M. R. Fisher, A. L. Murphree, C. J. Gomer, *Lasers Surg. Med.* **1995**, *17*, 2-31; b) W. R. Dichtel, J. M. Serin, C. Edder, J. M. J. Frechet, M. Matuszewski, L. S. Tan, T. Y. Ohulchanskyy, P. N. Prasad, *J. Am. Chem. Soc.* **2004**, *126*, 5380-5381; c) S. Kim, T. Y. Ohulchanskyy, H. E. Pudavar, R. K. Pandey, P. N. Prasad, *J. Am. Chem. Soc.* **2007**, *129*, 2669-2675.

[14]   a) P. N. Prasad, *Introduction to Biophotonics*, Wiley, New York **2003**; b) P. N. Prasad, *Nanophotonics*, Wiley, New York **2004**.

[15]   M. Albota, D. Beljonne, J. L. Bredas, J. E. Ehrlich, J. I. Fu, A. A. Heikal, S. E. Hess, T. Kogej, M. D. Levin, S. R. Marder, D. McCord-Maughon, J. W. Perry, H. Rockel, M. Rumi, G. Subramaniam, W. W. Webb, X. L. Wu, C. Xu, *Science* **1998**, *281*, 1653-1656.

[16]   L. Porres, O. Mongin, C. Katan, M. Charlot, T. ; Pons, J. Mertz, M. Blanchard Desce, *Org. Lett.* **2004**, *6*, 47.

[17]   a) Y. Meshalkin, *Kvantovaya Elektron.* **1996**, *23*, 551-552; b) W. R. Zipfel, R. M. Williams, R. Christie, A. Y. Nikitin, B. T. Hyman, W. W. Webb, *Proc. Natl. Acad. Sci. USA* **2003**, *100*, 7075-7080; c) G. F. White, K. L. Litvinenlo, S. R. Meech, D. L. Andrews, A. J. Thomson, *Photochem. Photobiol.* **2004**, *3*, 47-55.

[18]   a) G. S. He, J. D. Bhawalkar, C. F. Zhao, P. N. Prasad, *Appl. Phys. Lett.* **1995**, *67*, 2433-2435; b) G. S. He, L. X. Yuan, N. Cheng, J. D. Bhawalkar, P. N. Prasad, L. L. Brott, S. J. Clarson, B. A. Reinhardt, *J. Opt. Soc. Am. b-Opt. Phys.* **1997**, *14*, 1079-1087; c) A. Abbotto, L. Beverina, R. Bozio, S. Bradamante, C. Ferrante, G. A. Pagani, R. Signorini, *Adv. Mater.* **2000**, *12*, 1963; d) S. Charier, O. Ruel, J. B. Baudin, D. Alcor, J. F. Allemand, A. Meglio, L. Jullien, *Angew. Chem. Int. Ed.* **2004**, *43*, 4785-4788.

[19]   O. Mongin, A. Pla-Quintana, F. Terenziani, D. Drouin, C. Le Droumaguet, A.-M. Caminade, J.-P. Majoral, M. Blanchard-Desce, *New J. Chem.* **2007**, *31*, 1354-1367.

[20]   C. Li, C. L. Liu, Q. S. Li, Q. H. Gong, *Chem. Phys. Lett.* **2004**, *400*, 569-572.

[21]   a) M. Drobizhev, A. Karotki, M. Kruk, A. Rebane, *Chem. Phys. Lett.* **2002**, *355*, 175-182; b) M. Drobizhev, A. Karotki, M. Kruk, Y. Dzenis, A. Rebane, A. Meng, E. Nickel, C. W. Spangler, in *Nonlinear Optical Transmission and Multiphoton Processes in Organics, Vol. 5211* (Eds.: A. T. Yeates, K. D. Belfield, F. Kajzar, C. M. Lawson), **2003**, pp. 63-74; c) H. Rath, J. Sankar, V. PrabhuRaja, T. K. Chandrashekar, A. Nag, D. Goswami, *J. Am. Chem. Soc.* **2005**, *127*, 11608-11609; d) M. Drobizhev, Y. Stepanenko, A. Rebane, C. J. Wilson, T. E. O. Screen, H. L. Anderson, *J. Am. Chem. Soc.* **2006**, *128*, 12432-12433.

[22]   a) Y. Morel, A. Irimia, P. Najechalski, Y. Kervella, O. Stephan, P. L. Baldeck, C. Andraud, *J. Chem. Phys.* **2001**, *114*, 5391-5396; b) R. Anemian, J. C. Mulatier, C. Andraud, O. Stephan, J. C. Vial, *Chem. Commun.* **2002**, 1608-1609; c) K. D. Belfield, A. R. Morales, J. M. Hales, D. J. Hagan, E. W. Van Stryland, V. M. Chapela, J. Percino, *Chem. Mater.* **2004**, *16*, 2267-2273; d) S. J. Chung, M. Rumi, V. Alain, S. Barlow, J. W. Perry, S. R. Marder, *J. Am. Chem. Soc.* **2005**, *127*, 10844-10845.

[23]   a) O. Mongin, J. Brunel, L. Porres, M. Blanchard-Desce, *Tetrahedron Lett.* **2003**, *44*, 2813-2816; b) L. Porres, C. Katan, O. Mongin, T. Pons, J. Mertz, M. Blanchard-Desce, *J. Mol. Struct.* **2004**, *704*, 17-24; c) O. Varnavski, X. Yan, O. Mongin, M. Blanchard-Desce, T. Goodson, III, *J. Phys. Chem. C* **2007**, *111*, 149-162.

[24]   A. Adronov, J. M. J. Frechet, G. S. He, K. S. Kim, S. J. Chung, J. Swiatkiewicz, P. N. Prasad, *Chem. Mater.* **2000**, *12*, 2838-2843.

[25]   O. Mongin, T. R. Krishna, M. H. V. Werts, A. M. Caminade, J. P. Majoral, M. Blanchard-Desce, *Chem. Commun.* **2006**, 915-917.

[26]   C. Vonesch, F. Aguet, J. L. Vonesch, M. Unser, *IEEE Signal Processing Magazine* **2006**, *23*, 20-31.

[27]   a) M. Bruchez, M. Moronne, P. Gin, S. Weiss, A. P. Alivisatos, *Science* **1998**, *281*, 2013-2016; b) W. C. W. Chan, S. M. Nie, *Science* **1998**, *281*, 2016-2018.

[28]   J. V. Kim, S. S. Kang, M. L. Dustin, D. B. McGavern, *Nature* **2009**, *457*, 191-U185.

[29]   a) E. B. Voura, J. K. Jaiswal, H. Mattoussi, S. M. Simon, *Nat. Med.* **2004**, *10*, 993-998; b) M. Stroh, J. P. Zimmer, D. G. Duda, T. S. Levchenko, K. S. Cohen, E. B. Brown, D. T.

Scadden, V. P. Torchilin, M. G. Bawendi, D. Fukumura, R. K. Jain, *Nat. Med.* **2005**, *11*, 678-682.

[30]   A. R. Clapp, T. Pons, I. L. Medintz, J. B. Delehanty, J. S. Melinger, T. Tiefenbrunn, P. E. Dawson, B. R. Fisher, B. O'Rourke, H. Mattoussi, *Adv. Mater.* **2007**, *19*, 1921.

[31]   E. Buhleier, W. Wehner, F. Vogtle, *Synthesis-Stuttgart* **1978**, 155-158.

[32]   A. Adronov, J. M. J. Frechet, *Chem. Commun.* **2000**, 1701-1710.

[33]   a) D. Ormrod, B. Jarvis, *Am. J. Clin. Dermatol.* **2000**, *1*, 133-139; discussion 140-131; b) O. Mongin, C. Rouxel, A.-C. Robin, A. Pla-Quintana, T. R. Krishna, G. Recher, F. Tiaho, A.-M. Caminade, J.-P. Majoral, M. Blanchard-Desce, in *Nanobiosystems: Processing, Characterization, and Applications, Vol. 7040* (Eds.: E. M. Heckman, T. B. Singh, J. Yoshida), **2008**.

[34]   a) C. O. Turrin, J. Chiffre, J. C. Daran, D. de Montauzon, A. M. Caminade, E. Manoury, G. Balavoine, J. P. Majoral, *Tetrahedron* **2001**, *57*, 2521-2536; b) A. M. Caminade, V. Maraval, R. Laurent, C. O. Turrin, P. Sutra, J. Leclaire, L. Griffe, P. Marchand, C. Baudoin-Dehoux, C. Rebout, J. P. Majoral, *CR Chimie* **2003**, *6*, 791-801; c) A. M. Caminade, J. P. Majoral, *Prog. Polym. Sci.* **2005**, *30*, 491-505; d) C. Padie, M. Maszewska, K. Majchrzak, B. Nawrot, A.-M. Caminade, J.-P. Majoral, *New J. Chem.* **2009**, *33*, 318-326.

[35]   C. Le Droumaguet, A. Sourdon, E. Genin, O. Mongin, M. Blanchard-Desce, *Chem. Asian J.* **2013**, *8*, 2984-3001.

[36]   a) K. D. Belfield, K. J. Schafer, W. Mourad, B. A. Reinhardt, *J. Org. Chem.* **2000**, *65*, 4475-4481; b) K. D. Belfield, M. V. Bondar, O. V. Przhonska, K. J. Schafer, W. Mourad, *J. Lumin.* **2002**, *97*, 141-146; c) J. M. Hales, D. J. Hagan, E. W. Van Stryland, K. J. Schafer, A. R. Morales, K. D. Belfield, P. Pacher, O. Kwon, E. Zojer, J. L. Bredas, *J. Chem. Phys.* **2004**, *121*, 3152-3160; d) K. J. Schafer, S. Yao, K. D. Belfield, J. M. Hales, D. J. Hagan, E. W. Van Stryland, in *Genetically Engineered and Optical Probes for Biomedical Applications I, Vol. 5329* (Eds.: A. P. Brovko, D. J. Bornhop, R. Raghavachari, S. I. Achilefu), **2004**, pp. 201-206.

[37]   R. Gvishi, G. Berkovic, Z. Kotler, P. Krief, J. Y. Becker, M. Sigalov, L. Shapiro, V. Khodorkovsky, in *Photonics, Devices, and Systems Ii, Vol. 5036* (Eds.: M. Hrabovsky, D. Senderakova, P. Tomanek), **2003**, pp. 437-442.

[38]   W. Yang, P. S. Chan, M. S. Chan, K. F. Li, P. K. Lo, N. K. Mak, K. W. Cheah, M. S. Wong, *Chem. Commun.* **2013**, *49*, 3428-3430.

[39]   H.-Y. Ahn, S. Yao, X. Wang, K. D. Belfield, *Acs Appl. Matt. Interf.* **2012**, *4*, 2847-2854.

[40]   N. R., P. Danilevicius, C. A.I., M. Chatzinikolaidou, D. Gray, L. Flamigni, M. Farsari, G. D.T., *Chem. Mater.* **2014**.

[41]   H.-B. Sun, S. Kawata, *Two-Photon Photopolymerization and 3D Lithographic Microfabrication, Vol. 170*, DOI 10.1007/b94405, **2004**.

[42]   S. D. Gittard, R. Narayan, *Expert Rev. Med. Devices* **2010**, *7*, 343-356.

[43]   a) F. Claeyssens, E. A. Hasan, A. Gaidukeviciute, D. S. Achilleos, A. Ranella, C. Reinhardt, A. Ovsianikov, S. Xiao, C. Fotakis, M. Vamvakaki, B. N. Chichkov, M. Farsari, *Langmuir* **2009**, *25*, 3219-3223; b) M. Farsari, M. Vamvakaki, B. N. Chichkov, *J. Opt.* **2010**, *12*; c) C. Schizas, V. Melissinaki, A. Gaidukeviciute, C. Reinhardt, C. Ohrt, V. Dedoussis, B. N. Chichkov, C. Fotakis, M. Farsari, D. Karalekas, *Int. J. Adv. Manuf. Tech.* **2010**, *48*, 435-441.

[44]   S. Chandrasekaran, A. B. Frazier, *J. Microelectromech. Syst.* **2003**, *12*, 289-295.

[45] T. S. Drakakis, G. Papadakis, K. Sambani, G. Filippidis, S. Georgiou, E. Gizeli, C. Fotakis, M. Farsari, *Appl. Phys. Lett.* **2006**, *89*.

[46] J. M. Kim, J. J. Park, H.-J. Lee, K. W.-S., H. Muramatsu, S.-M. Chang, *Bioproc. Biosyst. Eng.* **2010**, *33*, 47-53.

[47] N. R. Schiele, D. T. Corr, Y. Huang, N. A. Raof, Y. Xie, D. B. Chrisey, *Biofabrication* **2010**, *2*.

[48] a) P. Tayalia, C. R. Mendonca, T. Baldacchini, D. J. Mooney, E. Mazur, *Adv. Mater.* **2008**, *20*, 4494-4498; b) H. Hidai, H. Jeon, D. J. Hwang, C. P. Grigoropoulos, *Biomed. Microdevices* **2009**, *11*, 643-652; c) T. M. Hsieh, C. W. B. Ng, K. Narayanan, A. C. A. Wan, J. Y. Ying, *Biomaterials* **2010**, *31*, 7648-7652.

[49] A. Doraiswamy, C. Jin, R. J. Narayan, P. Mageswaran, P. Mente, R. Modi, R. Auyeung, D. B. Chrisey, A. Ovsianikov, B. Chichkov, *Acta Biomater.* **2006**, *2*, 267-275.

[50] A. Ovsianikov, S. Schlie, A. Ngezahayo, A. Haverich, B. N. Chichkov, *J. Tissue Eng. Regen. Med.* **2007**, *1*, 443-449.

[51] A. Barth, J. E. T. Corrie, *Biophys. J.* **2002**, *83*, 2864-2871.

[52] J. Noguchi, A. Nagaoka, S. Watanabe, G. C. R. Ellis-Davies, K. Kitamura, M. Kano, M. Matsuzaki, H. Kasai, *J.Physiol.-London* **2011**, *589*, 2447-2457.

[53] J. A. Sanchez, J. Vergara, *Am. J. Physiol.* **1994**, *266*, C1291-C1300.

[54] A. Silanskas, M. Foss, W. Wende, C. Urbanke, A. Lagunavicius, A. Pingoud, V. Siksnys, *Biochemistry* **2011**, *50*, 2800-2807.

[55] H. Ando, T. Furuta, R. Y. Tsien, H. Okamoto, *Nat. Genet.* **2001**, *28*, 317-325.

[56] S. Kantevari, C. J. Hoang, J. Ogrodnik, M. Egger, E. Niggli, G. C. R. Ellis-Davies, *Chembiochem* **2006**, *7*, 174-180.

[57] Y. R. Zhao, Q. Zheng, K. Dakin, K. Xu, M. L. Martinez, W. H. Li, *J. Am. Chem. Soc.* **2004**, *126*, 4653-4663.

[58] V. Nikolenko, R. Yuste, L. Zayat, L. M. Baraldo, R. Etchenique, *Chem. Commun.* **2005**, 1752-1754.

[59] a) A. Banerjee, D. E. Falvey, *J. Org. Chem.* **1997**, *62*, 6245-6251; b) L. Kwangoo, D. E. Falvey, *J. Am. Chem. Soc.* **2000**, *122*, 9361-9366.

[60] J. A. Neville, E. Welch, D. J. Leffell, *Nat. Clin. Pract. Onc.* **2007**, *4*, 462-469.

[61] C. Sundararajan, D. E. Falvey, *J. Org. Chem.* **2004**, *69*, 5547-5554.

[62] Y. Zhu, C. M. Pavlos, J. P. Toscano, T. M. Dore, *J. Am. Chem. Soc.* **2006**, *128*, 4267-4276.

[63] O. D. Fedoryak, T. M. Dore, *Org. Lett.* **2002**, *4*, 3419-3422.

[64] A. S. C. Fonseca, M. S. T. Goncalves, S. P. G. Costa, *Tetrahedron* **2007**, *63*, 1353-1359.

[65] B. Curten, P. H. M. Kullmann, M. E. Bier, K. Kandler, B. F. Schmidt, *Photochem. Photobiol.* **2005**, *81*, 641-648.

2. Imidazole based derivatives for bioimaging

In this chapter two series of imidazole based derivatives with excited state proton transfer (ESIPT) property are presented. For comparison purposes their counterparts, in which the ESIPT was deliberately blocked, were investigated. It is known that ESIPT is very complex and its efficiency is affected not only by internal (e.g. substitution pattern) but also by external parameters (e.g. solvent). Therefore, the first series that has been studied is a collection of differently substituted molecules, designed with the aim of testing the influence of the molecular structure on ESIPT efficiency. Once determined the best scaffold in order to maximize the fluorescence quantum yield values, the second series of imidazoles was synthesized. It is formed by a number of molecules containing the sulfonamido group and various substituents.

The linear optical properties of all the derivatives are described below, whereas details about synthesis and 2PA absorption properties can be found elsewhere.[1] The compounds were synthesized by the group of Dr. Daniel T. Gryko, whereas the 2PA properties were determined by the group of Dr. Mireille Blanchard-Desce. Hence, it is shown that the molecular structure and the external medium can significantly influence the luminescence parameters of these ESIPT compounds. They display modest two photon absorption properties, but they open the way to use imidazole derivatives as fluorophores for bioimaging.

2.1. Introduction

Imidazole[2] derivatives, and particularly tetraphenylimidazoles, are attracting attention due to their photophysical properties. At the same time, ESIPT[3] has emerged in recent years as a very interesting phenomenon which can be applied to the design of fluorescent sensors.[4] ESIPT is a four state cycle based on the different acid- base properties of two tautomeric forms. They are enol or enamide (E) and keto or ketimide (K) forms (the second nomenclature is used when NH rather than OH is the group involved in H donation) respectively in the ground and excited states, leading to a very rapid proton transfer between a proton donor (-OH, $-NH_2$ groups) and a proton acceptor (C = O, -N = groups) found in the immediate proximity. Molecules undergoing ESIPT exhibit dual emission: a normal emission (at higher energy and having a mirror image of the absorption) arising from an excited species with similar geometry to the ground state and a Stokes shifted emission (6000 – 12 000 cm^{-1}) originating from a tautomer formed in the excited state. The relative intensities of these emissions are highly dependent on the molecular structure and on solvent

conditions (i.e. proticity). Although many functional dyes display ESIPT, only a handful of them are known to simultaneously exhibit also high fluorescence quantum yield. Among those studied extensively is a variety of 2-hydroxyphenylbenzoxazole-[5] and 2-hydroxyphenylbenzothiazole derivatives.[6] Very few derivatives and/or analogues of 2-(2-hydroxyphenyl)imidazole have been photophysically studied. Given the promising optical properties of the imidazole derivatives synthesized so far, it is desirable to gain in-depth knowledge on the structure-property relationship for this group of compounds. In particular, one can envision that π-expansion of multisubstituted imidazoles will significantly alter their optical properties, as is the case for many homoaromatic systems.[7] While phenanthro[9,10-*d*]imidazoles have been previously described,[8] derivatives possessing a 2-hydroxyphenyl group at position 2 of the imidazole core were studied only recently.[9]

Lately however, the fundamental work by Fahrni and co-workers[10] proved that replacing OH with sulphonamido group resulted in appreciably higher fluorescence quantum yields, while maintaining other beneficial optical parameters such as largely Stokes-shifted emission. As a consequence sulphonamidophenyl-benzimidazoles and phenanthroimidazoles are attracting high interest as fluorescent sensors[10c, 11] and as probes.[12] Aryl-substituted benzimidazoles and phenanthroimidazoles functionalized with tosylamido or dansylamido groups can provide well higher luminescence yields ($\phi_{fl} > 0.4$)[11-13] with respect to similar unsubstituted counterparts and the corresponding benzoxazoles. Wu et. al demonstrated that the substitution position in the tosylated compounds can play a significant role in keto tautomer emission energy. It was shown that inserting a donor methoxy group in *para* position of 2-(2'-arylsulfonamidophenyl)benzimidazole led to red shift of the emission maximum compared to unsubstituted fluorophore, whereas the substitution in *meta* position led to a blue shift.[10c] Since for biological applications the solubility in high polarity solvents is of importance, the role of donor and/or acceptor groups in water soluble 2-(2'-arylsulfonamidophenyl)benzimidazoles was investigated.[10b] None of the donor substituted derivatives exhibited dual emission in aqueous solution, whereas for some of the acceptor substituted compounds an additional band at higher energy was noticed. The quantum yield values were far higher for acceptor substituted compounds (ϕ_{fl} around 0.4) and well correlated with the observed Stokes shifts. More important, double substitution with both donor and acceptor groups led to the highest luminescence yield of the series, $\phi_{fl} = 0.46$.[10b]

In fluorescence imaging it is desirable to use functional dyes which can be excited using red or NIR light. Given that the majority of ESIPT-active compounds efficiently absorb UV or violet light, (hence tissue penetration is rather low and applications in biological imaging are very problematic) we were also interested in studying the two-photon absorption (2PA) cross-section of

the selected molecules (which in turn allows for excitation in biological window). The aim of this study is to explore the synhetic strategies to alter the basic imidazole-based ESIPT system and to investigate the optical properties of the new compounds. This would allow us to address one of the most important challenges regarding ESIPT systems, i.e. the wide tunability of chromophore absorption as well as proton transfer emission.

2.2. Results and discussion

2.2.1. Generic imidazole derivatives

A library of novel fourteen imidazole based derivatives (ESIPT and non ESIPT) was the object of photophysical investigation. All the ESIPT compounds, as well as their non-ESIPT counterparts were synthesized via Debus-Radziszewski method (see reference [1] for details). For sake of clarity, only the structures of some representative compounds are displayed in Chart 1, whereas the others can be found in reference [1].
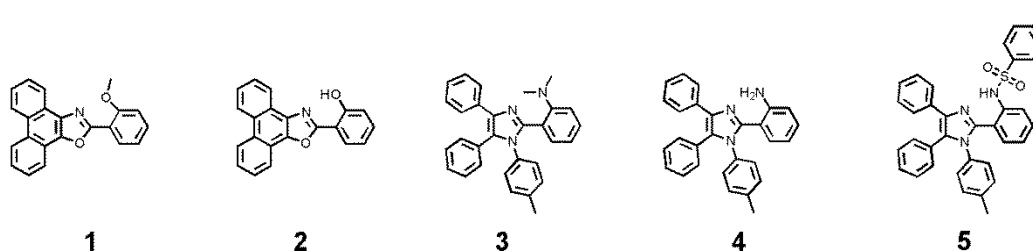
Chart 2.1. Structures of the selected compounds.

In order to ascertain the ESIPT properties of the new compounds, we have performed the examination in solvents of different dielectric constant and proticity, namely toluene (TOL), dichloromethane (DCM) and methanol (MeOH).

One photon absorption. As described in Chart 2.1, as representative for the series, the families **1** and **2**, and **3**, **4** and **5** respectively, were chosen. Their photophysical parameters are reported in Table 2.1, with two separate lines for E and the K forms.
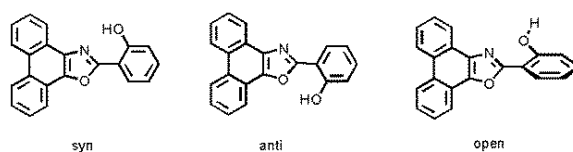
Chart 2.2. Possible conformers of compound **2**.

Compound **2** exists in three different conformations (Chart 2.2), similar to other benzoxazoles.[14] Two of them are planar, with -OH group oriented either toward the N (*syn*) or the O group (*anti*). In the third configuration (*open*), the phenoxy group lies in a plane perpendicular to the one containing the π–extended benzoxazole. In non-polar solvents, the first two conformers, and in particular the most stable *syn* which is capable of intramolecular proton transfer, are favored. On the contrary, in protic solvents, the *open* structure is stabilized by intermolecular hydrogen bond formation between the benzoxazole group and the solvent preventing an efficient ESIPT.

The absorption and emission spectra of the compounds are illustrated in Figure 2.1. The molar absorption coefficients of non-ESIPT models and ESIPT compounds are about 20 000 M^{-1} cm^{-1}, the typical range for $\pi - \pi^*$ transitions. Except sample **4** in MeOH, all the others display dual luminescence. As expected, in polar solvent MeOH, an increase of the luminescence of E and decrease or even suppression of K was noticed, which is actually the case of **4**. The weak emission maximizing at similar wavelengths with the models is coming from the E ground state tautomer, whereas the one with a large Stokes shift belongs to the K excited state tautomer. It can be noticed a strong decrease (almost 100 %) of the E luminescence compared to the one of the analogous model, favoring the formation of K tautomer (Figure 2.1, Table 1.1). The quantum yield values ϕ_{fl} were ranging from 0.001 to 0.05 for E, and they were increasing up to 0.4 for K.
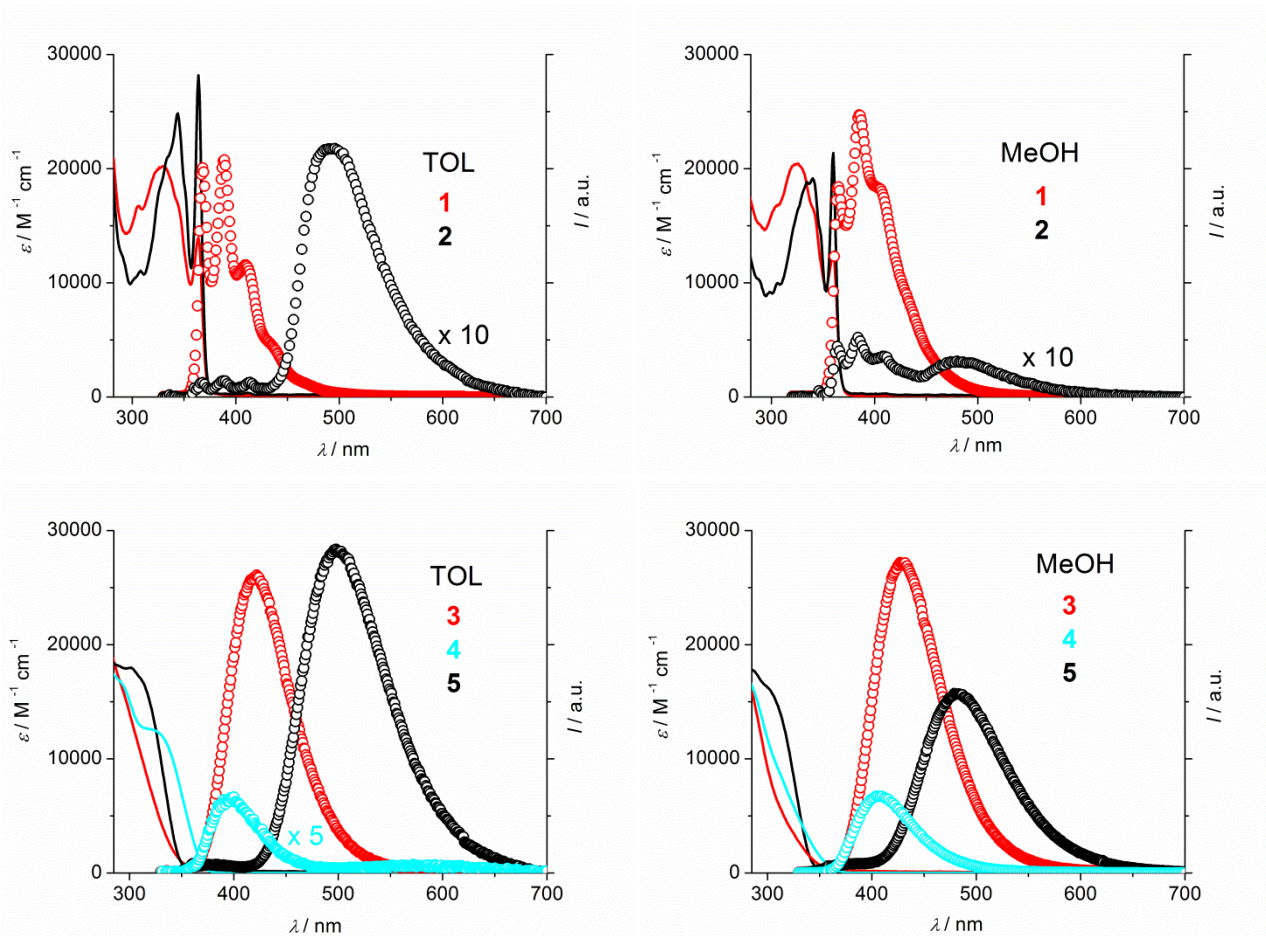
Figure 2.1. Absorption and emission spectra of the selected compounds in TOL and MeOH at room temperature. Data in DCM[1] not shown.

Time resolved data were measured by using a picosecond laser pulse and a Streak camera device for the picosecond lifetimes, while for the longer nanosecond values a Time Correlated Single Photon Counting (TCSPC) was used. The non-ESIPT models have lifetimes of several nanoseconds in all solvents (Table 2.1). The time resolved data display rapidly quenched E luminescence with $\tau \leq 20$ ps for ESIPT sample **2**, but with considerably longer lifetimes for K (Figure 2.2 and Table 2.1). With an instrumental resolution of 10 ps, the 10 ps measured lifetimes for **2** should be taken as the upper limit for τ. We cannot however exclude that the luminescence decay of E detected in the present experiment is not due to the ESIPT process. In similar compounds, in fact, much faster ESIPT processes have been reported, $\tau \ll 1$ ps, followed by a multi-exponential decay of E fluorescence ascribed to different conformation not undergoing ESIPT.[15] On the other side, in case of **4**, the proton transfer time, corresponding to the decay lifetime of E form, could be measured from the streak images; these values were 115, 70 and 320 ps in TOL, DCM and MeOH solutions, respectively. Whereas a weak K luminescence could be detected in TOL and DCM with the same *decay* lifetime registered as for the *decay* of E band, no K

luminescence was detected in MeOH. Identical lifetimes for E and K excited states in the consecutive reaction scheme (E* → K*→ K) mean that the lifetime of the intermediate K* tautomer is very low compared to its formation; the product does not accumulate and the exponential, apparent decay lifetime, is coincident with the formation lifetime.[16]

Table 2.1. Photophysical parameters of compounds **1-5** in TOL, DCM and MeOH at room temperature.

		TOL			DCM			MeOH		
		λ_{em}/nm	ϕ_{Fl}	τ/ns	λ_{em}/nm	ϕ_{Fl}	τ/ns	λ_{em}/nm	ϕ_{Fl}	τ/ns
1		368; 389; 410	0.53	2.69	368; 388; 409	0.58	2.78	365; 385; 405	0.602	2.56
2	E	367; 389; 413	0.003	0.02	365; 387; 414	0.001	≤ 0.01	364; 384; 410	0.009	≤ 0.01
	K	495	0.111	0.84	492	0.073	0.58	480	0.013	0.12
3		422	0.275	2.67	424	0.278	3.05	430	0.275	4.18
4	E	398	0.009	0.115[a]	397	0.007	0.07[a]	407	0.057	0.32
	K	572	0.004	<< 0.115	562	0.002	<< 0.08	-	-	-
5	E	375	0.004	0.05	378	0.004	0.05	379	0.004	-
	K	499	0.396	0.05[b]; 5.08	484	0.362	0.05[b]; 5.80	482	0.201	0.07[b]; 5.28

[a]See text for details. [b]Rise of K.

The ESIPT process in **5** had a lifetime of 50 ps in TOL and DCM and 75 ps in MeOH, as determined by the decay of E luminescence and the matching rise in K luminescence (Figure 2.2). In the case of MeOH solutions, the absorption at the exciting wavelength (355 nm) was low due to poor solubility and the resulting signal was very weak. In the MeOH case, the E*→K* reaction lifetime was determined only by the exponential rise in the K tautomer. As can be appreciated from the streak camera image in Figure 2.2, the K tautomer form was long lived, with a lifetime of ca. 5 ns in all solvents (Table 2.1), and could be measured more precisely with a nanosecond TCSPC apparatus. The combination of efficient formation and relatively long lifetime led to a remarkably high yield of the Stokes-shifted K luminescence (ϕ_{Fl} ca. 0.4 in TOL and ϕ_{Fl} ca. 0.2 in MeOH) with promising perspectives for its application.
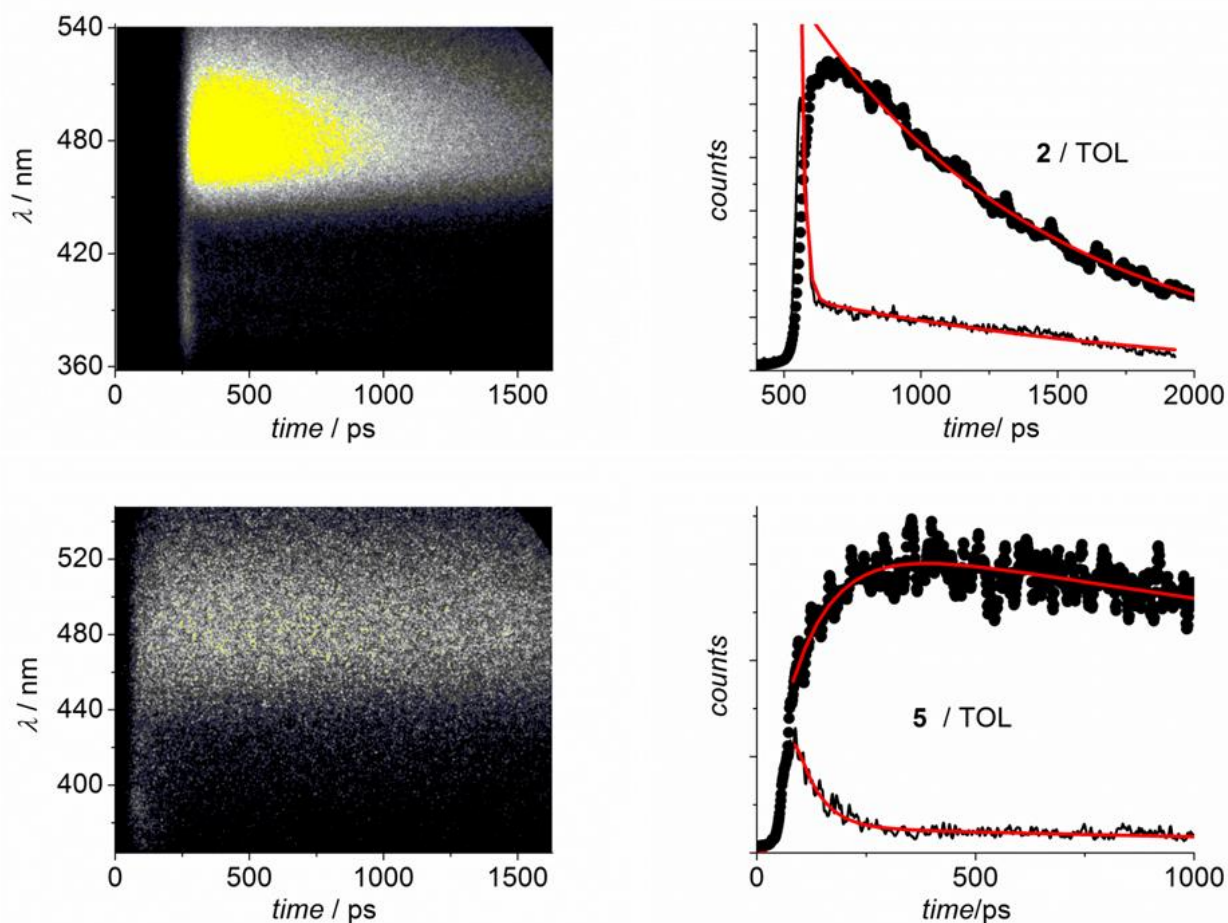
Figure 2.2. Streak camera images of **2** (upper line) and **5** (bottom line) in TOL at room temperature. The profiles of E and K are shown together with the corresponding fitting. Other data can be found in reference [1].

The photophysical properties of the compounds were studied in rigid matrices of TOL and MeOH at 77 K. In this thesis only the selected compounds (see Chart 2.1) are characterized, whereas the others are described into detail in reference [1]. Prompt and delayed luminescence together with the corresponding lifetimes were measured and the most important parameters for the selected compounds are collected in Table 2.2. Here, the fluorescence and phosphorescence maxima for each model and ESIPT compound are reported together with the lifetimes measured upon excitation at 331 nm by a nanosecond TCSPC apparatus both in E and K emission regions. It should be stressed that, due to the scattering of the solid matrix, the 77 K determinations are prone to larger errors than those at room temperature and the results should be taken with caution. The latter luminescence was measured with the use of a phosphorimeter with a 1 ms delay after excitation with a pulsed lamp, in order to get rid of the strong fluorescence signal.
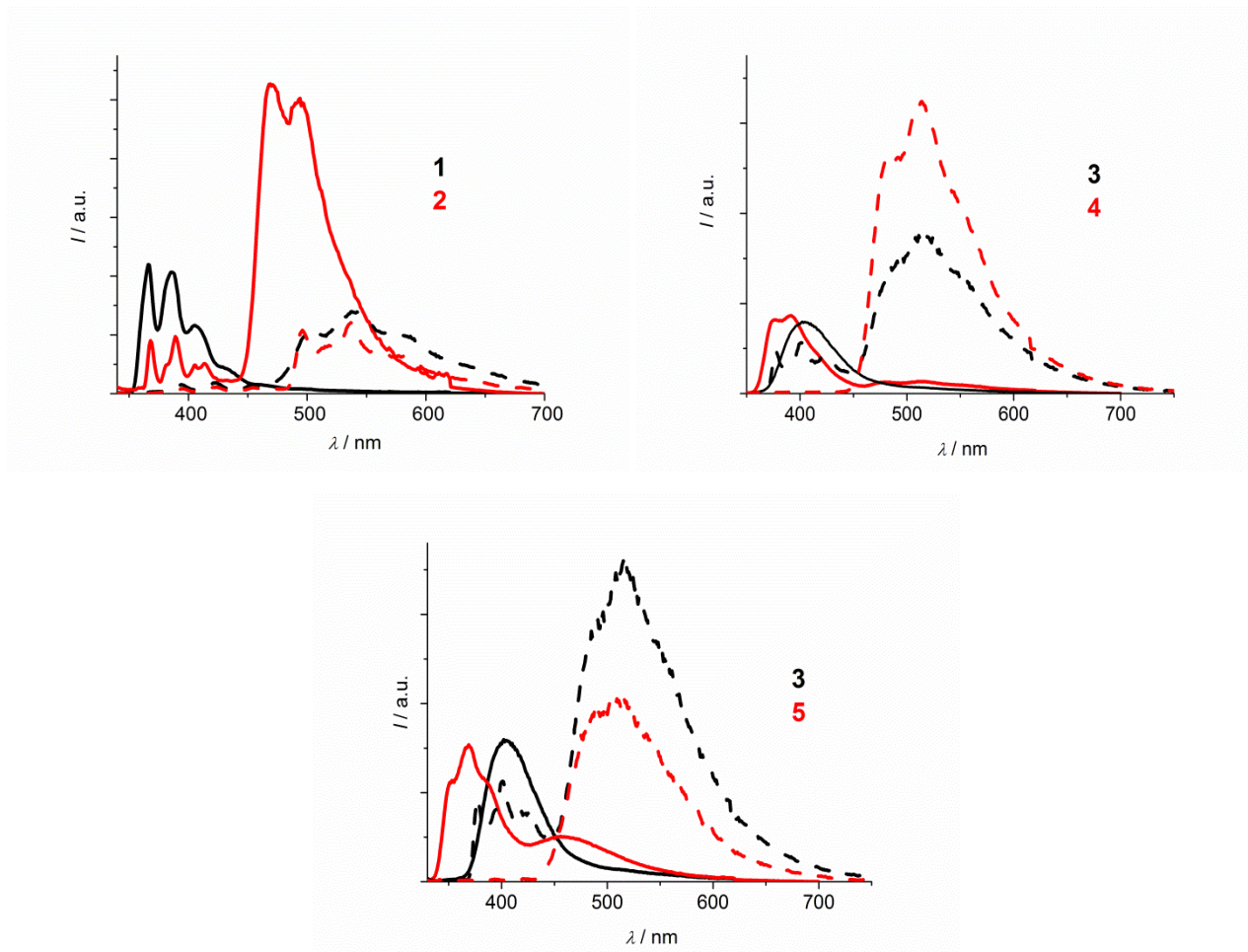
Figure 2.3. Arbitrarily scaled 77 K total luminescence (full line) and arbitrarily scaled delayed luminescence (dashed line) for model compounds (black) and corresponding ESIPT samples (red) in TOL. Other data can be found in reference [1].

The energy levels were calculated from the highest energy emission maxima. Those of E singlet excited states were well above 3 eV, whereas the corresponding triplet was 0.5-0.9 eV lower, a rather large energy gap (Table 2.2). The energy level of the excited singlet K form was very close, within 0.1-0.2 eV, to the triplet energy level of E form. No K phosphorescence was detected in the explored wavelength range. The fluorescence lifetimes of E at 77 K displayed, in most cases, a modest increase with respect to those at room temperature, showing that E→K tautomerism is a modestly activated process. A similar, unimportant increase in the lifetime was registered in several cases for K form. Accordingly, the relative emission of K to E forms was roughly similar for **2** and **4**, with respect to those at room temperature (see above), whereas very poor K emission was detected for **5** in the glass, indicating for the latter a thermally activated E→K process. It should be noted that the delayed emission spectrum not only shows the phosphorescence bands of the sample, but there is evidence of delayed fluorescence (Figure 2.3). Given the large excited singlet–triplet splitting in these molecules, as commented above, we consider this delayed

fluorescence as deriving from triplet-triplet processes (p-type delayed fluorescence). In agreement with this mechanism, the measured lifetime of delayed fluorescence was approximately half of that of phosphorescence.[17] It might be recalled that in a sample structurally similar to **5**, e-type (thermally activated) delayed fluorescence has been reported in air purged chloroform matrices.[18] In that case, the process was likely due to extremely low singlet-triplet splitting, on the order of 0.08 eV.

Table 2.2. Luminescence properties of the samples in TOL and MeOH at 77 K. K and E form properties for the ESIPT samples are reported in separate lines; fluorescence and phosphorescence data for E form are shown. The non-ESIPT model compounds are in gray cells.

	State	TOL			MeOH		
		λ_{em}/nm	τ/ns	E / eV	λ_{em}/nm	τ/ns	E / eV
1	^{1}1	366; 386; 405	1.7; 3.9	3.38	363; 383; 401	2.1; 4.3	3.41
	^{3}1	504; 539	436×10^6	2.46	498; 535	380×10^6	2.48
2	^{1}E	368; 389; 413	0.2	3.36	364; 384; 406	0.3	3.40
	^{3}E	496; 518; 537	150×10^6	2.50	494; 514; 535	119×10^6	2.51
	^{1}K	469; 494	3.8	2.64	472; 494	4.8	2.62
3	^{1}3	402	5.8	3.08	405	2.7; 8.3	3.06
	^{3}3	488; 516	795×10^6	2.54	507	263×10^6; 1.04×10^9	2.44
4	^{1}E	377; 392	1.8	3.28	395	2.8	3.13
	^{3}E	484; 514	1.16×10^9	2.56	520	238×10^6; 811×10^6	2.38
	^{1}K	478 [a]	n.d. [a]	2.59	507 [a]	n.d. [a]	2.44
5	^{1}E	353; 369; 385	2.0	3.51	364	2.4	3.40
	^{3}E	487; 509	908×10^6	2.54	508	487×10^6; 1.23×10^9	2.44
	^{1}K	456	5.3	2.71	n.d. [a]	n.d. [a]	-

[a] E phosphorescence overshadows the fluorescence of K form.

To get further insight into the excited state dynamics of these compounds, we performed transient absorption measurements in the nano-millisecond range to detect the presence of intermediates. The absorption spectra registered at the end of an 18 ns laser pulse in air-free solutions of the model compounds and corresponding ESIPT samples in TOL and MeOH solutions are shown in Figure 2.4. Excitation was at 355 nm, except in the case of **5** in MeOH solutions, which displayed a too low absorbance at 355 nm and was therefore excited at 266 nm. The solutions were optically matched and the laser intensity was constant, so that signals from different samples can be directly compared.
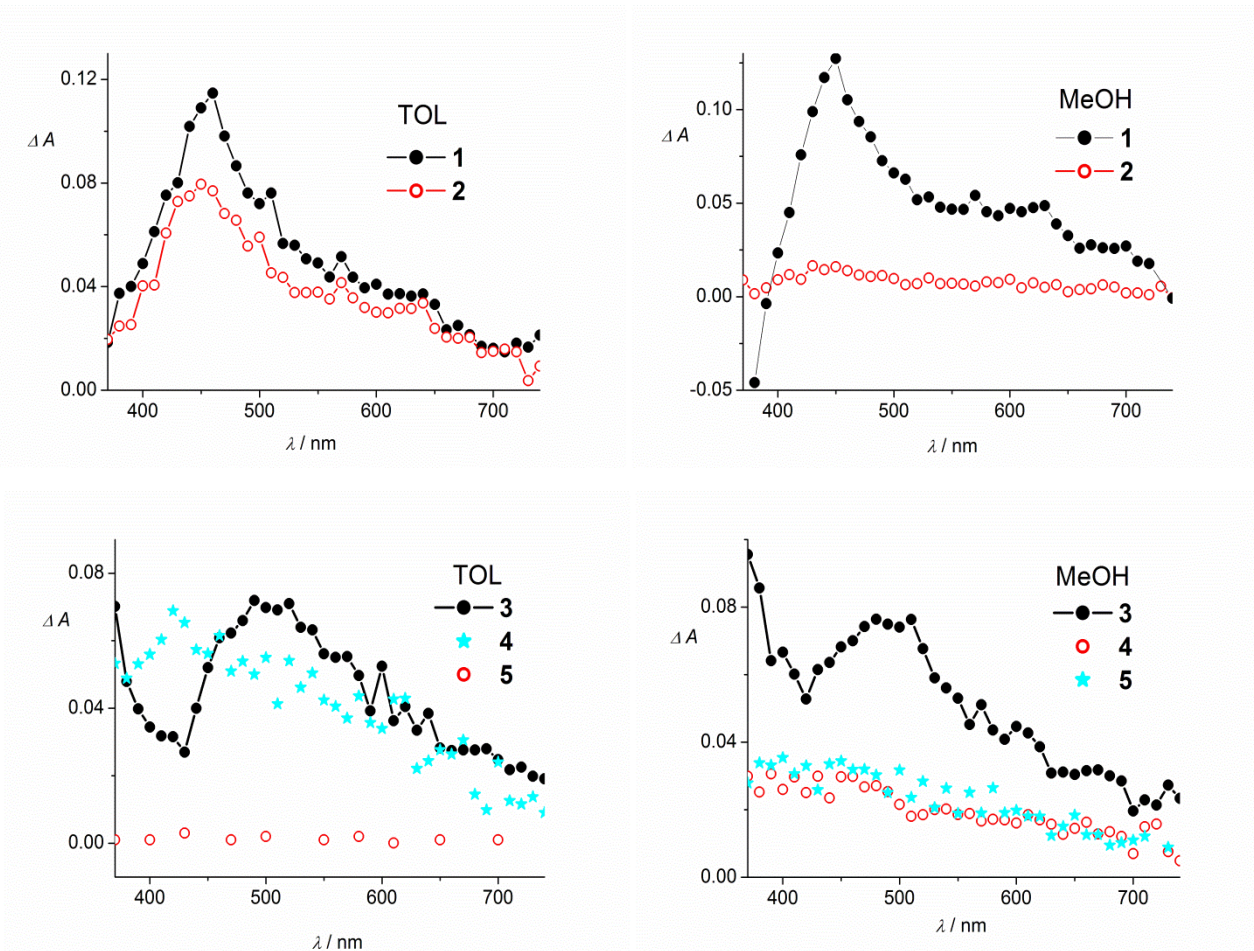
Figure 2.4. End of pulse spectra after excitation of the samples with a 18 ns laser pulse (3 mJ, at 355 or 266 nm) for optically matched solutions with *A*=0.9: models **1** and **3** (full circles) ESIPT samples **2**, **4** (open circles) and **5** (stars). Other data can be found in the reference [1].

The model samples (indicated by full circles) showed an intense band in the range 460-500 nm. The lifetimes were all on the order of tens of microseconds (Table 2.3) and the rates with oxygen were on the order of $2\text{-}4 \times 10^9$ M^{-1} s^{-1} both in TOL and MeOH solutions, typical of the triplet quenching reaction by oxygen.[19] We compared the transient absorbance measured in the ESIPT samples (Figure 2.4) to that measured in the model compounds. We noted that in sample **2** (and model **1**) and sample **4** (and model **3**), the same spectral shapes were obtained and hence we can assume that the same triplet was formed in the two cases. This is true both in TOL and in MeOH, with the only notable difference that the triplet yield in TOL was reduced to 60-70% with respect to that of the model, whereas in MeOH, it was reduced to ca. 10%. What it is remarkable is that there was no strict correlation between the yield of the parent singlet E form and that of the corresponding E triplet. For example, E singlet excited state in **2** compared to model **1** was ca. 0.5% in TOL and 1.5% in MeOH (Table 2.1), numbers quite different from those reported above for the triplet excited states. The behavior of **4** and **5** in TOL compared to the common model **3** were quite different from each other, with a value of almost zero for **4** and a broad band with a maximum at

34

420 nm for **5**. We tentatively ascribe this latter spectrum to the absorption of the triplet state of K form. K singlet was in fact formed in quite remarkable yield in TOL solutions of **5**. The yield of K triplet was lower for **5** in MeOH, where the yield of K form was decreased, to about 50%. **4** in MeOH had a band around 470 nm, similar to that of the model **3** in the same solvent, but with a lower yield, in agreement with the parent singlet excited state yield. The assignment in the case of **4** in MeOH is that of an E triplet due to similarities with the non-ESIPT model compounds.

Table 2.3. Triplet excited state spectral features, lifetimes and reaction rates with oxygen in TOL and MeOH solutions at 295 K.

	TOL			MeOH		
	λ_{max}/nm	τ^a /μs	k_q / $M^{-1}s^{-1}$	λ_{max}/nm	τ^a /μs	k_q / $M^{-1}s^{-1}$
1	460	17.5	2.2×10^9	450	51.4	1.6×10^9
2	450	27.4	1.6×10^9	450	72.7	1.3×10^9
3	500	25.1	2.8×10^9	490	18.9	5.9×10^9
4	n.d.	n.d.	n.d.	470	20.2	1.2×10^9
5	420	65.4	1.9×10^9	430	22.5	1.6×10^9

[a] Air-free solutions.

Two photon absorption. The non-linear optical measurements were performed by using the two-photon excited fluorescence (TPEF) method by the group of Dr. M. Blanchard-Desce. The data are collected in Table 4. Dye **4** had the highest 2PA cross section value (about 100 GM), while compound **2** possessed the lowest value (~5 GM).

Table 2.4. Two-photon absorption (2PA) cross-section of compounds **2**, **4** and **5**. Data measured by the group of Dr. M. Blanchard-Desce.

Compound	Solvent	λ_{2PA}^{max1} (nm)	σ_2^{max1} (GM)
2	$CHCl_3$	710	5
4	$CHCl_3$	<700	>95
5	$CHCl_3$	-	-

2.2.2. Sulphonamido imidazole derivatives

Prompted by the results obtained for the ESIPT derivatives containing a sulphonamido group in the molecule ($\phi_{fl} > 0.4$, τ_{keto} ca. 5 ns), a new small series of imidazole-based derivatives was synthesized by using the same Debus-Radziszewski method.[1b] Chart 2.3 illustrates the structures of the sulfonamide series, including the compound **5** previously reported for comparative purposes.
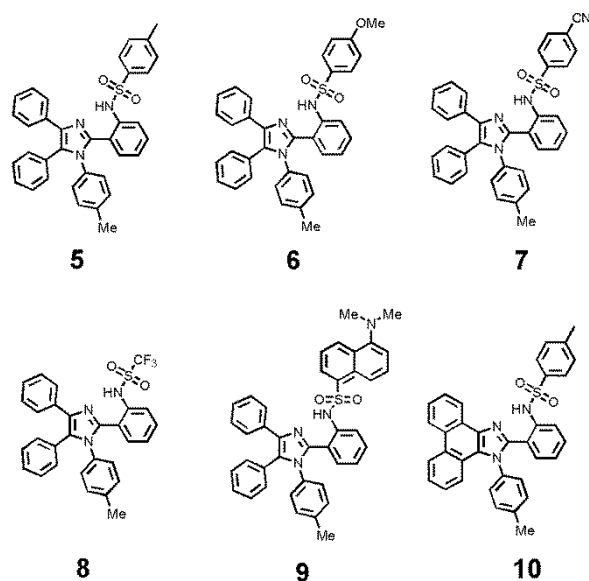
Chart 2.3. Structures of the investigated compounds.

Only the linear optical properties of these compounds were studied. Similar with the series reported above, they were tested in TOL, DCM and MeOH, in order to get information about the ESIPT property in various media. The most important data are collected in Table 2.5. The investigated tetraphenyl imidazoles exhibit similar broad and intense absorption spectra up to 350 nm, and the main band is accompanied by a weaker one up to 400 nm (data not shown). The molar absorption coefficients of the main UV band vary between 14 000 to 20 000 cm^{-1} M^{-1}, typical range for allowed π-π* transitions, and in agreement with other 2-(2'-tosylaminophenyl)benzimidazole derivatives reported in the literature.[10]
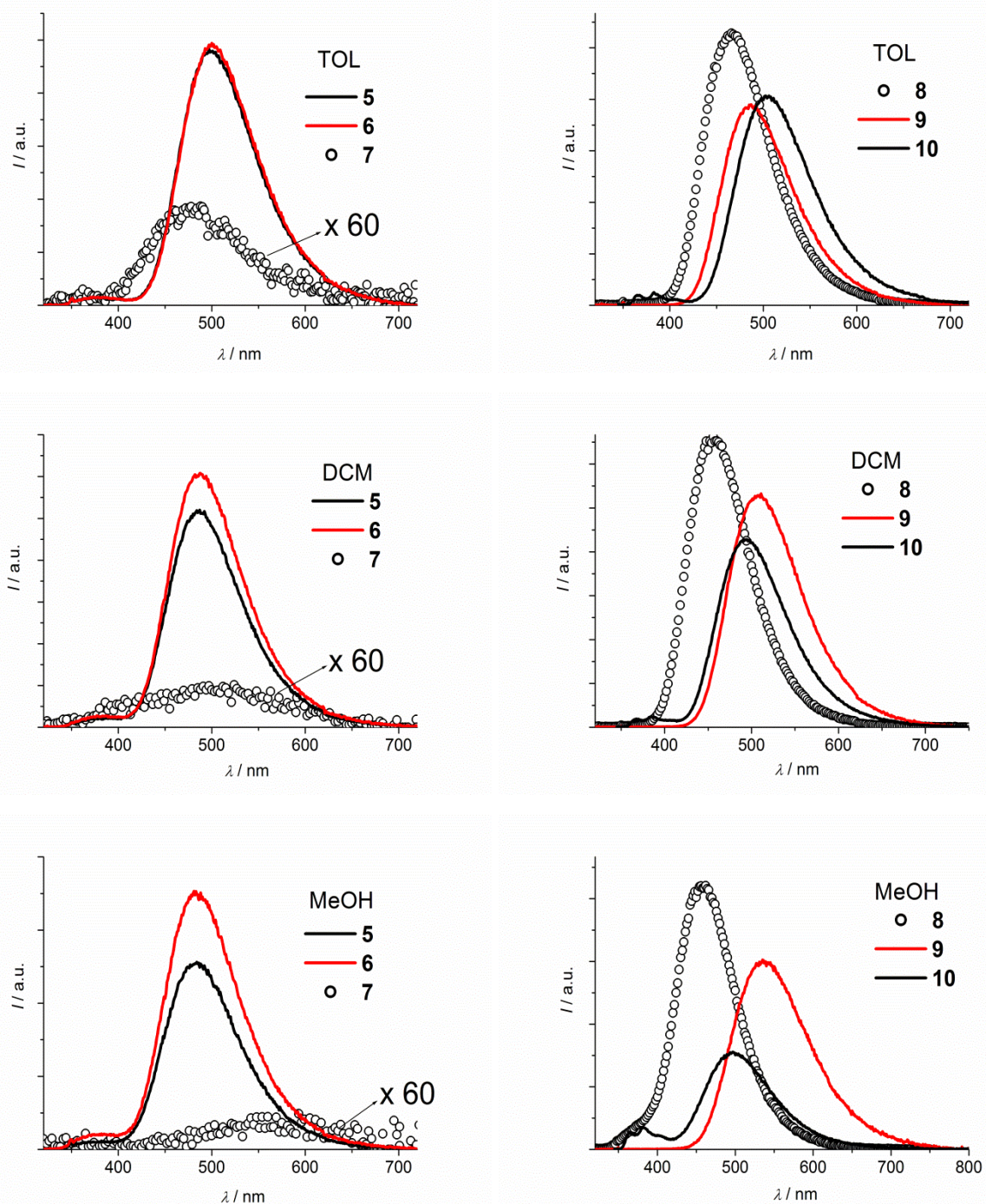
Figure 2.5. Luminescence spectra of optically matched compounds in TOL (first line), DCM (middle line) and MeOH (lower line) at room temperature. Excitation wavelength was 317 nm.

As seen from the Figure 2.5, except for the case of **7** which does not display a satisfactory luminescence, the samples are quite bright and the properties of the K tautomers are in line with those formerly reported for related compounds: emission quantum yields in apolar aprotic solvents of the order of 0.5 with lifetimes of the order of several nanoseconds, from 5 to 11 ns (Table 2.5).[10a, b, 12] What is undoubtedly new for these compounds is the detection of the weak E fluorescence and, in several cases, of the resolution of the ESIPT process lifetime which can be as

37

high as 190 ps, rather unusual for an ESIPT process. The reason has perhaps to be ascribed to higher activation energy of the process in NH acids, characterized by a weaker hydrogen bond, as formerly pointed out.[20]

Table 2.5. Photophysical parameters of the studied compounds in TOL, DCM and MeOH at room temperature. The properties of the E and K forms are on different lines. **5** is reported in Table 2.1.

		TOL			DCM			MeOH		
		λ_{em}/ nm	ϕ_{fl}	τ / ns	λ_{em}/nm	ϕ_{fl}	τ / ns	λ_{em}/nm	ϕ_{fl}	τ / ns
6	E	373	0.005	0.06	377	0.006	0.09	380	0.005	0.04
	K	500	0.393	0.06[a]; 5.20	488	0.420	0.08 [a]; 5.98	481	0.238	0.05[a]; 5.40
7	E	368	< 0.001	< 0.01	399	< 0.001	< 0.01	554	< 0.001	0.89
	K	470	0.003	3.46	525	0.002	5.88			
8	E	-	-	-	-	-	-	370	0.008	< 0.01
	K	465	0.561	5.18	456	0.596	5.23	462	0.383	5.57
9	E	–	–	–	–	–	–	–	–	–
	K	487	0.434	11.68	509	0.574	17.24	536	0.343	13.57
10	E	365; 383; 408	0.007	0.15	368; 384; 407	0.011	0.16	364; 381; 404	0.015	0.19
	K	506	0.468	0.14 [a]; 4.25	495	0.515	0.16 [a]; 4.86	497	0.171	0.16[a]; 2.39

[a] Rise.

77 K determinations in matrices of TOL and MeOH were performed. Both prompt and delayed luminescence spectra were acquired. Lifetimes of the various components were also measured and they are given in Table 2.6. Similar with the results reported above for the first series, delayed luminescence ascribed to E form was recorded for the samples, whereas no K phosphorescence was detected in the experimental window. The fluorescence lifetimes were longer than the ones at room temperature, and the biexponential lifetimes present in some cases (Table 2.6) were assigned to the aggregates formed by lowering the temperature. The phosphorescence lifetimes were $(0.2 - 2.7) \times 10^9$ sec.

Table 2.6. Luminescence parameters in TOL and MeOH at 77 K. **5** is reported in Table 2.2.

	State	TOL λ_{em}/nm	TOL τ/ns	TOL E / eV	MeOH λ_{em}/nm	MeOH τ/ns	MeOH E / eV
6	^{1}E	352; 369; 388	1.9	3.52	349; 365; 385	2.2	3.55
	^{3}E	512; 538	0.4×10^9; 1.3×10^9	2.42	511	0.8×10^9	2.42
	^{1}K	462	5.2	2.68	491	0.7 ; 6.3	2.52
7	^{1}E	434	-	2.85	-	-	-
	^{3}E	479; 503	1.3×10^9	2.58	506	0.9×10^9	2.45
	^{1}K	490	9.9	2.53	493	1.3 ; 15.4	2.51
8	^{1}E	355; 364	1.4	3.49	-	-	-
	^{3}E	472; 500	1.2×10^9	2.62	462; 490	0.2×10^9; 0.7×10^9	2.68
	^{1}K	423	3.2	2.93	409	1.5 ; 4.5	3.03
9	^{1}E	395; 423; 453[b]	-	3.14	-	-	-
	^{3}E	532	0.5×10^9	2.33	566	0.4×10^9	2.19
	^{1}K	472	14.4	2.62	476	19.5	2.60
10	^{1}E	361; 381; 403	4.2	3.43	359; 377; 396	6.6	3.45
	^{3}E	469; 503; 539; 590	1.7×10^9	2.64	439; 468; 499; 537	2.7×10^9	2.82
	^{1}K	-	-	-	-	-	-
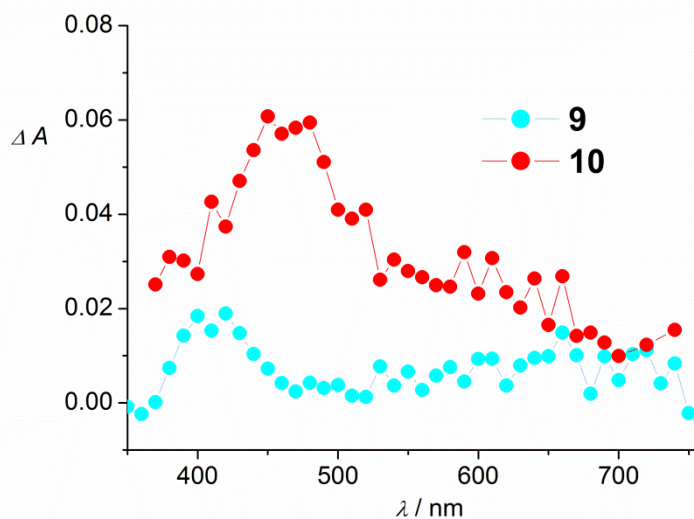
Figure 2.6. Transient absorption spectra of **9** and **10** with 18 ns laser pulse (355 or 266 nm, 3 mJ) for DCM solutions with $A = 0.7$ at the excitation wavelength. Other data can be found in reference [1b].

As concluded above, the transient spectrum of the E triplet displayed a broad absorption band around 460-500 nm. On the contrary, a much weaker transient absorption band detected in some samples around 420 nm and below was tentatively ascribed to the K triplet. DCM and MeOH solutions of the samples were probed at room temperature by nanosecond flash photolysis.

Transient absorption spectra of **9** and **10** in optically matched DCM solutions are shown in Figure 2.6. Except for compound **7**, for which no transient was identified, all the others showed E or K triplet absorption (Figure 2.6). The triplet lifetimes were of tens of microseconds, and the reaction rates with oxygen of 10^9 $M^{-1}cm^{-1}$.

2.3. Conclusions

Photophysical properties of two series of imidazole based derivatives displaying ESIPT were studied. These were compared with those of the reference samples where the possibility of ESIPT occurrence was blocked. The excited state dynamics of the samples displaying ESIPT were fully elucidated. The emission quantum yields of the sulfonamide series, range from 0.4 to 0.6 in aprotic solvents and the Stokes shift is tuned over a large range from 6000 to 15 000 cm^{-1} allowing a control of the emission wavelength from 460 to 560 nm. The tautomerization reaction in the singlet excited state showed variable lifetimes from less than 10 ps to a value on the order of few hundred picoseconds; the lifetime of the singlet excited K form varied from less than one hundred picoseconds to several nanoseconds at room temperature. Luminescence experiments at 77 K permitted us to derive phosphorescence spectra of the E form and to determine the relevant lifetimes in the millisecond-second range. The triplet absorption features assigned to the E (with broad maxima between 450 and 520 nm) and the K forms (with a less intense peaks at about 420 nm) were identified.

These results are not only of theoretical significance in that they provide new insight into factors influencing the photophysics of ESIPT-capable molecules, but they may also open the door to practical applications. Structurally accessible imidazole derivatives can serve as ideal platforms to design more complex systems based on the N---NHSO$_2$ proton cycle in the excited state.

2.4. References

[1]   a) K. Skonieczny, A. I. Ciuciu, E. Nichols, V. Hugues, M. Blanchard-Desce, L. Flamigni, D. T. Gryko, *J. Mat. Chem.* **2012**, *22*, 20649-20664; b) A. I. Ciuciu, L. Flamigni, K. Skonieczny, D. T. Gryko, *Phys. Chem. Chem. Phys.* **2013**, *15*, 16907-16916; c) A. I. Ciuciu, K. Skonieczny, D. Koszelewski, D. T. Gryko, L. Flamigni, *J. Phys. Chem. C* **2013**, *117*, 791-803.

[2]   a) M. R. Grimmet, *Comprehensive Heterocyclic Chemistry, Vol. 5*, ed. A. R. Katritzky and C. W. Rees, Pergamon, **1984**; b) M. R. Grimmet, *Comprehensive Heterocyclic Chemistry II, Vol. 3*, ed. A. R. Katritzky, C. W. Rees and E. F. V. Scriven, Pergamon, New York, **1996**; c) P. Molina, A. Tarraga, F. Oton, *Org. Biomol. Chem.* **2012**, *10*, 1711-1724.

[3]   a) A. Douhal, F. Lahmani, A. H. Zewail, *Chem. Phys.* **1996**, *207*, 477-498; b) C. Fang, R. R. Frontiera, R. Tran, R. A. Mathies, *Nature* **2009**, *462*, 200-U274; c) J. E. Kwon, S. Y. Park, *Adv. Mat.* **2011**, *23*, 3615-3642.

[4]   a) A. D. Roshal, A. V. Grigorovich, A. O. Doroshenko, V. G. Pivovarenko, *J. Phys. Chem. A* **1998**, *102*, 5907; b) J. S. Kim, D. T. Quang, *Chem. Rev.* **2007**, *107*, 3780; c) D. A. Svechkarev, G. V. Karpushina, L. L. Lukatskaya, A. O. Doroshenko, *Cent. Eur. J. Chem.* **2008**, *6*, 443–449; d) S. M. Landge, K. Tkatchouk, D. Benitez, D. A. Lanfranchi, M. Elhabiri, W. A. G. III, I. Aprahamian, *J. Am. Chem. Soc.* **2011**, *133*, 9812; e) B. Wang, V. Eric, E. V. Anslyn, *Chemosensors: Principles, Strategies, and Applications*, Wiley, **2011**.

[5]   a) A. Mordzinski, A. Grabowska, W. Kuhnle, A. Krowczynski, *Chem. Phys. Lett.* **1983**, *101*, 291; b) W. Frey, F. Laermer, T. Elsaesser, *J. Phys. Chem.* **1991**, *95*, 10391; c) K. Das, N. Sarkar, D. Majumda, K. Bhattacharyya, *Chem. Phys. Lett.* **1992**, *198*, 443; d) M. Fores, M. Duran, M. Sola, L. Adamowicz, *J. Phys. Chem. A* **1999**, *103*, 4413; e) M. Rini, J. Dreyer, E. T. J. Nibbering, T. Elsaesser, *Chem. Phys. Lett.* **2003**, *374*, 13; f) H. Wang, H. Zhang, O. K. Abou-Zied, F. E. R. C. Yu, M. Glasbeek, *Chem. Phys. Lett.* **2003**, *367*, 599; g) Y. Pang, W. Chen, *Hydrogen Bonding and Transfer in the Excited State, Vol. 2*, ed. K.-L. Han and G.-J. Zhao, Wiley, Chichester, **2011**; h) W. Chen, E. B. Twum, L. Li, B. D. Wright, P. L. Rinaldi, Y. Pang, *J. Org. Chem.* **2012**, *77*, 285–290.

[6]   a) K. Ding, S. J. Courtney, A. J. Strandjord, S. Flom, D. Friedrich, P. F. Barbara, *J. Phys. Chem.* **1983**, *87*, 1184–1188; b) S. R. Grando, C. M. Pessoa, M. R. Gallas, T. M. H. Costa, F. S. Rodembusch, E. V. Benvenutti, *Langmuir* **2009**, *25*, 13219; c) D. Yao, S. Zhao, J. Guo, Z. Zhang, H. Zhang, Y. Liu, Y. Wang, *J. Mater. Chem.* **2011**, *21*, 3568.

[7]   R. G. Harvey, *Polycyclic Aromatic Compounds*, Wiley, New York, **1997**.

[8]   A. H. Cook, D. H. Jones, *J. Chem. Soc.* **1941**, 278–282.

[9]   A. I. Shienok, L. S. Koltsova, N. L. Zaichenko, V. S. Marevtsev, *Russ. Chem. Bull.* **2002**, *51*, 2050.

[10]   a) C. J. Fahrni, M. M. Henary, D. G. VanDerveer, *J. Phys. Chem. A* **2002**, *106*, 7655-7663; b) M. M. Henary, Y. Wu, J. Cody, S. Sumalekshmy, J. Li, S. Mandal, C. J. Fahrni, *J. Org. Chem.* **2007**, *72*, 4784–4797; c) Y. Wu, P. V. Lawson, M. M. Henary, K. Schmidt, J. L. Bredas, C. J. Fahrni, *J. Phys. Chem. A* **2007**, *111*, 4584–4595.

[11]   a) M. M. Henary, Y. Wu, C. J. Fahrni, *Chem. Eur. J.* **2004**, *10*, 3015–3025; b) Y. M. Chung, B. Raman, D.-S. Kim, K. H. Ahn, *Chem. Commun.* **2006**, 186–188.

[12]   a) C.-H. Chui, Q. Wang, W.-C. Chow, M. C.-W. Yuen, K.-L. Wong, W.-M. Kwok, G. Y.-M. Cheng, R. S.-M. Wong, S.-W. Tong, K.-W. Chan, F.-Y. Lau, P. B.-S. Lai, K.-H. Lam, E. Fabbri, X.-M. Tao, R. Gambari, W.-Y. Wong, *Chem. Commun.* **2010**, *46*, 3538–3540; b) M. K. Nayak, *J. Photochem. Photobiol. A* **2012**, *241*, 26–37.

[13]   Y. Wu, X. Peng, J. Fan, S. Gao, M. Tian, J. Zhao, S. Sun, *J. Org. Chem.* **2007**, *72*, 62-70.

[14]   a) O. K. Abou-Zied, R. Jimenez, E. H. Z. Thompson, D. P. Millar, F. E. Romesberg, *J. Phys. Chem. A* **2002**, *106*, 3665-3672; b) S. R. Vazquez, M. C. R. Rodriguez, M. Mosquera, F. Rodriguez-Prieto, *J. Phys. Chem. A* **2008**, *112*, 376-387.

[15]   C. H. Kim, D. W. Chang, S. Kim, S. Y. Park, J. Taiha, *Chem. Phys. Lett.* **2008**, *450*, 302−307.

[16]   J. W. Moore, R. G. Pearson, in *Kinetics and Mechanism. A Study of Homogeneous Chemical Reactions Third Edition*, Wiley-Intersience, **1981**, pp. 290-296.

[17]   a) C. A. Parker, in *Photoluminescence of Solutions*, Elsevier Publishing Company, Amsterdam, **1968**, pp. 97-125; b) J. B. Birks, in *Photophysics of Aromatic Molecules*, Wiley-Interscience, London, **1970**.

[18]   S. Park, O.-H. Kwon, Y.-S. Lee, D.-J. Jang, S. Y. Park, *J. Phys. Chem. A* **2007**, *111*, 9649-9653.

[19]   S. L. Murov, I. Carmichael, G. L. Hug, in *Handbook of Photochemistry*, 2 ed., ed. Marcel Dekker Inc., New York, **1993**, pp. 289-293.

[20]   M. N. Khimich, L. D. Popov, A. S. Burlov, B. M. Uzhinov, *J. Fluoresc.* **2012**, *22*, 1095–1100.

3. Imidazo[1,2-*a*]pyridine derivatives for bioimaging

In the present chapter the linear optical properties of novel synthesized imidazo[1,2-*a*]pyridine derivatives are detailed. The reason of choosing this class of compounds as potential fluorophores for bioimaging, relies on the fact that their photophysical properties could be very interesting and at the same time, their 2PA properties were unknown. The compounds were synthesized by the group of Dr. Daniel T. Gryko, whereas the non-linear optical properties were measured by the group of Dr. Mireille Blanchard-Desce.

The first part of the work describes a series of imidazo[1,2-*a*]pyridine monomer molecules by varying mainly the substituents, but in some cases also their position on the scaffold. The idea was to identify the substituent capable of tuning the luminescence properties and further, to imply the substituted molecule in the construction of quadrupolar systems (Donor-Acceptor-Donor). Starting from the simple molecule, bis-imidazo[1,2-*a*]pyridines (D-A-D) linked at C5 (at pyridine ring) were constructed in order to increase the 2PA cross-sections. The second part of the work is focused on the photophysical study of another series of bis-imidazo[1,2-*a*]pyridines with linkage at C3 (at imidazole ring). The properties of the dimeric quadrupolar structures were studied by comparison with the corresponding imidazo[1,2-*a*]pyridine monomer.[1] The aim of the work was to identify the structure property relationship, in view of using these compounds for two photon excited fluorescence microscopy.

3.1. Introduction

Imidazo[1,2-*a*]pyridines have attracted attention due to their biological activity[2] and have been intensively investigated since the beginning of the last century.[3] It is already known that imidazo[1,2-*a*]pyridines display, in general, very good luminescent properties (ϕ_{fl} ca. 0.5-0.8)[4] in solution. Enhancing the fluorescence properties of imidazo[1,2-*a*]pyridines both in terms of emission quantum yield and of Stokes shift as well as tuning their emission wavelength is important not only for application in fluorescence microscopy, but also for optical materials. Therefore, we explored the possibility of exploiting different substitution pattern on the imidazo[1,2-*a*]pyridine scaffold. Several studies on imidazo[1,2-*a*]pyridines take advantage of the excited state intramolecular proton transfer (ESIPT)[4-5] process, both in solutions and in the solid state.[6] In

other cases interesting luminescence properties of new imidazo[1,2-*a*]pyridine derivatives were presented, however quantitative data on fluorescence quantum yields were not reported.[7]

Experimental studies made on series of imidazo[1,2-*a*]pyridines showed that the fluorescence quantum yield can be considerably increased to ca. 0.8 by substitution at C2 by naphthyl or phenyl derivatives.[4, 8] Currently, successful results involving imidazo[1,2-*a*]pyridines in terms of luminescence properties, particularly in polar solvents, are limited. A recent report based on combinatorial synthesis and screening showed that derivative of imidazo[1,2-*a*]pyridine drug, Zolpidem, can lead to luminescence quantum yields from $\phi_{fl} = 0.11$ to $\phi_{fl} = 0.89$ in dimethylsulphoxide solutions.[9]

The advantage of using this drug-like scaffold for the design of fluorescence probes for in vivo imaging is that these molecules can potentially retain their molecular recognition ability and, as such, be used as specific probes targeting biologically relevant dedicated sites.

The aim of the work was to increase both ϕ_{fl} and σ_2 in quadrupolar systems based on differently substituted imidazo[1,2-*a*]pyridines. We report in this chapter the optical properties of a series of imidazo[1,2-*a*]pyridine monomers together with more complex bis-imidazo[1,2-*a*]pyridines having the dimerization linkage at different positions.

3.2. Results and discussion

3.2.1. Bis-imidazo[1,2-*a*]pyridines dimerized at C5

As mentioned in the introduction part, the photophysical properties of the imidazopyridine derivatives are influenced by the position and the type of the substituent. Since we are interested in systems with high luminescence quantum yield for bioimaging, we have constructed a consistent library of monomers and dimers, all differently substituted, and the several representative structures are described in this chapter (Chart 3.1). All the others together with the details about synthetic procedure (via Gevorgyan method) are found in reference [1]. As can be noticed from Chart 3.1., the selected compounds display some differences in their molecular structure and they will be pointed out along the discussion.
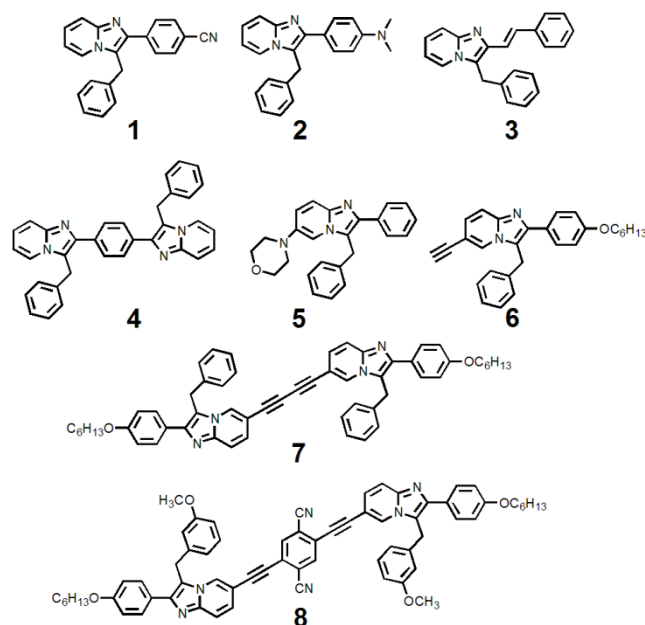
Chart 3.1. Structures of the selected compounds.

One photon absorption. In the present study we have measured the linear optical properties of the mentioned compounds in toluene (TOL) and dichloromethane (DCM) solutions, both at room temperature and 77 K. This allowed us to gain some insight on the nature of the emitting states of these samples. The most important parameters are reported in Table 3.1.
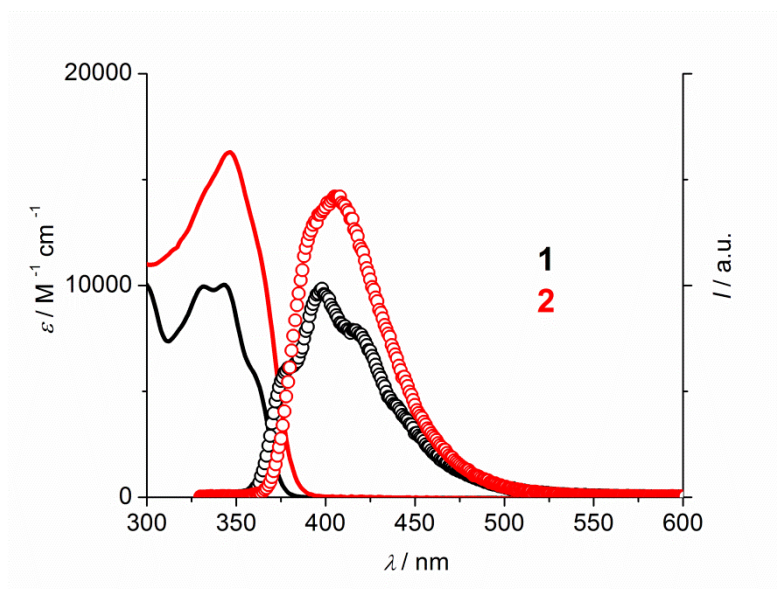
Figure 3.1. Absorption and emission spectra of **1** and **2** in TOL at room temperature. Excitation wavelength was 325 nm for optically matched solutions.

Figure 3.1 displays the absorption and emission spectra of **1** and **2** in TOL. These compounds are characterized by the presence of electron withdrawing cyano (in **1**) and electron

donor dimethylamino group (in **2**) on the phenyl (C2). The absorption and emission spectra of **1** has intense and structured bands, whereas in **2** a bathochromic shift of the order of 20 nm and a smoothing of the spectral structure can be detected. This might be ascribed to the increased strength of the electron releasing group, giving some charge transfer (CT) character to the lowest excited singlet. Moreover, it seems that the presence in the molecule of a strong electron donor in **2** increased its luminescence yield (ϕ_{fl} = 0.56 in TOL and 0.48 in DCM) at least 1.5 times compared to **1** (ϕ_{fl} = 0.37 in TOL and 0.33 in DCM). Luminescence of both samples is slightly affected by the polarity of the solvent (Table 3.1).
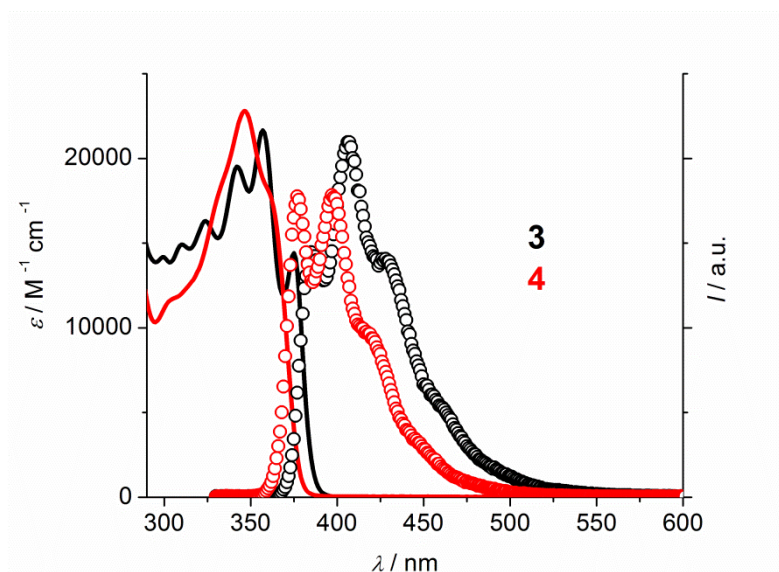
Figure 3.2. Absorption and emission spectra of **3** and **4** in TOL at room temperature. Excitation wavelength was 325 nm for optically matched solutions.

Compounds **3** and **4** are characterized by extended π conjugated systems. Sample **3** possesses a double bond to increase the conjugation length and **4** is a dimer of 3-benzyl-imidazo[1,2-a]pyridine connected by 1,4-phenylene bridge. Noteworthy are the higher molar absorption coefficients and luminescence quantum yields (Table 3.1) of these samples compared to the previous ones. From Figure 3.2 it can be noticed that **3** displays a slight bathochromic shift both in absorption and consistently, in emission. As observed previously for imidazo[1,5-a]pyridines,[10] also in our case the introduction of additional π-systems in the molecules led to increased quantum yield values (ϕ_{fl} = 0.67 in TOL, 0.63 in DCM for **3** and ϕ_{fl} = 0.63 in TOL and 0.68 in DCM for **4**).
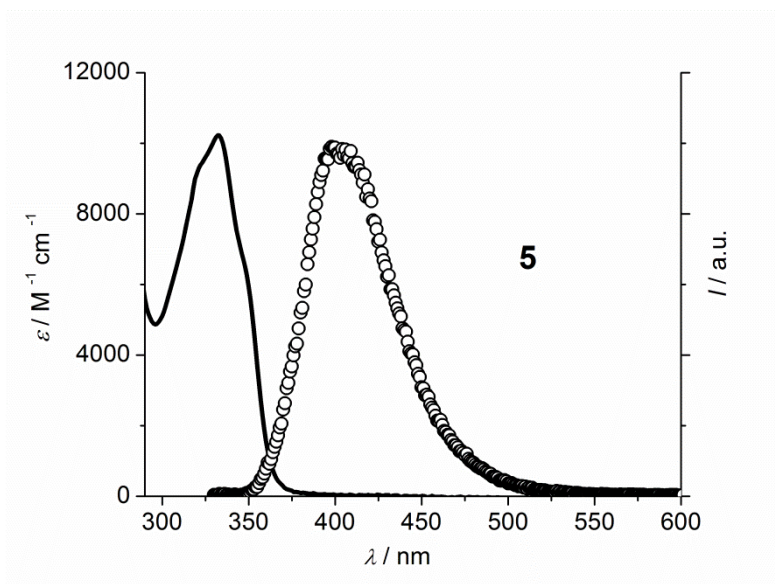
Figure 3.3. Absorption and emission spectra of **5** in TOL at room temperature. Excitation wavelength was 325 nm.

Alternatively to the functionalization at imidazole ring, the substitution at the six-membered ring was considered. In compound **5**, a moderately good electron donor, morpholine,[11] was introduced at position 6 of 3-benzyl-2-phenyl-imidazo[1,2-*a*]pyridine. Morpholine gives a charge transfer character to the lowest excited state, as noticed from the structureless luminescence spectrum from Figure 3.3. The luminescence quantum yield is dramatically decreased compared to previous cases, to $\phi_{fl} = 0.16$ in TOL and even more in DCM (Table 3.1).

Finally, the dimeric structures **7** and **8** with linkage at pyridine ring were investigated in TOL and DCM (Figure 3.4). The two dimers, with linkage at pyridine ring (C5), have a different center: 7 has two ethynyl groups, whereas **8** possesses a more complex diethynyl with the insertion of a 1,4-dicyanobenzene (Chart 3.1). Their photophysical properties are discussed together with the ones of the corresponding monomer model **6.** The molar absorption coefficients of the dimers were considerably higher with respect to the monomer **6** (Figure 3.4), indicating an extended conjugation in the molecule. It is obvious that apart from intensity, compound **7** has an absorption spectrum not so different from that of the model. Dimer **8** displays a different spectrum compared to the other samples. It shows a largely bathochromically shifted absorbance up to 450 nm, as expected from its extended π-conjugation. The luminescence of the dimer **7** is similar to that of **6**, but ca. 20 nm bathochromically shifted. On the contrary, **8** displays a largely shifted luminescence not only with respect to the model, but also with respect to its own absorption spectrum (Figure 3.4 and Table 3.1). The bathochromic shift of **8** increases dramatically in DCM, with ca. 100 nm. This implies that the structures of the emitting state and the ground state are rather different. This might be the case

47

for an emitting state with a strong CT character, given by the strong dicyanobenzene electron acceptor. The luminescence quantum yield in TOL of both **7** and **8,** and monomer, is about $\phi_{fl} = 0.3$. In DCM, whereas **6** and **7** were almost unaffected by the change in the solvent polarity, dimer **8** registered a consistent drop of the luminescence to $\phi_{fl} = 0.06$ (Table 3.1).
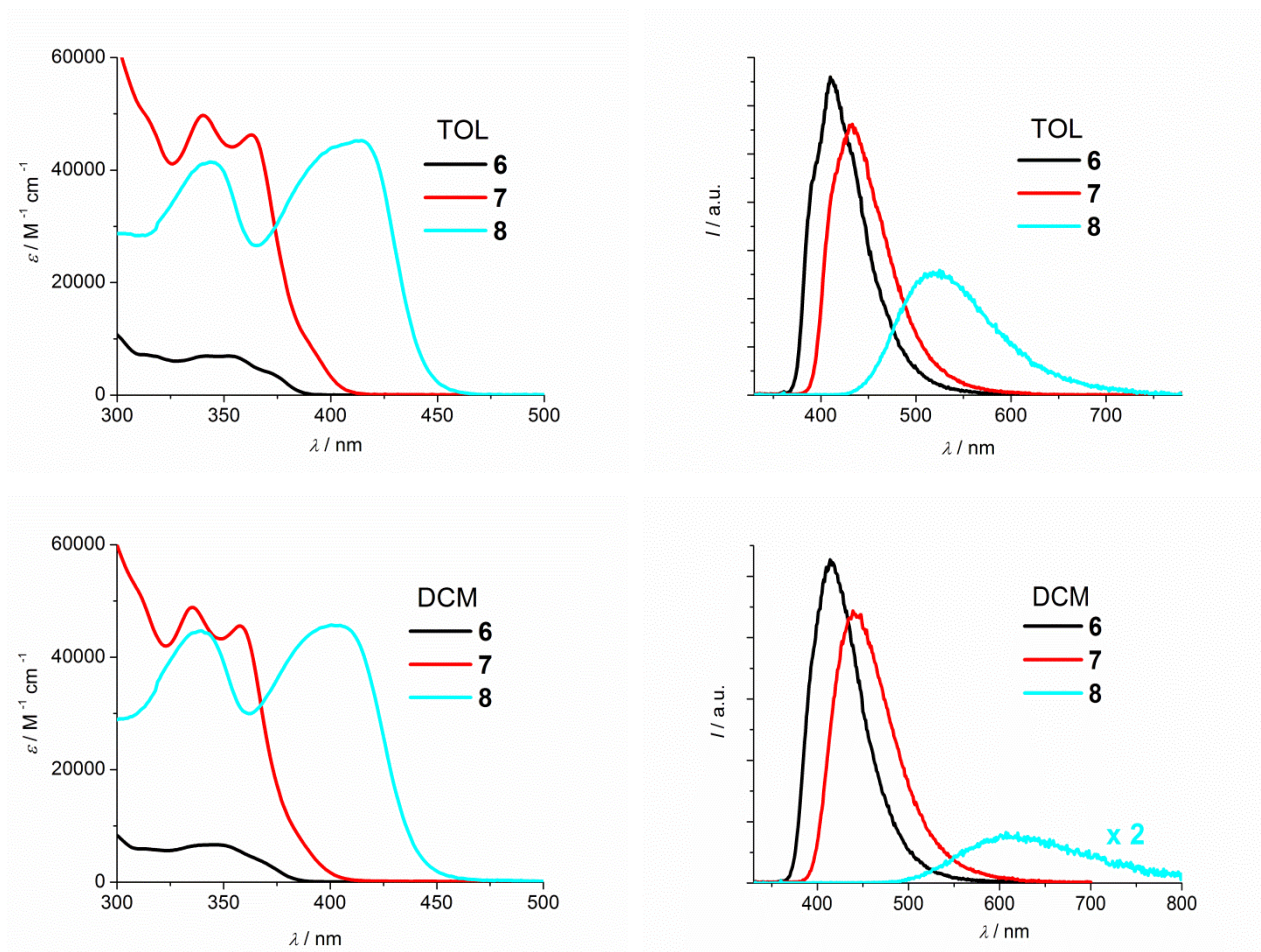
Figure 3.4. Absorption and emission spectra of **6, 7** and **8** in TOL and DCM at room temperature. Excitation wavelength was 325 nm for optically matched solutions.

Time resolved data obtained with a Time Correlated Single Photon Counting (TCSPC) apparatus show lifetimes of $1 - 3$ ns for all the investigated compounds, both in TOL and DCM (Table 3.1). Exception makes the dimer **8** in TOL, for which a longer excited state lifetime of about 11 ns was measured.

Table 3.1. Photophysical parameters of the studied compounds in TOL and DCM solutions at room temperature.

	TOL			DCM		
	λ_{em}^{max}/ nm	ϕ_{fl}	τ/ns	λ_{em}^{max}/ nm	ϕ_{fl}	τ/ns
1	378, 397, 416	0.37	2.87	401, 420	0.33	2.66
2	392, 407	0.56	2.16	429	0.48	2.20
3	385, 406, 428	0.67	2.89	384, 406, 428	0.63	2.98
4	377, 398, 418	0.63	1.99	375, 395, 415	0.68	2.13
5	402	0.16	3.62	417	0.11	3.39
6	390, 410, 434	0.30	3.58	414	0.30	3.23
7	413, 432	0.33	3.82	439	0.30	3.72
8	523	0.33	11.60	622	0.06	3.00

Excitation spectra taken at the emission maxima overlaid perfectly with the corresponding absorption spectra indicating a genuine emission from the lowest excited state and a high purity of the samples (data not shown).[1b]

Luminescence experiments at 77 K on glassy TOL matrices were performed, and the photophysical parameters for the selected compounds are collected in Table 3.2. The prompt luminescence is hipsochromically shifted with respect to that at room temperature by ca. 15 nm in all monomer samples (Tables 3.1 and 3.2). Most of the investigated molecules showed clear structured delayed luminescence[1b] with lifetimes in the milliseconds-seconds range (Table 3.2).

Figure 3.5 shows the prompt luminescence spectra in TOL of the dimers **7** and **8**, and their model **6**. Dimer **7** is bathochromically shifted with respect to **6** but still structured, similar to room temperature data. Differently, **8** shows broad prompt luminescence with a hypsochromic shift of 70 nm with respect to the room temperature luminescence (Table 3.2), and phosphorescence around 600 nm. The lifetimes measured at 77 K are not significantly different from room temperature data (Table 3.2), indicating activationless processes for the deactivation of the emitting state. The bi-exponential lifetime in a few cases is explained by the presence of aggregates formed at low temperatures.
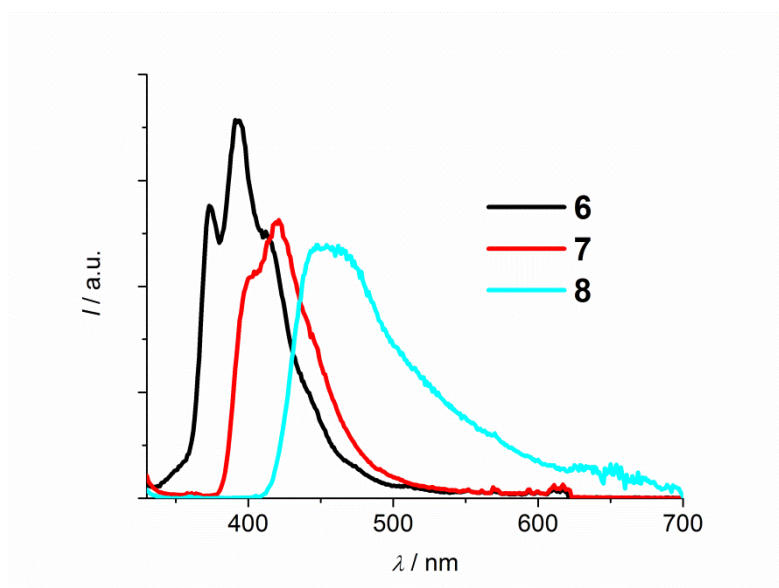
Figure 3.5. Arbitrary scaled luminescence spectra of **6, 7** and **8** in TOL at 77 K. Excitation wavelength was 325 nm.

Table 3.2. Photophysical parameters of the studied compounds in TOL glassy matrices at 77 K.

		77 K		
	State	λ_{em}^{max}/ nm	τ/ns	E/ eV
1	^{1}1	365, 384, 405, 430	2.84	3.39
	^{3}1	468, 501, 540, 584	1.45×10^9	2.65
2	^{1}2	377, 397, 417	1.93	3.28
	^{3}2	464, 497, 536, 575	1.35×10^9	2.68
3	^{1}3	378, 399, 423, 448	2.34	3.29
	^{3}3	540	2.4×10^6; 30×10^6	2.30
4	^{1}4	367, 388, 409	1.48	3.38
	^{3}4	465, 500, 527, 567	1.40×10^9	2.48
5	^{1}5	392	4.47	3.16
	^{3}5	555	89×10^6; 359×10^6	2.23
6	^{1}6	373, 394, 413, 441	3.99	3.32
	^{3}6	475, 511, 553, 602	1.09×10^9	2.61
7	^{1}7	401,421	4.58	3.09
	^{3}7	496, 532, 581	130.5×10^6; 323×10^6	2.50
8	^{1}8	453	4.48 ; 10	2.73
	^{3}8	548, 574, 619	226×10^6	2.16

Two photon absorption. The two photon absorption cross sections measured in the group of Dr. M. Blanchard-Desce are reported in Table 3.3, with the highest value (120 GM) obtained for the dimer **8.** Other details can be found in reference [1b].

Table 3.3. Two-photon absorption data of **1, 4, 6, 7, 8** derived from TPEF measurements[12] in toluene. Data measured by the group of Dr. M. Blanchard-Desce.

	$\lambda_{TPA}{}^{max}$ / nm	$\sigma_2{}^{max}$ / GM
1	≤ 700	≥ 18
4	≤ 700	≥ 16
6	≤ 700	≥ 8.5
7	720	51
8	800	33
	720	120

3.2.2. Bis-imidazo[1,2-*a*]pyridines dimerized at C3

The modest results described above for the first bis-imidazo[1,2-*a*]pyridines synthesized particularly for the use in bioimaging, determined us to approach a new strategy on the same class of compounds. Whereas in the first series the position C3 was blocked and the variation of the substituent was made mainly at C2, in the new series, both C2 and C3 are involved. Moreover, the most important feature of the novel D-A-D systems constructed from the corresponding monomer models is the linkage made at the imidazole ring. These have as centers pyrazine or 1,4-dicyanobenzene rings. Details about the synthesis of the compounds via Ortoleva-King-Chichibabin method can be found in reference [1a], whereas their structures are shown in Chart 3.2.
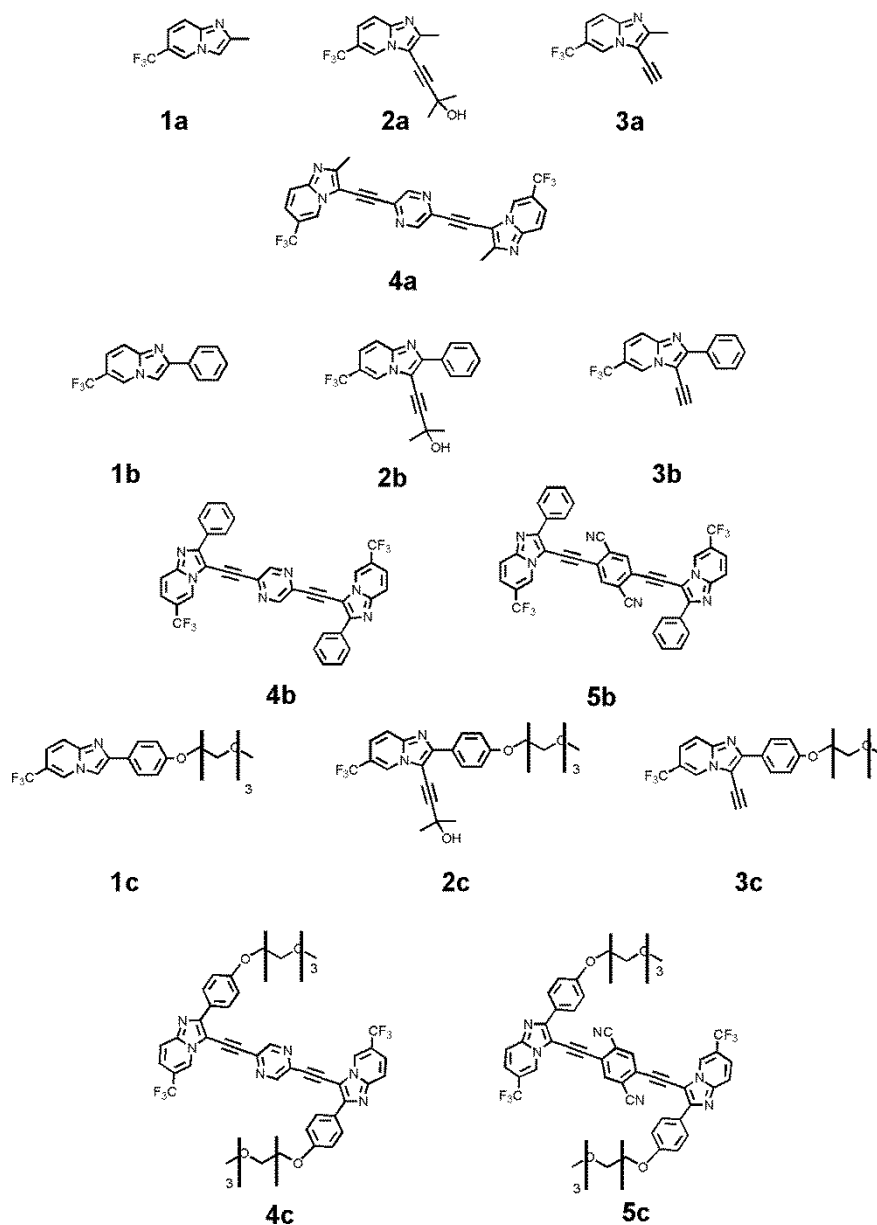
Chart 3.2. Structures of the investigated compounds.

One photon absorption. Photophysical properties of the imidazopyridine dimers were investigated and compared to the ones of the corresponding monomer models. Steady state and time resolved experiments were performed in toluene (TOL) and dichloromethane (DCM), at room temperature (295 K) and 77 K. The most important parameters obtained at 295 K are collected in Table 3.4.
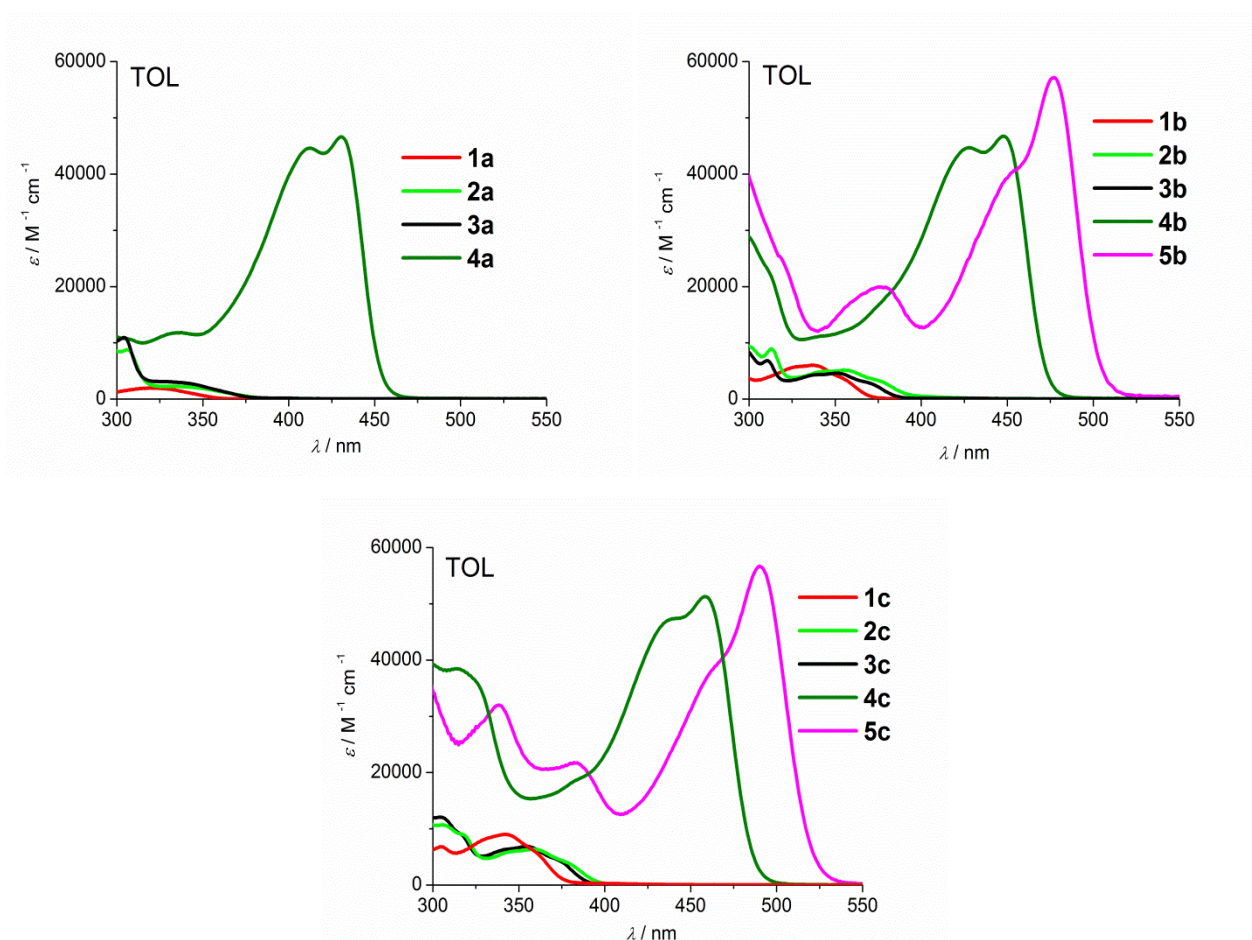
Figure 3.6. Absorption spectra of dimers and monomers in TOL at room temperature.

Figure 3.6. shows the absorption spectra of the dimers together with the corresponding monomer models. The monomers **1a-c** display a single broad band (320-340 nm) and a molar absorption coefficient (ε) increasing upon substitution from ca. 10^3 to ca. 10^4 M^{-1} cm^{-1}. The monomers **2a-c** and **3a-c** have similar absorption features, with a structured band around 300 nm (ε ca. 10 000 M^{-1} cm^{-1}) and a broader one around 340-360 nm (ε ca. 5 000 M^{-1} cm^{-1}). The absorption spectra of the dimers are characterized by an intense vibrational band (ε ca. 50 000 M^{-1} cm^{-1}) around 480-490 nm for the 1,4 –dicyano benzene-containing dimers **5b-c** and around 420-460 nm for the ones having a pyrazine bridge, **4a-c**. Sample **5b** raised some solubility problems preventing a careful determination of the molar absorption coefficient. Therefore its absorption spectrum is

normalized in Figure 3.6 to that of the similar compound **5c**. It can be noticed that the absorption spectra of the dimers are entirely different from the superposition of the absorption properties of the component monomers, a clear indication of an extensive electronic delocalization in the quadrupolar structures.
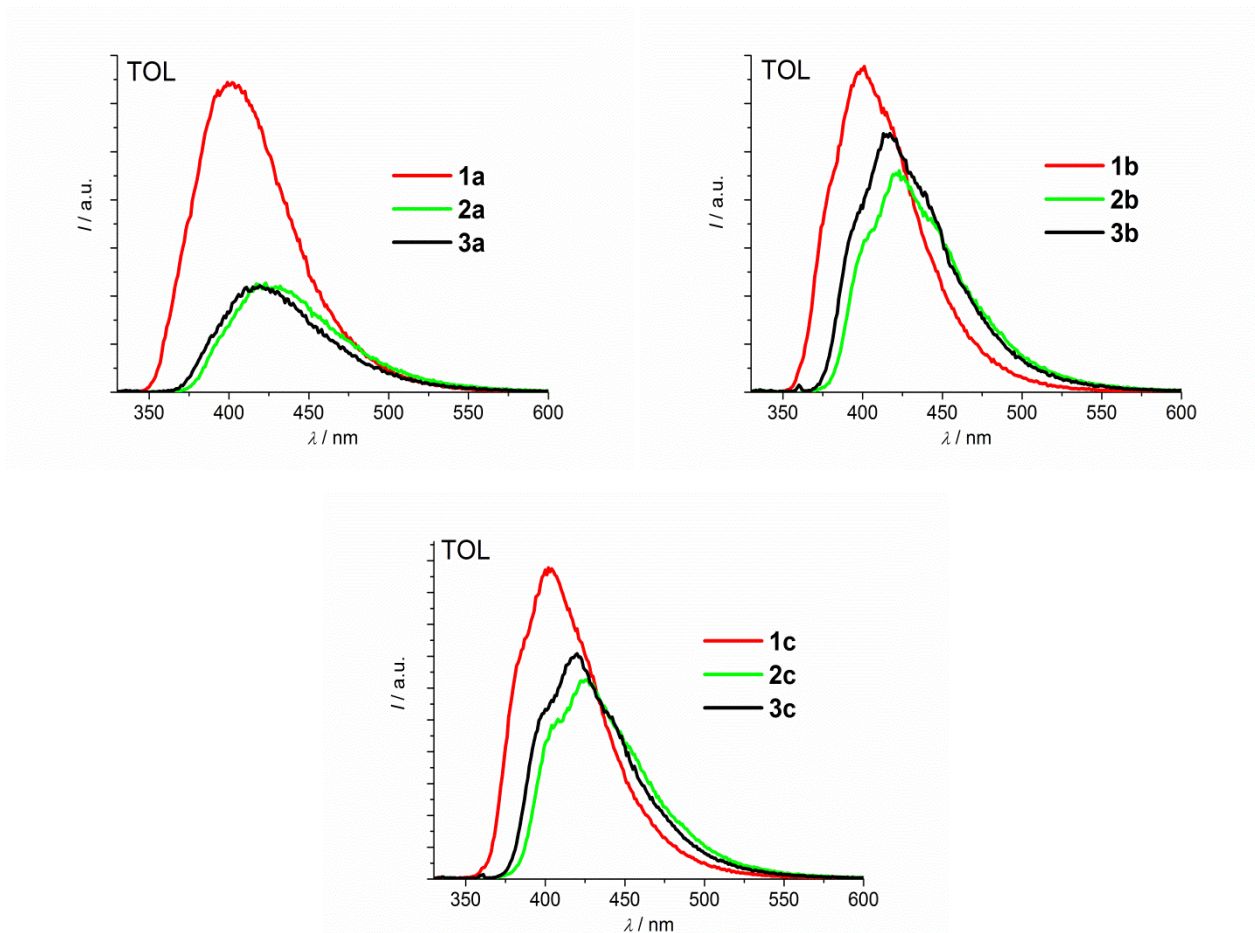
Figure 3.7. Luminescence spectra of the monomers in TOL at room temperature. Excitation wavelength was 325 nm for optically matched solutions.

The emission spectra of the monomers in TOL are presented in Figure 3.7 and their photophysical parameters are reported in Table 3.4. The emission maximizes around 380-420 nm and displays good mirror images of the absorption spectra, being ascribed to the lowest singlet excited state, very likely $\pi-\pi^*$ in nature. From Table 3.4 it can be deduced that the **a** series shows the lowest emission quantum yield (ϕ_{fl} =0.06-0.17) whereas the **c** series the highest one (0.17-0.23). Moreover, within each **a**, **b**, **c** series, the family **1**, exhibited the highest emission yield: 0.17 for **1a**, 0.18 for **1b** and 0.23 for **1c** (Table 3.4). As expected, compounds **2** and **3** of each series, differing only for the presence of a tertiary alcohol at the alkyne substituent, have similar properties. Steady

state data in DCM showed that the emission quantum yield for each dye was independent of the solvent polarity (Table 3.4).[1a]
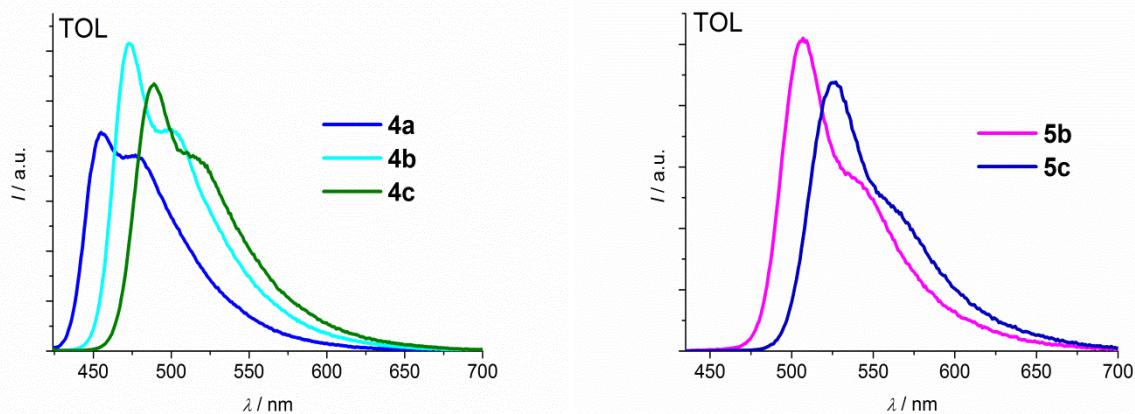
Figure 3.8. Luminescence spectra of the dimers in TOL at room temperature. Excitation wavelength was 424 nm for optically matched solutions.

The luminescence spectra of dimers in TOL are reported in Figure 3.8. The emission of **4a-c** is located around 470-520 nm, whereas of **5b-c** is around 510-570 nm. Also in this case the emission spectra display a good mirror image with the absorption spectra and they are ascribed to the lowest $\pi-\pi^*$ singlet excited state. They have remarkably high emission quantum yields, up to 0.93 in TOL, which decrease in DCM, in general by less than 10%. Only in the case of the less substituted **4a** structure, the drop in emission quantum yield from TOL to DCM is from 0.69 to 0.35 (Table 3.4). In the case of samples **4a-c,** a slight bathochromic shift occurs in more polar solvents, a confirmation of some charge transfer character. An increased conjugation in the other bis-imidazo[1,2-*a*]pyridines **5b-c** stabilizes the $\pi-\pi*$ excited state and weakens the CT character, making their luminescence less affected by the solvent polarity (Table 3.4). Within the same solvent, a bathochromic shift by increasing substitution from series **a** to **b** and **c** can be noticed.

Fluorescence lifetimes of 1-3 ns were determined for the entire library of compounds (with the exception of sample **1a** which has a $\tau > 6$ ns) and found to be independent of solvent polarity (Table 3.4). The measured lifetimes are in agreement with those of similar imidazole-based monomer compounds reported in the literature.[1b, 6d, 13]

Excitation spectra measured on the emission maxima of both monomers and bis-imidazo[1,2-*a*]pyridines overlay perfectly the corresponding absorption spectra, indicating a genuine emission from the lowest excited state and the absence of contaminants.[1a]

Table 3.4. Photophysical parameters of the investigated compounds in TOL and DCM at room temperature. Monomers are in grey cells.

	TOL			DCM		
	λ_{em}^{max}/nm	ϕ_{fl}	τ/ns	λ_{em}^{max}/nm	ϕ_{fl}	τ/ns
1a	402	0.17	6.33	400	0.20	6.56
2a	423	0.06	3.20	422	0.07	3.16
3a	419	0.06	2.91	418	0.07	2.80
4a	455; 477	0.69	1.38	470; 490	0.35	1.35
1b	379; 401; 416	0.18	2.40	374; 394; 415	0.19	2.15
2b	401; 423; 444	0.13	2.63	400; 420; 442	0.13	2.48
3b	396; 416; 440	0.15	2.86	394; 413; 433	0.15	2.67
4b	473; 500	0.93	1.49	480; 503	0.88	1.81
5b	507; 541	0.92	2.31	507; 540	0.83	2.66
1c	385; 402; 417	0.23	2.24	384; 403; 416	0.24	1.98
2c	408; 426; 448	0.17	2.55	405; 424; 446	0.18	2.41
3c	399; 420; 438	0.19	2.75	398; 419; 436	0.19	2.54
4c	489; 517	0.87	1.73	498; 525	0.82	2.27
5c	525; 562	0.84	2.67	529; 563	0.80	3.25

Steady state and time resolved measurements at 77 K were performed and the parameters are collected in Table 3.5. The prompt luminescence of the monomer imidazo[1,2-a]pyridines is slightly hypsochromically shifted with respect to the one at room temperature. Structured delayed luminescence was recorded between 450 – 650 nm.[1a]
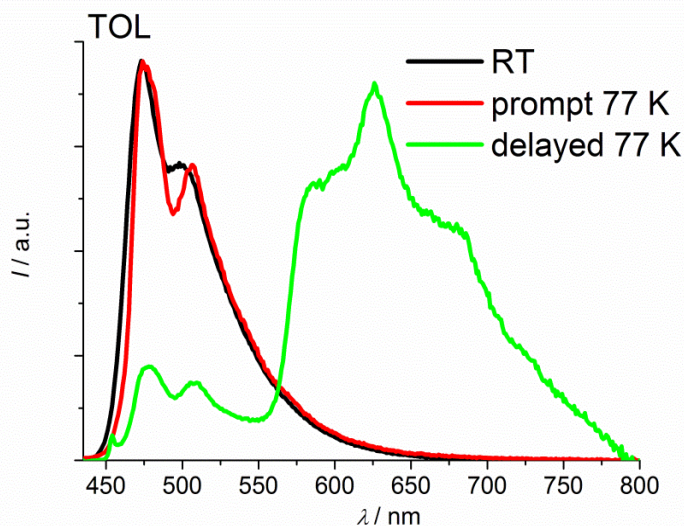
Figure 3.9. Arbitrary scaled RT luminescence in TOL and 77 K total and delayed luminescence of **4b** in TOL with 50% EtI, upon excitation at 424 nm.

As representative for the series it was chosen the dimer **4b** and Figure 3.9 shows its room temperature and 77 K emission spectra. As it can be noticed from Figure 3.9, a fluorescence more resolved than at room temperature or, in some cases, a slightly hypsocromically shifted one was detected at 77 K. As no trace of phosphorescence was detected, we utilized the heavy atom effect (ethyl iodide - EtI), which increases spin-orbit coupling and hence the triplet yield. With the addition of EtI, well-defined structured phosphorescence spectra above 550 nm were recorded for the dimers. Since the presence of EtI not only enhances the excited singlet to excited triplet conversion, but also the excited triplet to ground state singlet conversion, the corresponding triplet lifetimes are not reported in Table 3.5.

Table 3.5. Photophysical parameters of the investigated compounds in TOL at 77 K. Monomers are in grey cells.

	State	λ_{em}^{max}/nm	τ/ns	E/eV
		TOL		
1a	^{1}1a	381	5.50	3.25
	^{3}1a	469; 500; 527	0.98×10^9	2.64
2a	^{1}2a	395; 422; 452	3.61	3.14
	^{3}2a	479; 509; 549	1.08×10^9	2.59
3a	^{1}3a	394	3.10	3.14
	^{3}3a	469; 500; 540	1.31×10^9	2.64
4a	^{1}4a	455; 485	2.36	2.72
	^{3}4a	612; 669	-	2.02
1b	^{1}1b	366; 384; 404	2.58	3.38
	^{3}1b	476; 508; 541	1.02×10^9	2.60
2b	^{1}2b	391; 413; 432	4.08	3.17
	^{3}2b	479; 511; 550	1.09×10^9	2.59
3b	^{1}3b	381; 400; 420	4.27	3.25
	^{3}3b	476; 505; 538	1.29×10^9	2.60
4b	^{1}4b	473; 504	1.42	2.62
	^{3}4b	585; 626; 680	-	2.12
5b	^{1}5b	492; 524	2.30	2.52
	^{3}5b	554; 595; 638	-	2.23
1c	^{1}1c	367; 385; 404	2.31	3.37
	^{3}1c	476; 507; 533	0.85×10^9	2.60
2c	^{1}2c	394; 418; 442	3.40	3.14
	^{3}2c	481; 510; 549	0.96×10^9	2.57
3c	^{1}3c	381; 401; 424	3.65	3.25
	^{3}3c	467; 501; 543	1.11×10^9	2.65
4c	^{1}4c	487; 517	1.70	2.54
	^{3}4c	553; 592; 635	-	2.24
5c	^{1}5c	509; 541	2.60	2.43
	^{3}5c	592; 650; 707	-	2.09

Two photon absorption. The non-linear optical properties are reported in Table 3.6. There can be noticed the high 2PA cross-sections for compounds **5b** and **5c** ($\sigma_2 \geq 800$ GM), which lead to high two photon brightness values (730 GM for **5b** and 640 GM for **5c**).

Table 3.6. Two-photon absorption properties of bis-imidazo[1,2-*a*]pyridines in DCM. Data measured by the group of Dr. M. Blanchard-Desce. [1a]

	$2\lambda_{\mathrm{OPA}}^{\mathrm{max}}$/nm	$\lambda_{\mathrm{TPA}}^{\mathrm{max}}$/nm	σ_2^{max}/GM	$\sigma_2^{\mathrm{max}}\phi_{\mathrm{fl}}$/GM
4a	848	≤700	≥500	>180
4b	880	730	640	560
4c	900 620	750	550	450
5b	942 748	770	880	730
5c	968 762	800	800	640

3.3. Conclusions

The first comprehensive study of optical properties of substituted imidazo[1,2-*a*]pyridines monomers has been performed at room temperature in solutions of different polarity (TOL and DCM) and at 77 K in rigid TOL glass. It proved that it is possible to tune their linear optical properties by changing the substituents at position 2 and/or 3. Their photophysical results were rationalized in terms of substitution pattern. We also reported the luminescence properties of bis-imidazo[1,2-*a*]pyridines by comparing them to the ones of the corresponding monomers.

Most of the investigated monomer imidazo[1,2-*a*]pyridines have shown good luminescence quantum yields, ranging between 0.2 and 0.7, both in toluene and dichloromethane. The highest quantum yields were obtained for the samples substituted by electron donor group at C2 or with increased conjugation at same position. The bis-imidazo[1,2-*a*]pyridines (linked at pyridine ring - position 5) treated in the first part, had modest luminescence yields (ca. 0.3 in TOL) and high solvent polarity dependence for one sample. More interesting, the bis-imidazo[1,2-*a*]pyridines (linked at imidazole ring - position 3) characterized in the second part, displayed very high luminescence, close to unity in some cases. Moreover, the influence of the solvent polarity on the fluorescence properties was modest (<10%) in this case.

Phosphorescence spectra are easily recorded for monomers and dimers linked at pyridine ring in TOL matrix at 77 K. In the case of bis-imidazo[1,2-*a*]pyridines linked at C3, phosphorescence could be observed by adding a heavy-atom solvent. The fluorescence lifetimes are of the order of several nanoseconds, both at room temperature and 77K, whereas phosphorescence lifetimes for monomers are of the order of seconds.

The most important finding is that linking two imidazo[1,2-*a*]pyridine moieties at position 3 offers significant advantages over similar D-A-D architectures linked at position 5. In particular, as both fluorescence quantum yield is 2.5 times higher and σ_2 is ~10 times larger, these quadrupolar compounds show significant two-photon brightness (500-750 GM). Among them, the dye which combines hydrophilic core (pyrazine) and substituents (4-(oligoethyleneglycol)phenyl) holds promise as a new two-photon probe for bioimaging.

3.4. References

[1] a) A. I. Ciuciu, D. Firmansyah, V. Hugues, M. Blanchard-Desce, D. T. Gryko, L. Flamigni, *J. Mater. Chem.* **2014**, DOI:10.1039/C4TC00234B; b) D. Firmansyah, A. I. Ciuciu, V. Hugues, M. Blanchard-Desce, L. Flamigni, D. T. Gryko, *Chem. Asian J.* **2013**, *8*, 1279-1294.

[2] a) J. C. Teulade, G. Grassy, J. P. Girard, J. P. Chapat, M. Simeondebuochberg, *Eur. J. Med. Chem.* **1978**, *13*, 271-276; b) E. Abignente, A. F., E. Luraschi, C. Saturnino, F. Rossi, E. Lampa, M. Cazzola, E. Brandinelli, R. Marrazzo, E. Marmo, *Rend. Atti. Accad. Sci. Med. Chir.* **1985**, *139*, 313; c) E. Abignente, A. F., E. Luraschi, C. Saturnino, F. Rossi, E. Lampa, M. Cazzola, E. Brandinelli, R. Marrazzo, E. Marmo, *Chem. Abstr.* **1986**, *105*, 126822z; d) S. Z. Langer, S. Arbilla, J. Benavides, B. Scatton, in *Gaba and Benzodiazepine Receptor Subtypes: Molecular Biology, Pharmacology, and Clinical Aspects, Vol. 46*, **1990**, pp. 61-72; e) E. Abignente, *Actual. Chim. Ther.* **1991**, *18*, 193-214; f) E. Abignente, *Chem. Abstr.* **1991**, *115*, 256028n; g) A. Elhakmaoui, A. Gueiffier, J. C. Milhavet, Y. Blache, J. P. Chapat, O. Chavignon, J. C. Teulade, R. Snoeck, G. Andrei, E. Declercq, *Bioorg. Med. Chem. Lett.* **1994**, *4*, 1937-1940; h) T. Ueda, K. Mizushige, K. Yukiiri, T. Takahashi, M. Kohno, *Cerebrovasc. Dis.* **2003**, *16*, 396-401; i) K. F. Byth, J. D. Culshaw, S. Green, S. E. Oakes, A. P. Thomas, *Bioorg. Med. Chem. Lett.* **2004**, *14*, 2245-2248; j) T. S. Harrison, G. M. Keating, *Cns Drugs* **2005**, *19*, 65-89; k) R. B. Lacerda, C. K. F. de Lima, L. L. da Silva, N. C. Romeiro, A. L. P. Miranda, E. J. Barreiro, C. A. M. Fraga, *Bioorg. Med. Chem.* **2009**, *17*, 74-84.

[3] A. E. Tschitschibabin, *Ber. Dtsch. Chem. Ges. A* **1924**, *57*, 2092 –2101.

[4] H. Tomoda, T. Hirano, S. Saito, T. Mutai, K. Araki, *Bull. Chem. Soc. Jpn.* **1999**, *72*, 1327-1334.

[5]   A. Douhal, F. Amatguerri, A. U. Acuna, *J. Phys. Chem.* **1995**, *99*, 76-80.

[6]   a) T. Mutai, H. Tomoda, T. Ohkawa, Y. Yabe, K. Araki, *Angew. Chem. Int. Ed.* **2008**, *47*, 9522-9524; b) H. Shono, T. Ohkawa, H. Tomoda, T. Mutai, K. Araki, *ACS Appl. Mater. Interfaces* **2011**, *3*, 654-657; c) A. J. Stasyuk, M. Banasiewicz, M. K. Cyranski, D. T. Gryko, *J.Org.Chem.* **2012**, *77*, 5552-5558; d) T. Mutai, H. Sawatani, T. Shida, H. Shono, K. Araki, *J. Org. Chem.* **2013**, *78*, 2482-2489.

[7]   a) Y. Q. Ge, J. Jia, H. Yang, X. T. Tao, J. W. Wang, *Dyes Pigm.* **2011**, *88*, 344-349; b) A. T. Khan, R. S. Basha, M. Lal, *Tetrahedron Lett.* **2012**, *53*, 2211-2217.

[8]   J. Catalan, E. Mena, F. Fabero, F. Amatguerri, *J. Chem. Phys.* **1992**, *96*, 2005-2016.

[9]   O. N. Burchak, L. Mugherli, M. Ostuni, J. J. Lacapere, M. Y. Balakirev, *J. Am. Chem. Soc.* **2011**, *133*, 10058-10061.

[10]   a) F. Shibahara, R. Sugiura, E. Yamaguchi, A. Kitagawa, T. Murai, *J. Org. Chem.* **2009**, *74*, 3566-3568; b) F. Shibahara, E. Yamaguchi, A. Kitagawa, A. Imai, T. Murai, *Tetrahedron* **2009**, *65*, 5062-5073; c) E. Yamaguchi, F. Shibahara, T. Murai, *J. Org. Chem.* **2011**, *76*, 6146-6158; d) F. Shibahara, Y. Dohke, T. Murai, *J. Org. Chem.* **2012**, *77*, 5381-5388; e) Y. Shigemitsu, T. Mutai, H. Houjou, K. Araki, *J. Phys. Chem. A* **2012**, *116*, 12041-12048.

[11]   a) Y. Y. Zhao, M. R. Wasielewski, *Tetrahedron Lett.* **1999**, *40*, 7047-7050; b) X.-F. Zhang, J. Wang, *J. Phys. Chem. A* **2011**, *115*, 8597-8603.

[12]   O. Mongin, L. Porrès, M. Charlot, C. Katan, M. Blanchard-Desce, *Chem. Eur. J.* **2007**, *13*, 1481 – 1498.

[13]   A. I. Ciuciu, K. Skonieczny, D. Koszelewski, D. T. Gryko, L. Flamigni, *J. Phys. Chem. C* **2013**, *117*, 791-803.

4. Organic nanodots for bioimaging

As a final approach in identifying new two photon absorbers for bioimaging purposes, we have investigated four organic dendrimers of various sizes. Unlike the systems presented in the previous chapters, these compounds have the advantage of possessing significant 2PA cross sections. In combination with a reduced toxicity (given mainly by the absence of metals in the structure), solubility in solvents of high polarity (i.e. dimethylsulphoxide) and a high luminescence quantum yield, the investigated organic nanodots could have important values of two photon brightness ($\phi_{fl}\ \sigma_2$).

Our aim in this work was to elucidate the excited state properties of these dendrimers, and to do this, steady state and time resolved methods were employed. Synthesis and 2PA measurements were performed by the group of Dr. Mireille Blanchard-Desce.

4.1. Introduction

Organic dendrimers (nanodots or ONDs) were developed as alternative to semiconductor quantum dots (QDs) for bioimaging purposes. Though the QDs have gained popularity due to their extremely large two photon (2PA) cross-sections (two photon brilliance $\phi_{fl}\ \sigma_2 > 47\ 000$ GM) and intense luminescence properties, they suffer of some drawbacks (i.e. biological toxicity).[1] Therefore, an alternative route implying organic nanodots (ONDs) was developed. This approach is based on the confinement of a large number of optimized chromophores to build nano-objects of defined and controlled structure. The novel 'soft' ONDs proved to have competitive 2PA properties,[2] and this could be attained by grafting a large number of fluorophores displaying significant 2PA properties on the surface of a dendrimeric platform. Whereas the luminescence of ONDs can be tuned by acting on the nature of the fluorophore, the minimization of the toxicity can be obtained by rigorous choice of the dendritic scaffold. It was shown that phosphorous dendrimers possess low toxicity and biodegradability, as required in biomedical applications.[3] In order to increase their solubility in aqueous media, nanodots with shielding dendrimeric layers and peripheral charged groups were synthesized.[4] Apart from solubility, also the problem of the low luminescence in biological medium (water) should be overcome,[4c] since the maintenance of a high emission is of importance in imaging applications.

It is also known that the luminescence properties of these dendrimers can be significantly affected by the formation of dimers or aggregates between adjacent chromophores.[5] Processes like

energy or electron transfer, excimer formation or exciton annihilation[6] can also lead to changes in the optical response.

Within this context, we aimed at the development of novel water soluble phosphorous based ONDs with optimized cross-sections (σ_2) values in the biological window (700 – 1100 nm), while maintaining high luminescence yields (ϕ_{fl}). Fluorene chromophore was chosen to decorate the core, since it was successfully involved up to date in the construction of ONDs with large multiphoton absorption.[7] The optical characterization of the new compounds was performed by steady state and time resolved spectroscopy.

4.2. Results and discussion

We have investigated four dendrimers synthesized *via* divergent method (from the core to the outer part) and characterized by the presence of cationic groups on their periphery. The number of charged groups varies between 24 (**3, 6**) and 48 (**4, 5**). The compounds are structured on a central phosphazene ring on which were grafted 12 (**3, 4, 6**) or 24 (**5**) fluorene chromophores. Their photophysical properties were compared to the ones of the fluorene models **1** and **2**. The structures of the investigated compounds are shown in Chart 4.1. Chart 4.2 contains a schematic representation of ONDs, in order to simplify the visualization of the dendrimers for the reader. The compounds were investigated in a series of solvents of different polarity: THF ($\varepsilon = 7.58$), DCM ($\varepsilon = 8.93$), DMF ($\varepsilon = 36.7$) and DMSO ($\varepsilon = 46.4$), according to their solubility.

One photon absorption. The absorption spectra of the dendrimers in all solvents show a reasonably good superposition with the sum of the spectra of the 12 or 24 chromophores which compose them, in the region of absorption of the fluorene unit, i.e. 350-450 nm. A considerably higher absorption coefficient is observed around 300 nm, due to the absorption contribution of the phosphazene center and of the aromatic groups situated on the dendrimers' branches. As representative for the series, the absorption spectrum of **5** in DMSO is compared with the sum of 24 spectra of the fluorene model **1** in Figure 4.1.
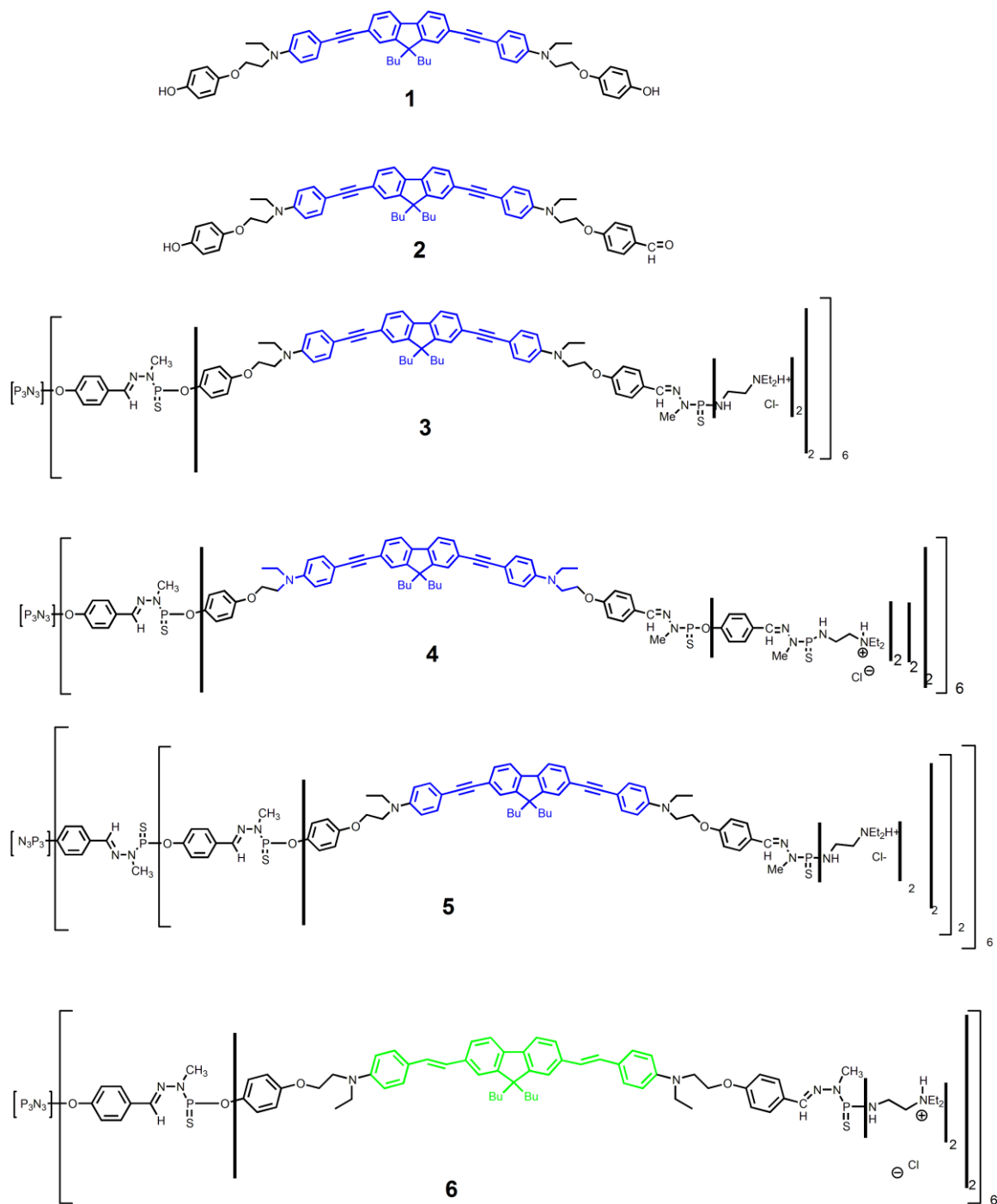
Chart 4.1. Structures of the investigated compounds. Fluorene chromophore is highlighted in the corresponding color of the emission.
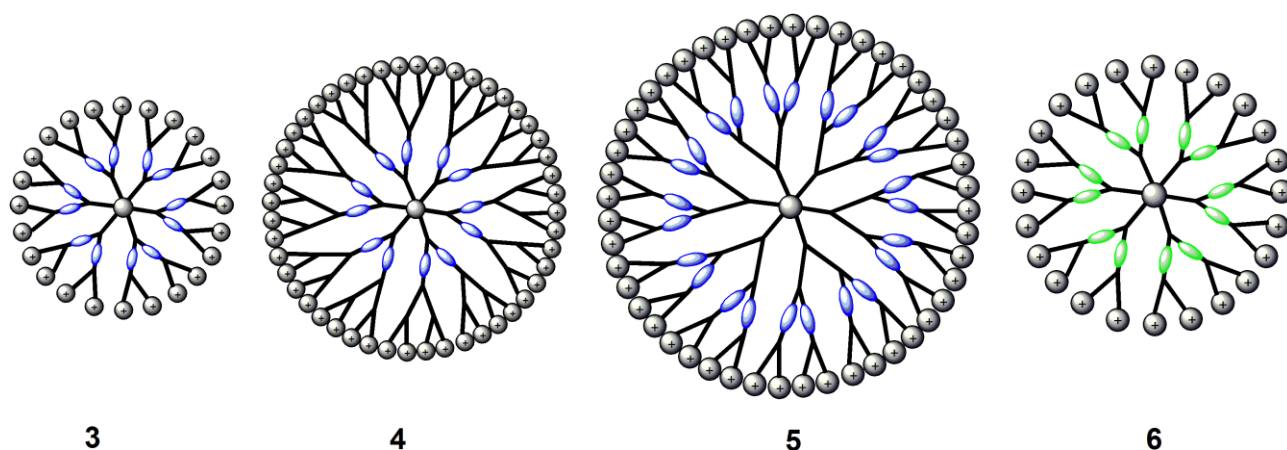
Chart 4.2. Schematic structures of the investigated ONDs. Fluorene chromophore is highlighted in the corresponding color of the emission.

A comparison of the absorption spectra of all the compounds in the same solvent, i.e. DCM, is shown in Figure 4.2 left. It is evident that the maximum of absorption of the dendrimers **3, 4** and **5** is unshifted with respect to models **1** and **2**, whereas **6** is red-shifted by ca. 27 nm. The same trend occurs in all the examined solvents. This can be explained by considering that the fluorene unit in **6** is differently substituted. In **6**, in fact, the chromophore is connected *via* ethenyl, whereas in the other dots the connection is made by ethynyl linkers. The type of connection has been proven to affect the photophysical properties of the dendrimers: the more extended conjugation introduced by the double bonds causes a red shift of the absorption transition of the fluorene chromophore.[8]
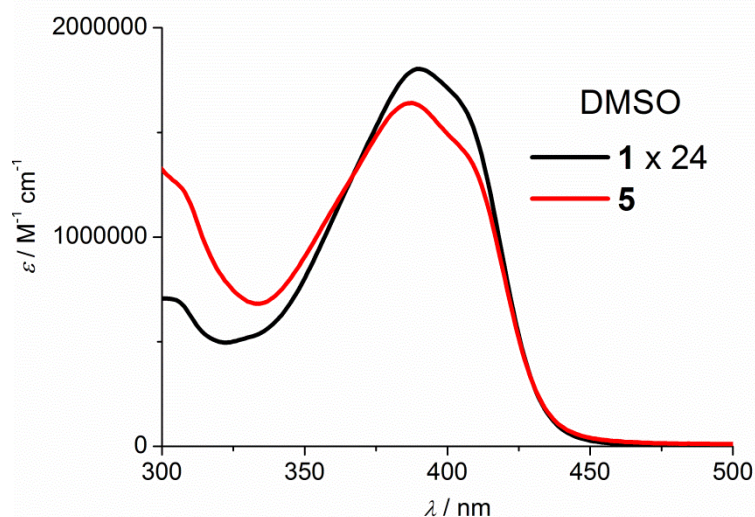
Figure 4.1. Absorption spectrum of **5** compared with the absorption spectrum of the model **1** multiplied by 24 in DMSO solutions.
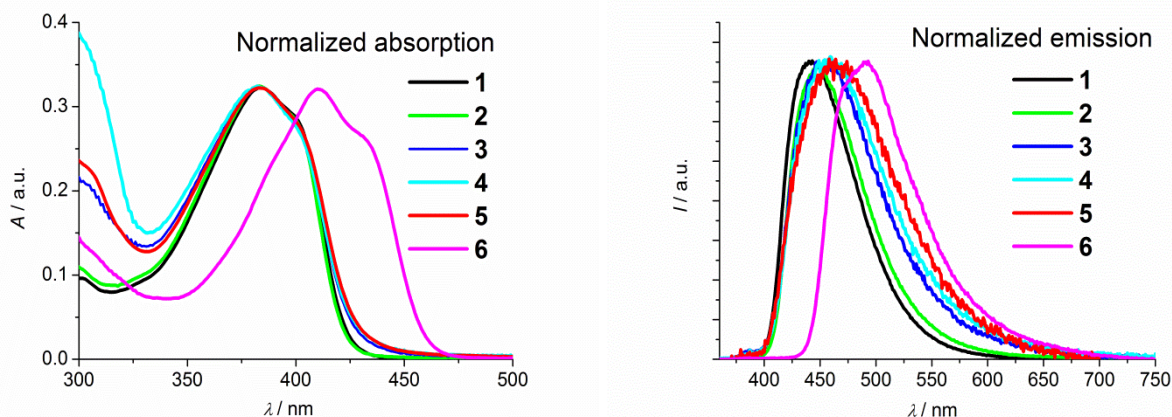
Figure 4.2. Arbitrary scaled absorption spectra (left) and emission spectra (right) of samples **1-6** in DCM solutions.

All the examined compounds show a moderate solvatochromism, with the absorption band slightly shifting to lower energy while increasing the polarity of the solvent.

The normalized luminescence of the samples **1-6** in DCM is presented in Figure 4.2 right. This shows the normalized emission spectra of models **1** and **2** and the different dendrimers in DCM solvent. One can notice that **6** displays a bathochromic shift of $10 - 40$ nm with respect to the other compounds (Table 4.1 and Figure 4.2 right), in agreement with the absorption behavior and ascribable to the increased conjugation introduced by the ethylene linkers in the structure. A similar trend can be observed by comparing the emission maxima of the compounds in each examined solvent (Table 4.1).
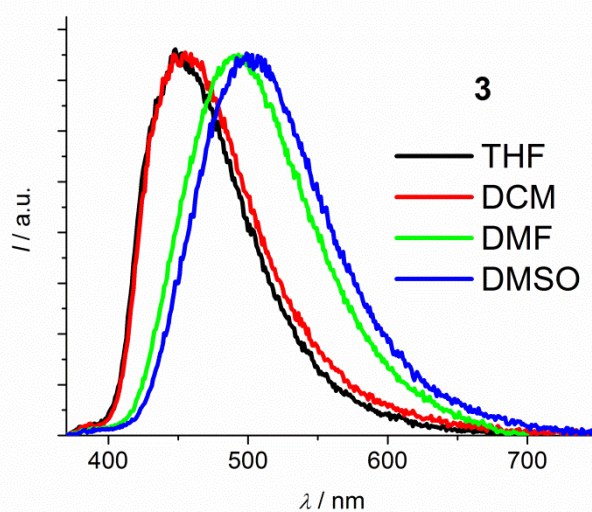
Figure 4.3. Arbitrary scaled emission spectra of **3** in all solvents at room temperature.

At variance with the absorption, the emission of the examined dots and of the models is strongly influenced by the polarity of the solvent, as noticed for representative dendrimer **3** (Figure 4.3). While the maxima are almost invariant when passing from THF to DCM, they show bathochromic shifts ranging from 30 to 50 nm when moving to DMF and DMSO, solvents with high dielectric constants (Table 4.1). A pronounced fluorescence solvatochromism has been noticed for 1 and similar fuorene based quadrupolar molecules[4c, 9] and has been ascribed to the polar nature of the relaxed excited state where a symmetry breaking occurs. The data show that this seems to be effective also in the present newly designed dots with peripheral charges.

As mentioned above, an interesting outcome is the dependence of the fluorescence quantum yield of the compounds on the polarity of the solvent. It can be noticed that while models **1** and **2** show a high yield that ranges from ca. 0.6 to 0.8 in all solvents, similarly to what previously reported for related compounds,[4b, 8, 9b] the dots show different behaviors (Table 4.1). Dendrimer **6** appears to be slightly affected by the polarity of the solvent, ϕ_{fl} about 0.5 -0.6 in all solvents, i.e. slightly lower than that of the model. For all other dendrimers **3**, **4** and **5**, an important drop in the quantum yields occur in all the examined solvents, with trends not directly correlated to the polarity of the medium. Their luminescence is quenched to about 12 % that of the models in THF and DCM ($\phi_{fl} = 0.07 - 0.11$), and to 20-26% in DMF and DMSO ($\phi_{fl} = 0.13 - 0.16$) (Table 4.1). These values are lower, to some extent, with respect to other dendrimers based on similar fluorene chromophores lacking charged groups on the periphery.[2, 4b, c, 9b, 10] It can be noticed that neither the number of branches nor the number of charges influences the luminescence features of these dendrimers.

Time resolved experiments led to the measured lifetimes collected in Table 4.1. Models **1** and **2** have a short lifetime (≤ 1 ns) in the less polar solvents and longer than one ns in more polar media, in agreement with previously reported data.[4c] The interesting outcome is that while **6** shows a perfect monoexponential decay ($\tau = 1.1 - 1.4$ ns) in all the solvents except DMSO, the other dendrimers **3, 4** and **5** show always bi-exponential decays. One of the measured lifetimes is very similar to that of models i.e. 0.9 -1.4 ns, whereas the other is much shorter, of the order of hundreds of picoseconds (Table 4.1). The percentage distribution of each lifetime is around 50:50 within experimental uncertainties for **3** and **4**, whereas is around 65:35 (short lifetime: long lifetime) within experimental uncertainties, for **5**. These results lead to speculate on the presence of at least two populations of fluorophores, one with an excited state unaffected and the other quenched by some still unidentified process.

If one assumes, within the same solvent, a constancy of the radiative rate constant k_r in the dendrimers **3, 4** and **5** compared to the model **1** ($k_r = \phi_1/\tau_1$), the expected fluorescence yield (ϕ_{calc}) in case of the cromophore quenching can be calculated from the kinetic data (τ_1 and τ_2) and the

fraction of the two observed lifetimes (f_1 and f_2) reported in Table 4.1, as: $\phi_{calc} = k_r (f_1 \, \tau_1 + f_2 \, \tau_2)$. For **3, 4** and **5** the calculated luminescence yield in each solvent is well higher than the experimental one, i.e. in DCM is 0.35, 0.39 and 0.29 respectively against an experimental value which is ca. ¼ of the calculated one for all dots. This means that part of the luminescence is lost in the time resolved determinations and suggests that a static quenching, i.e. faster than the time resolution of the experiments, occur between closely spaced fluorene units. Moreover, this occurs for a large majority of the chromophores, from 50% to 75%. So, in addition to the quenching process measured on the picosecond time scale and reported on Table 4.1 there must be at least another quenching process which escapes our detection, with a lifetime of the order of few picoseconds or lower.

Transient absorbance. Flash photolysis experiments have been performed for selected compounds in order to get more information on the excited state dynamics of the fluorophores in the dots. Figure 4.4 shows the end of pulse spectra of **5** and model **1** in air-free DMSO. The spectra obtained for both solutions are similar, displaying bleaching features at 390 nm and positive features around 500 nm and 750 nm, typical of the fluorene triplet excited state.[11] The lifetime in **1** is 250 μs. It can be noticed that the ΔA values of the spectra registered for **5** are well lower than those of the fluorene model and the triplet lifetime is greatly reduced, to 450 ns. The low ΔA in **5** can be interpreted by considering that the parent singlet excited state is also decreased to ca. 20% than the model **1** (Table 4.1). On the other hand the reduction of the triplet lifetime can be ascribed to the trapping of molecular oxygen inside the dendrimer branches or to self-quenching by fluorene ground states in the high concentration of the dot microenvironment. The reaction rate with oxygen of **1** is of the order of 10^9 M^{-1} s^{-1} in DMSO solutions, typical of triplet quenching reaction by oxygen.[12] No effect on the triplet lifetime of **5** (450 ns) was noticed upon equilibrating the solution with air.

Table 4.1. Fluorescence data at room temperature of dots and models in air-equilibrated THF, DCM, DMF and DMSO at 295K; n.s. –not soluble. The concentrations used are of the order of 10^{-7} M.

		λ_{em}^{max} / nm	ϕ_{fl}	ϕ_{calc}	τ /ns
THF	**1**	450 [a]	0.80 [a]		1.02
$\varepsilon = 7.58$	**2**	448	0.73		0.96
	3	448	0.11	0.45	0.16 (47%); 0.95 (53%)
	4	n.s	n.s		n.s
	5	n.s	n.s		n.s
	6	493	0.64	-	1.12
DCM	**1**	443	0.74		0.98
$\varepsilon = 8.93$	**2**	447	0.62		0.87
	3	454	0.09	0.35	0.14 (57%); 0.91 (43%)
	4	459	0.11	0.39	0.15 (58%); 1.04 (42%)
	5	464	0.07	0.29	0.12 (70%); 1.00 (30%)
	6	491	0.54	-	1.12
DMF	**1**	486	0.57		1.51
$\varepsilon = 36.71$	**2**	492	0.59		1.43
	3	490	0.15	0.34	0.38 (44%); 1.33 (56%)
	4	492	0.15	0.34	0.40 (50%); 1.39 (50%)
	5	488	0.16	0.23	0.26 (60%); 1.11 (40%)
	6	509	0.61	-	1.42
DMSO	**1**	501 [a]	0.78 [a]		1.46
$\varepsilon = 46.45$	**2**	501	0.63		1.45
	3	503	0.14	0.49	0.24 (42%); 1.41 (58%)
	4	n.s.	n.s.		n.s
	5	490	0.13	0.43	0.31 (60%); 1.53(40%)
	6	520	0.47	-	0.36 (32%); 1.94 (68%)

[a] Data from reference [4c].
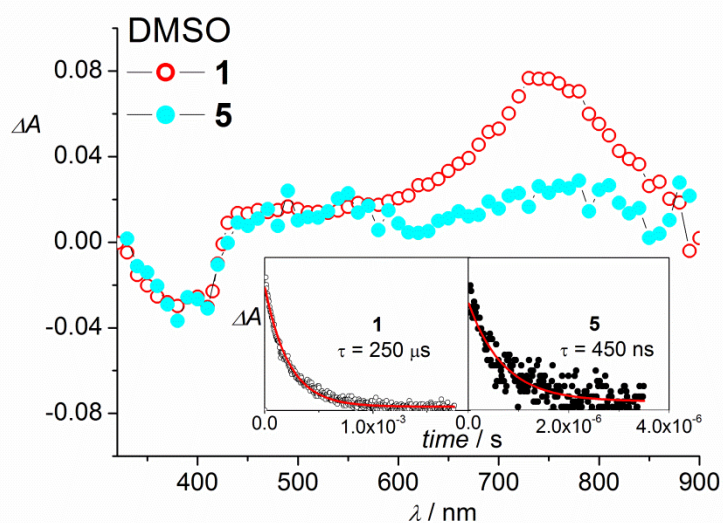
Figure 4.4. End of pulse spectra after excitation of the samples with an 18 ns laser pulse (3 mJ at 355 nm) for optically matched solutions with *A* = 0.8 in DMSO.

Discussion. On the basis of the collected data we will here try to identify the possible reasons for the important quenching of fluorescence detected in some of the dots, in particular in media which provide a highly polar microenvironment, since this is a serious drawback for the use of these luminophors for imaging in physiological conditions.

Energy transfer from excited fluorene to any other component of the dot is excluded on the basis of thermodynamic grounds. The energy of fluorene excited state (model **1**) is around 2.8 eV, whereas all other components, in particular the central phosphazene core, has a much higher energy, of the order of 3.5 eV.[13] We also examine the possibility that the luminescence drop observed in more polar solvents is ascribable to a photoinduced electron transfer process from the fluorene singlet excited state to other units present in the dot. This process can occur if the energy stored in the fluorene chromophore excited state, 2.8 eV, is sufficient to promote the oxidation of fluorene and the reduction of the possible electron acceptor. The charged surface of the dot and the stabilization effect of the medium/high polarity solvents could provide a polar microenvironment favorable to the charge separated state formation. Nevertheless, the oxidation potential of fluorene is of the order of 1.58 V *vs*. SCE,[14] and the reduction potential of phosphazene compounds similar to the central unit are of the order of -3 V *vs*. SCE.[15] The energy necessary to allow the electron transfer would be too high, and the process cannot occur.

Having excluded electron and energy transfer, one of the most likely processes for the quenching of the chromophores might be the formation of stacked non-fluorescent fluorene structures. These might be formed either by fluorene units belonging to different dots (intermolecular aggregation) after interpenetration of the branches, or by chromophores belonging

to the same dot (intramolecular aggregation). An intramolecular aggregation of the fluorene units in the flexible chains constituting the dots **3**, **4**, **5**, would be quite expected. Nonetheless, the similar results obtained in the lifetime and exponential distribution in samples **3** and **5** characterized by the presence of respectively 12 and 24 fluorene chromophores, do not seem to support intramolecular aggregation. Such increase in the number of chromophores, yielding a more crowded microenvironment, would in fact be expected to favor the stacking process and alter to a large extent the quenching. As a matter of fact we have a slightly higher contribution by the fast process in **5**, 65% with respect to 50% in **3**, but this is not so pronounced to positively identify intramolecular aggregation as the source of the detected quenching. It might however be a con-cause.

On the other hand, it has formerly been shown that similar water soluble rod-like dendrimers are susceptible to aggregation.[4c] Accordingly, a possible explanation for the results could be an intermolecular aggregation phenomenon. To investigate this possibility, we designed an experiment where solutions of the dendrimers were prepared by varying their concentration of two orders of magnitude and the fluorescence lifetimes were measured (Table 4.2). If this hypothesis is true, an increase in aggregation phenomenon with the concentration would be expected and hence a change in the ratio of the two lifetimes in favor of the fast one. It is clear that no significant differences in the lifetime values or percentage distributions are observed. However, if we imagine that the aggregation of these dots proceeds *via* micelle formation, i.e. only above a certain threshold aggregation occurs and the aggregates are characterized by an identical size, i.e by the same number of components. Under these conditions, where an increase in concentration changes the number of aggregates but not their size, one might expect that the ratio between the interdigitized chromophores and the one exposed to the solvents remain constant with the overall concentration of dendrimers. This hypothesis needs a confirmation but it seems to be at the moment the most likely one.

It should be noted that the completely different behavior of **6**, where an emission quantum yield similar to that of the monomer and a mono-exponential lifetime is observed in all solvents (except the highly polar DMSO), supports the aggregation hypothesis as responsible of the quenching since the rigidity of the ethylene linkers prevents the conformational flexibility necessary for the staking. Unfortunately this confirmation cannot give us any indication about the intra- or the inter-molecular aggregation hypothesis.

Table 4.2. Lifetimes at 295 K measured by TCSPC in air-equilibrated solutions of different concentrations (C) of **3**, **4** and **5**, upon excitation at 373 nm.

		C/M	τ/ns	C/M	τ/ns
THF ε=7.58	**3**	2.9×10^{-6}	0.13 (48%); 0.95 (52%)	5.2×10^{-8}	0.14 (50%); 0.94 (50%)
DCM ε=8.93	**3**	3.8×10^{-6}	0.18 (57%); 1.0 (43%)	5.2×10^{-8}	0.21 (58%); 1.0 (42%)
	4	1.1×10^{-6}	0.15 (50%); 1.0 (50%)	5.2×10^{-8}	0.15 (52%); 1.0 (48%)
	5	6.1×10^{-7}	0.16 (73%); 0.98 (27%)	3.0×10^{-8}	0.17 (72%); 1.1 (28%)
DMF ε=36.71	**3**	2.8×10^{-6}	0.39 (56%); 1.3 (44%)	4.2×10^{-8}	0.31 (51%); 1.2 (49%)
	4	1.4×10^{-6}	0.36 (49%); 1.3 (51%)	4.2×10^{-8}	0.42 (56%); 1.4 (44%)
	5	8.5×10^{-7}	0.29 (68%); 1.2 (32%)	3.0×10^{-8}	0.31 (66%); 1.2 (34%)
DMSO ε=46.45	**3**	1.5×10^{-6}	0.36 (48%); 1.6 (52%)	5.2×10^{-8}	0.47 (49%); 1.5 (51%)
	5	7.3×10^{-7}	0.36 (68%); 1.5 (32%)	3.0×10^{-8}	0.28 (66%); 1.3 (34%)

Two photon absorption. The two photon absorption properties of the compounds are currently under investigation in the group of Dr. M. Blanchard-Desce.

4.3. Conclusions

Four different dendrimers characterized by the presence of charges on the periphery were characterized by means of steady state and time resolved spectroscopy. All but one (where the chromophore is connected *via* ethenyl instead of ethynyl linkers) showed a high loss of the luminescence, independent of the polarity of the solvent. It seems that the type of chromophore/connection involved in the molecular structure affects the optical properties. The

quenched emission in polar solvents was characterized by biexponential lifetimes, indicative of two different populations. Energy/ electron transfer processes were excluded as potential cause for the luminescence loss, due to unfavorable thermodynamic conditions. The results were discussed on the basis of the occurrence of aggregation processes that are responsible of the quenching of the chromophores.

4.3. References

[1]   a) D. R. Larson, W. R. Zipfel, R. M. Williams, S. W. Clark, M. P. Bruchez, F. W. Wise, W. W. Webb, *Science* **2003**, *300*, 1434-1436; b) X. Michalet, F. F. Pinaud, L. A. Bentolila, J. M. Tsay, S. Doose, J. J. Li, G. Sundaresan, A. M. Wu, S. S. Gambhir, S. Weiss, *Science* **2005**, *307*, 538-544; c) R. Hardman, *Environ. Health Perspect.* **2006**, *114*, 165-172.

[2]   O. Mongin, T. R. Krishna, M. H. V. Werts, A. M. Caminade, J. P. Majoral, M. Blanchard-Desce, *Chem. Commun.* **2006**, 915-917.

[3]   a) M. Maszewska, J. Leclaire, M. Cieslak, B. Nawrot, A. Okruszek, A. M. Caminade, J. P. Majoral, *Oligonucleotides* **2003**, *13*, 193-205; b) J. Solassol, C. Crozet, V. Perrier, J. Leclaire, F. Beranger, A. M. Caminade, B. Meunier, D. Dormont, J. P. Majoral, S. Lehmann, *J. Gen. Vir.* **2004**, *85*, 1791-1799.

[4]   a) T. R. Krishna, M. Parent, M. H. V. Werts, L. Moreaux, S. Gmouh, S. Charpak, A.-M. Caminade, J.-P. Majoral, M. Blanchard-Desce, *Angew. Chem. Int. Ed.* **2006**, *45*, 4645-4648; b) O. Mongin, C. Rouxel, A.-C. Robin, A. Pla-Quintana, T. R. Krishna, G. Recher, F. Tiaho, A.-M. Caminade, J.-P. Majoral, M. Blanchard-Desce, in *Nanobiosystems: Processing, Characterization, and Applications, Vol. 7040* (Eds.: E. M. Heckman, T. B. Singh, J. Yoshida), **2008**; c) C. Rouxel, M. Charlot, O. Mongin, T. R. Krishna, A.-M. Caminade, J.-P. Majoral, M. Blanchard-Desce, *Chem. Eur. J.* **2012**, *18*, 16450-16462.

[5]   W. West, S. Pearce, *J. Phys. Chem.* **1965**, *69*, 1894-1903.

[6]   G. De Belder, G. Schweitzer, S. Jordens, M. Lor, S. Mitra, J. Hofkens, S. De Feyter, M. Van der Auweraer, A. Herrmann, T. Weil, K. Mullen, F. C. De Schryver, *Chemphyschem* **2001**, *2*, 49-55.

[7]   a) B. A. Reinhardt, L. L. Brott, S. J. Clarson, A. G. Dillard, J. C. Bhatt, R. Kannan, L. X. Yuan, G. S. He, P. N. Prasad, *Chem. Mater.* **1998**, *10*, 1863-1874; b) R. Kannan, G. S. He, L. X. Yuan, F. M. Xu, P. N. Prasad, A. G. Dombroskie, B. A. Reinhardt, J. W. Baur, R. A. Vaia, L. S. Tan, *Chem. Mater.* **2001**, *13*, 1896-1904; c) O. Mongin, L. Porres, L. Moreaux, J. Mertz, M. Blanchard-Desce, *Org. Lett.* **2002**, *4*, 719-722; d) O. K. Kim, K. S. Lee, Z. Huang, W. B. Heuer, C. S. Paik-Sung, *Opt. Mater.* **2003**, *21*, 559-564; e) K. D. Belfield, A. R. Morales, B. S. Kang, J. M. Hales, D. J. Hagan, E. W. Van Stryland, V. M. Chapela, J. Percino, *Chem. Mater.* **2004**, *16*, 4634-4641.

[8]   a) C. Katan, S. Tretiak, M. H. V. Werts, A. J. Bain, R. J. Marsh, N. Leonczek, N. Nicolaou, E. Badaeva, O. Mongin, M. Blanchard-Desce, *J. Phys. Chem. B* **2007**, *111*, 9468-9483; b)

O. Mongin, L. Porres, M. Charlot, C. Katan, M. Blanchard-Desce, *Chem. Eur. J.* **2007**, *13*, 1481-1498.

[9]   a) F. Terenziani, A. Painelli, C. Katan, M. Charlot, M. Blanchard-Desce, *J. Am. Chem. Soc.* **2006**, *128*, 15742-15755; b) C. Katan, M. Charlot, O. Mongin, C. Le Droumaguet, V. Jouikov, F. Terenziani, E. Badaeva, S. Tretiak, M. Blanchard-Desce, *J. Phys. Chem. B* **2010**, *114*, 3152-3169.

[10]   O. Mongin, A. Pla-Quintana, F. Terenziani, D. Drouin, C. Le Droumaguet, A.-M. Caminade, J.-P. Majoral, M. Blanchard-Desce, *New J. Chem.* **2007**, *31*, 1354-1367.

[11]   S. M. Fonseca, J. Pina, L. G. Arnaut, J. S. de Melo, H. D. Burrows, N. Chattopadhyay, L. Alcacer, A. Charas, J. Morgado, A. P. Monkman, U. Asawapirom, U. Scherf, R. Edge, S. Navaratnam, *J. Phys. Chem. B* **2006**, *110*, 8278-8283.

[12]   S. L. Murov, I. Carmichael, G. L. Hug, *Handbook of Photochemistry*, 2nd ed., ed. Marcel Dekker Inc., New York, **1993**.

[13]   N. Chattopadhyay, B. Haidar, A. Mallick, S. Sengupta, *Tetrahedron Lett.* **2005**, *46*, 3089-3092.

[14]   a) R. H. Goldsmith, L. E. Sinks, R. F. Kelley, L. J. Betzen, W. H. Liu, E. A. Weiss, M. A. Ratner, M. R. Wasielewski, *Proc. Natl. Acad. Sci. U. S. A.* **2005**, *102*, 3540-3545; b) P. Hapiot, C. Lagrost, F. Le Floch, E. Raoult, J. Rault-Berthelot, *Chem. Mater.* **2005**, *17*, 2003-2012.

[15]   H. R. Allcock, M. T. Stein, J. A. Stanko, *J. Am. Chem. Soc.* **1971**, *93*, 3173-3178.

5. Systems for other applications

So far in this thesis, different two photon absorbers were characterized for applications in fluorescence microscopy. As part of TOPBIO project aiming at development of new 2PA systems for biomedical use, the current chapter is presenting novel compounds with other potential applications. Here, two photon polymerization and two photon uncaging of biologically active molecules were considered.

Since both domains are relatively new by means of 2PA methods, we believe that our contribution together with others' in the mentioned fields can be of significant value. The synthesis of the samples used as photoinitiators was made by the group of Dr. Daniel T. Gryko, whereas of the systems for uncaging by the group of Dr. Harry Anderson (in both cases *via* multi-step synthesis). The 2PA properties of the photoinitiators were determined by Dr. Maria Farsari's group. The biocompatibility tests were conducted by the group of Dr. Maria Chatzinikolaidou.

5.1. Two photon initiators for photopolymerization

5.1.1. Introduction

Besides the biomedical applications mentioned in Chapter 1, two photon polymerization (2PP) technique finds applications in photonic crystals,[1] optical storage,[2] biomolecule scaffolds[3] etc. The method has attracted considerable attention due to the fabrication of 3D structures with micro- and nanoscale dimensions. Among others, a 9 nm resolution has been reported recently.[4]

The photoinitiator, capable of creating the reactive species, requires large two photon absorption cross-sections (σ_2) and high efficiency. These can guarantee an elevated writing speed and low polymerization threshold. A lot of work has been done in the field by using already available UV photoinitiators,[5] but they proved to have low σ_2 values leading to long exposure times of the material and implicitly, damage.

Between the compounds tested as photoinitiators for 2PP (see Chapter 1), ketocoumarins presents great interest due to the enhancement of σ_2 values by the proper molecular design. Moreover, in order to be efficient as polymerization photoinitiator, the sample needs to display high intersystem crossing to the triplet state which is usually the "active" state and, consequently a low emission is indicative of high population of the triplet state.[6] In fact, ketocoumarins are known for

possessing low luminescence[7] and high intersystem crossing yields,[7a] making them efficient triplet sensitizers. Though many studies reported the ketocoumarins as photosensitizers in one photon polymerization[8] only few derivatives have been used for 2PA photopolymerization.[7b, 7d, 9] Still, there is no clear information about the 2 PA polymerization and burning thresholds.

Here, the optical properties of several bis-ketocoumarins are investigated as function of the central core and terminal parts. In fact, the solubility issue has been solved by the introduction of branched-alkyl chains at the end of the amino moieties. It is also known that the type of central ring can affect the photophysical properties of the system.[10] Since cycloketones are commercially available at relatively low costs, testing the effects of ring size on photophysical properties could be a useful method to overcome the synthetic economic issues. In the end, the 2PA properties of the compounds were measured and their capability as photoinitiators was tested by fabricating 3D microstructures. The migration and proliferation of cells seeded on these microstructures were evaluated.

5.1.2. Results and discussion

Experiments on the compounds showed in Chart 5.1 were conducted in two solvents of different polarity, toluene (TOL) with $\varepsilon = 2.38$ and dichloromethane (DCM), $\varepsilon = 8.93$.
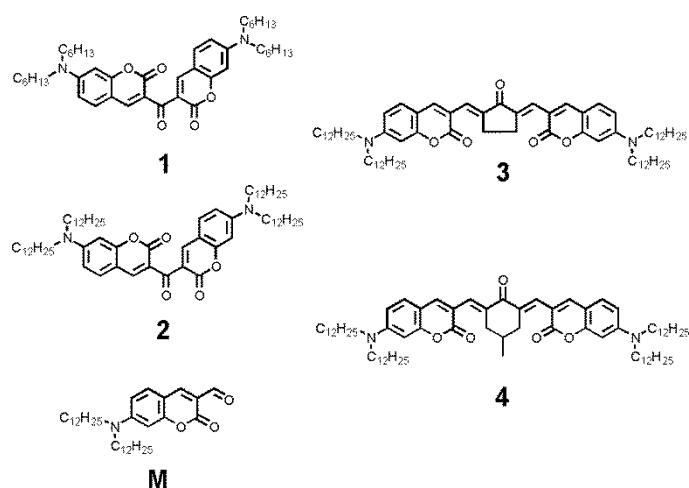
Chart 5.1. Structures of the investigated bis-ketocoumarins and their monomer model **M**.

One photon absorption. Representative for the series, the absorption spectra in the two solvents of the samples **1** and **3** are displayed in Figure 5.1 and the most important data are collected in Table 5.1.
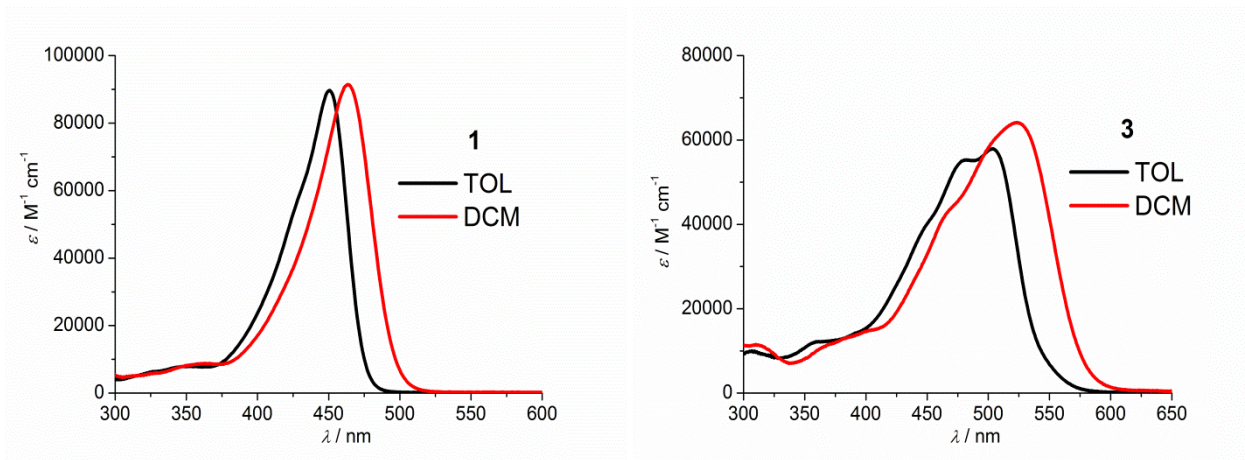
Figure 5.1. Absorption spectra of **1** and **3** in TOL and DCM solutions.

The absorption spectra of **1** and **2** are almost identical with an absorption maximizing at 450 nm and with a molar absorption coefficient (ε) value close to 100 000 M^{-1} cm^{-1} (Figure 5.1). The data are not dissimilar from the ones of the monomer **M** though in the latter the maximum is 10 nm hypsochromically shifted and the molar absorption coefficient is almost half (Table 5.1). The compounds **3** and **4** show bathochromically shifted broader spectra in comparison to **M**, indicative of an extended conjugation ($\varepsilon = 60\ 000 - 80\ 000$ M^{-1} cm^{-1}). The absorption spectra of all samples shift bathochromically in DCM, from 10 nm to 25 nm. The bathochromic shift is indicative of a transition which occurs at lower energy in the polar solvent and it might be due either to a destabilization of the ground state or to a stabilization of the excited state in the vertical transition.

The fluorescence spectra from solutions with matched optical density in TOL and DCM are reported in Figure 5.2 and the luminescence data are collected in Table 5.1. The monomer **M** displays a strong fluorescence quantum yield, 0.576 in TOL and 0.656 in DCM. The spectral features and the fluorescence quantum yields (ϕ_{fl}) of **1** and **2** are almost identical, only slightly bathochromically shifted with respect to those of the monomer **M**, but with a much lower fluorescence quantum yield compared to that of **M**. They display a low ϕ_{fl}, of the order of a few percent in both TOL and DCM. Sample **4** has a ϕ_{fl} slightly higher than that of the former samples, of the order of 5-10% of that of **M**, whereas the compound **3** has a noticeable luminescence, of the order of 50% of that of the reference monomer **M**. The trend of ϕ_{fl} within the series is similar in both solvents, with a higher luminescence quantum yield in DCM compared to TOL for **3**, **4** and **M**, whereas **1** and **2** have a lower ϕ_{fl} in DCM. One can notice that the Stokes shift (Δ_{ss}) are in general

higher in DCM than in TOL but from a qualitative viewpoint, Δ_{ss} for the various samples in TOL parallel the one in DCM, with a larger Stoked shifted emission for sample **3** and even more for **4**. For the latter, a value of ca. 2200 and 3400 cm^{-1} is detected in TOL and DCM respectively. These values testify the large change in polarity from the ground to the relaxed excited state. An increased charge transfer character in the excited state is compatible with the observations. Accordingly, as observed for the absorption features the vibronic structure present in the emission spectra of **3** and **4** in TOL solutions, is lost in DCM. The reported data are in agreement with other reports on similar samples.[7a, b]
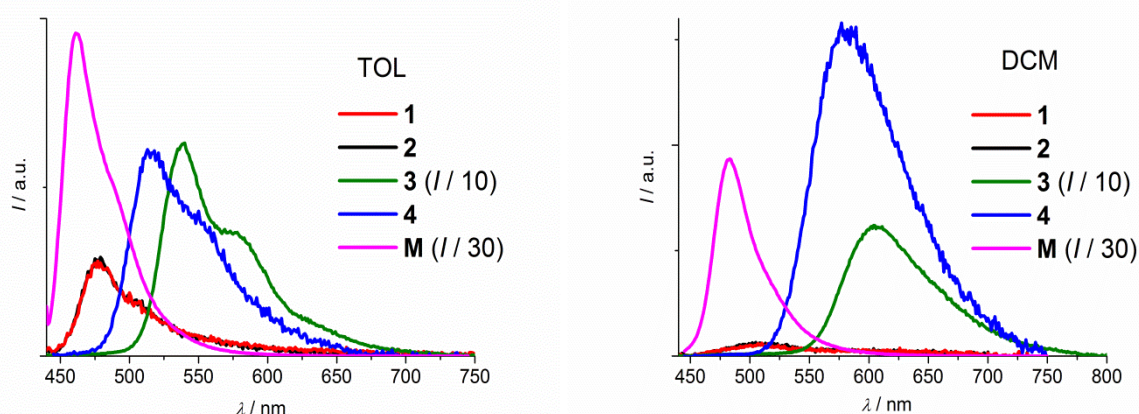
Figure 5.2. Room temperature corrected luminescence spectra in TOL (left) and DCM (right), λ_{exc} is 440 nm and $A_{440\,nm} = 0.10$ for all samples.

The data on lifetimes are missing in the literature also for the already published ketocoumarines. This might be due to the subnanosecond lifetime of the bis-ketocoumarine derivatives, which require nonstandard time resolved luminescence techniques. In addition to a Time Correlated Single Photon Counting (TCSPC) apparatus, we have used Streak camera device with 10 ps resolution. This allowed to measure the luminescence lifetime of all samples, as reported in Table 5.1. Streak camera images and the derived lifetime decays of **4** are shown in Figure 5.3. At variance with the cases of samples **3**, **4** and **M** which have a strict exponential decay lifetime, **1** and **2** display a bi-exponential decay in both solvents, with a major component with tens of picosecond lifetime and a 15%-20% component with about two hundred picosecond lifetime. The presence of a double exponential, ascribable to two different types of populations in the excited state, has been formerly reported for a similar compound and ascribed to the presence of different conformers.[7c]

Table 5.1. Spectroscopic and photophysical parameters of the samples at room temperature.

	$\varepsilon/M^{-1}cm^{-1}$ (λ_{abs}^{max}/nm)	λ_{em}^{max}/nm	Δ_{ss}/cm^{-1}	ϕ_{fl}	τ/ns	k_{rad}/sec^{-1}
			TOL			
1	89700 (451)	477	1210	0.010	0.05 (80%) 0.16 (20%)	2.0×10^8
2	91000 (450)	475	1170	0.010	0.05 (80%) 0.16 (20%)	2.0×10^8
3	55100 (479); 57900 (504)	540; 578 (sh)	1320	0.251	0.900	2.8×10^8
4	72100 (460)	514; 558 (sh)	2280	0.025	0.07	3.6×10^8
M	52700 (440)	462	1080	0.576	1.95	2.9×10^8
			DCM			
1	91400 (464)	506	1790	0.003	0.01 (85%) 0.17 (15%)	3.0×10^8
2	93700 (464)	504	1710	0.003	0.02 (85%) 0.19 (15%)	1.5×10^8
3	64100 (523)	605	2590	0.313	1.2	2.6×10^8
4	75800 (485)	582	3440	0.078	0.27	2.9×10^8
M	56200 (450)	483	1520	0.656	2.47	2.6×10^8

Whereas the monomer lifetime is in the nanosecond range, the biscoumarin samples display lifetimes of the order of tens/hundreds of picoseconds. The lifetimes in DCM solutions are higher than those in TOL for sample **3**, **4** and **M**, whereas they are slightly lower for samples **1** and **2**. This parallels the trend of luminescence quantum yield, in fact the calculated radiative rate constants k_{rad} $=\phi_{fl}/\tau$ are, for all samples, almost unaffected by solvent polarity, within experimental error.[11] This, in broad terms, indicates that the triplet yield (ϕ_{isc}) which occurs from the lowest singlet excited state in competition with the radiative deactivation, should also be unaffected by the solvent. From the polymerization viewpoint, the formation of a high triplet yield is crucial. The maximum achievable triplet yield is the difference between unity and the emission quantum yield. From this simplified approach, the lower limiting triplet yield can be derived for sample **6a**, which has the highest emission quantum yield, ϕ_{fl} = 0.25 and 0.31 in TOL and DCM respectively. 2PA photopolymerization is a very complex process, therefore the number of parameters affecting the process is quite large. However, as formerly pointed out,[10] the luminescence properties and hence the triplet yield formation can give a broad indication.
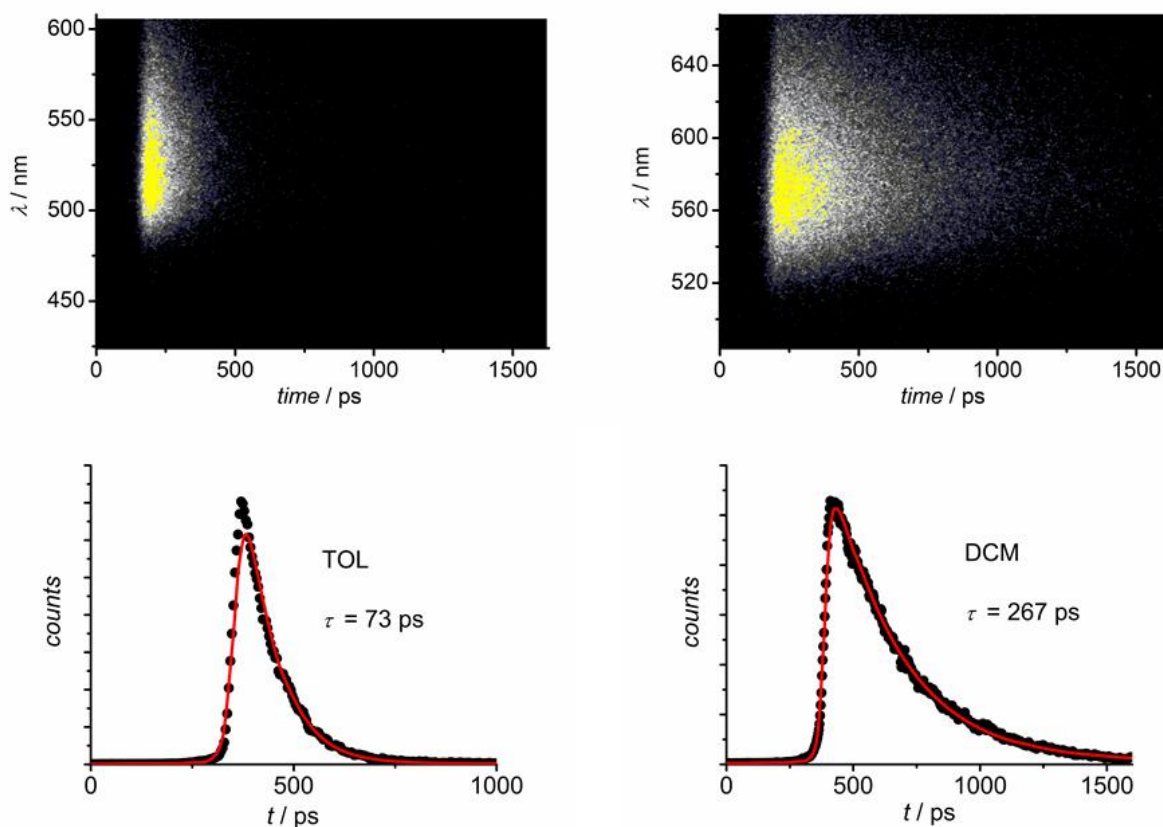
Figure 5.3. Streak camera images (upper line) of compound **4** in TOL and DCM. The time decays registered on the emission maxima with the exponential fitting are shown (bottom line).

As a final step in the characterization of the lowest excited states of the samples, we determined the luminescence properties at 77 K in a rigid TOL glass. The results of the luminescence experiments at 77 K are summarized in Table 5.2. This determination gives a precise E_{00} for the singlet excited level, for which we conventionally assume the energy of the emission maxima at 77 K, and it can provide the triplet energy level from the phosphorescence spectra.

In samples **1** and **2** a high triplet quantum yield is expected, based on the literature data (ϕ_{isc}= 0.92)[7a] for very similar samples. The phosphorescence of samples **1 - 4** can be detected in TOL glasses, whereas for monomer **M**, the use of a heavy atom solvent as ethyl iodide (EtI) is required (Figure 5.4). The presence of the EtI increases the spin orbit coupling and consequently the triplet yield and allows detection of the phosphorescence of **M**, characterized by a high luminescence quantum yield and hence by a low ϕ_{isc}. Figure 5.4 illustrates some representative examples of the fluorescence and phosphorescence spectra detected at 77 K. The phosphorescence lifetime is about 25 ms for all samples.

The singlet-triplet splitting is of the order of 0.36 - 0.40 in samples **1 - 4** and increases to 0.54 in monomer **M**. A larger splitting is commonly associated to a more difficult intersystem crossing, and apparently this is the case here.
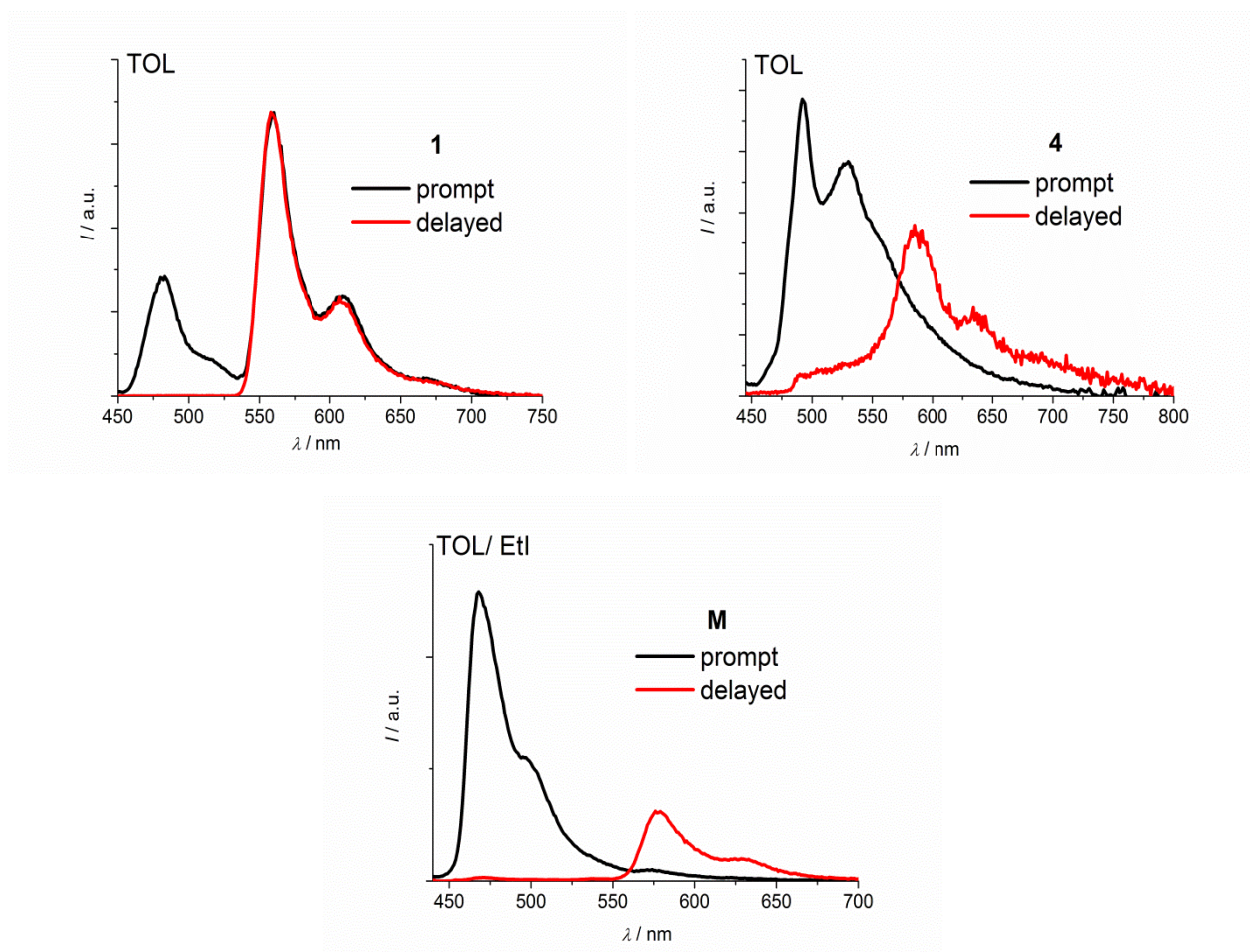
Figure 5.4. Arbitrarily scaled prompt and delayed luminescence measured in glassy solutions at 77 K for 1 and **4** in TOL and for **M** in TOL/EtI. Excitation was at 430 nm.

Table 5.2. Band maxima and energies of fluorescence and phosphorescence in TOL solid matrix at 77 K. For model **M**, the solvent is TOL: EtI (1:1).

	State	λ_{em}^{max}/nm	E/eV
77 K			
1	^{1}1	482	2.57
	^{3}1	560; 609	2.21
2	^{1}2	482	2.57
	^{3}2	559; 607	2.21
3	^{1}3	494; 545	2.51
	^{3}3	587; 625	2.11
4	^{1}4	493; 529	2.51
	^{3}4	587; 629	2.11
M	^{1}M	462; 494	2.68
	^{3}M	578; 631	2.14

80

Two photon absorption. 2PA properties of the compounds were investigated by using the Z-scan technique in the group of Dr. Maria Farsari. The 2PA cross-sections values are collected in Table 5.3 and a photograph illustrating some microstructures fabricated with the investigated compounds as photoinitiators is shown in Figure 5.5. More details can be found in reference [12].
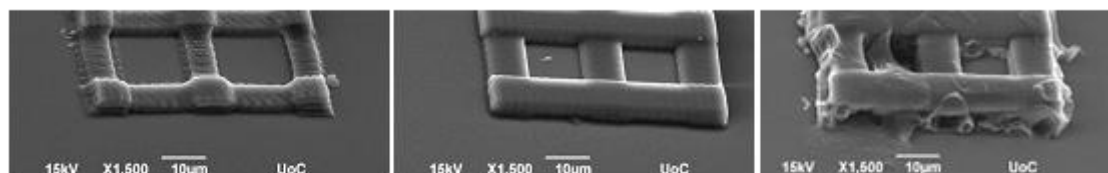
Figure 5.5. Microstructures fabricated in Dr. Maria Farsari's lab by using the investigated compounds as photoinitiators.

Table 5.3. 2PA cross-section values of the compounds measured by Z-scan technique in DCM at 800 nm. Data measured in the group of Dr. Maria Farsari.

	C_M	σ_2/ GM
1	0.01	153
2	0.01	90
3	0.01	55
4	0.01	401

Cells adhesion and proliferation on various materials surfaces and on the polystyrene control surface were tested in the group of Maria Chatzinikolaidou. The cells were monitored between 1 and 7 days, as shown in Figure 5.6. A clear proliferation increase with a dense layer of well-spread flattened cells completely covering all material surfaces was observed.
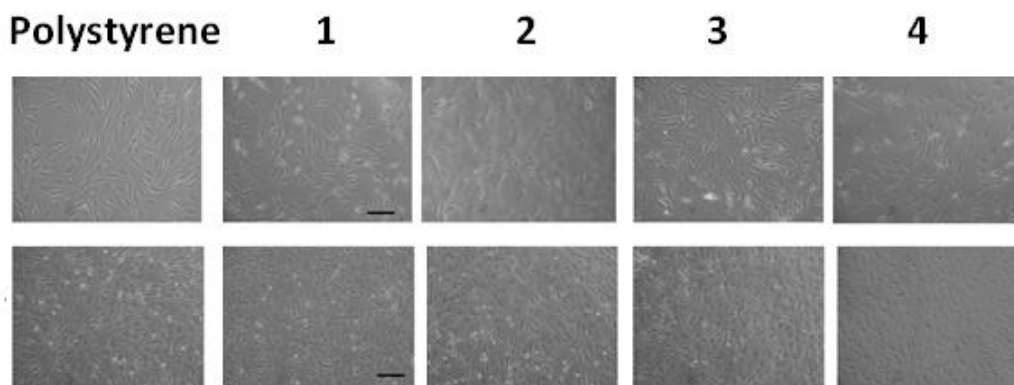
Figure 5.6. Optical microscopy images of pre-osteoblastic cells seeded on polystyrene and custom-made photoinitiators **1- 4**: after 1 day (upper line) and 7 days (bottom line). Scale bar represents 50 μm.

5.1.3. Conclusions

A series of four biscoumarins photoinitiators, together with their monomeric model, were photophysically studied by means of steady state and time resolved techniques. The experimental data showed that the central ring affects significantly their photophysical properties. Whereas simple biscoumarins showed strong solvent dependency, registering a decrease of luminescence and lifetime in more polar DCM, the ones possessing a central ring behaved contrarily, with an increase in the parameters. Intense phosphorescence spectra were detected for some of the compounds, indicative of an efficient triplet formation.

By using these structures as photoinitiators, 3D microstructures were successfully fabricated. The experimental results showed that the compound with the highest 2PA cross-section has the lowest fabrication window, whereas the simple biscoumarins showed the largest one. This is in agreement with photophysical data, which proved that in the former compounds the triplet is formed with high quantum yield.

5.2. Two photon systems for uncaging purposes

5.2.1. Introduction

Two photon uncaging (or photolysis) represents a non-invasive and optimum method for the release of molecules in biological systems.[13] It has the advantage of being a fast process and non-invasive for the release, up to the cellular level. A variety of biomolecules as enzymes,[14] proteins,[15] nucleotides[16] or neurotransmitters[17] were released by using photolysis method.

Recently, the two photon uncaging *via* photoinduced electron transfer process (PeT) gained a lot of interest. This strategy involves the transfer of one electron from the electron donor (2PA photosensitizer) to the electron acceptor (uncaging group), followed by the immediate release of the caged molecule. Although many groups can be used as caging groups in PeT systems, phenacyl esters, picolinium esters and nitrobenzil derivatives are attracting considerable interest. Falvey et al. pioneered the work in photolysis processes *via* photoinduced electron transfer. They developed the first PeT uncaging system for the trapped phenacyl.[18] They started by using *N,N*- dimethylaniline as photosensitiser[19], and continued with the use of a covalently linked system.[20] Both *N,N*-dimethylaniline and anthracene were linked to phenacyl uncaging group with ester bonds. Only *N,N*- dimethylaniline showed the release of acetic acid upon irradiation, whereas anthracene showed no evidence of uncaging. It was assumed that the anthracene triplet state prevented the formation of the charge separated state, and consequently the molecule could not be released. Phenacyl groups exhibiting very high protecting and deprotecting quantum yields (>80%), have been reported.[18]

The same group established that picolinium salts are capable of uncaging *via* PeT.[21] The uncaging of acetic acid from *N*-methyl-4-picolinium acetate perchlorate from a variety of donors (as BODIPY, carbazole and coumarin derivatives) was demonstrated using ^{1}H NMR spectroscopy.[21] Moreover, the electron transfer occurrence was proved by flash photolysis experiments, since transient absorption bands at 410, 690 and 770 nm were detected. The peak at 410 nm corresponds to the *N*-methyl-4-picolinium radical ion, while the other peaks are related to the donor radical cation.

Up to date there are no examples of uncaging of nitrobenzyl *via* PeT, but the group was used to cage phosphates, carboxylic acids, alcohols and amines by Norrish type II mechanism.[22]

Regarding the caged groups, the neurotransmitter γ-aminobutyric acid (GABA) is a good candidate due to its biological function. Furthermore, the research performed to date on the release of GABA is rather limited. Two-photon uncaging of GABA was demonstrated by using a

nitroindoline derivative in brain tissue.[23] A recent work of Specht et al. reported that only EANBP-GABA can release quantitatively GABA *in vitro* with uncaging cross-section over 1 GM.[24]

Within this context, three dyads designed for optimized intramolecular PeT and in view of caging GABA, are reported. The characterization of the electron transfer process was performed by steady state and time resolved methods. The results obtained on the charge separated state, should be able to help in the evaluation of the use of these arrays as uncaging systems for neurotransmitter GABA and help in the design of optimized 2PA uncaging systems.

5.2.2. Results and discussion

One photon absorption. The photophysical measurements of the compounds shown in Chart 5.2 were performed in non-polar toluene (TOL, $\varepsilon = 2.38$) and polar methanol (MeOH, $\varepsilon = 32.66$). The absorption spectra of the dyads and models in MeOH are collected Figure 5.7.
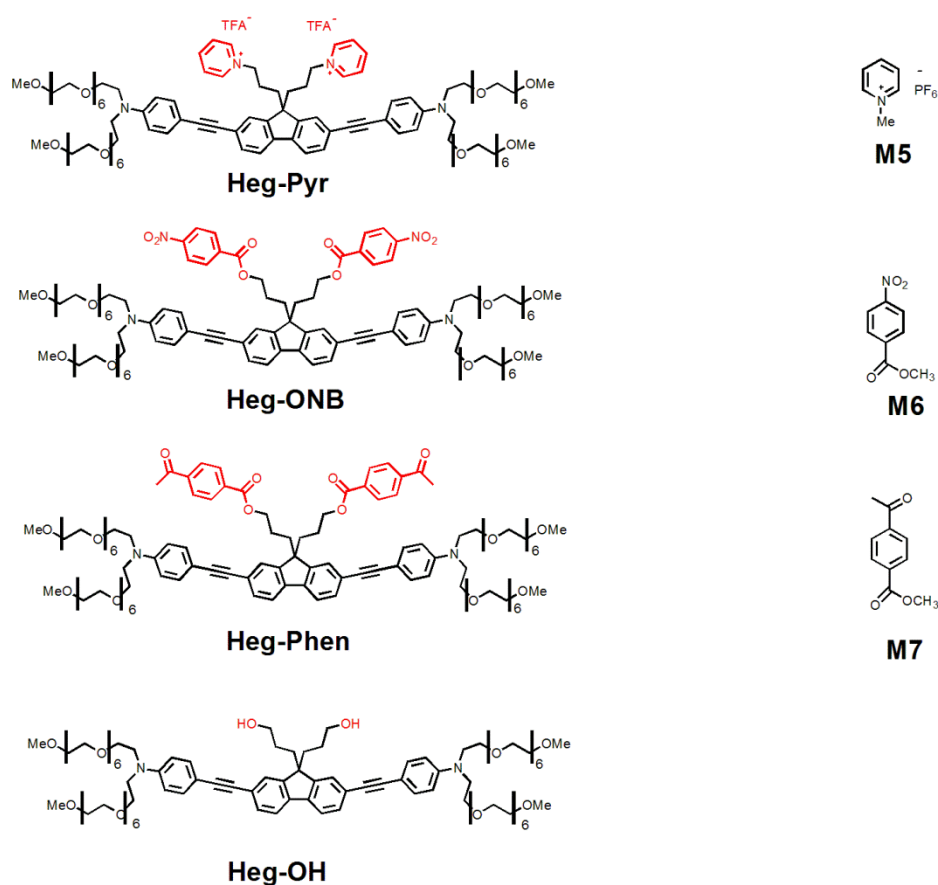
Chart 5.2. Structures of the investigated compounds.
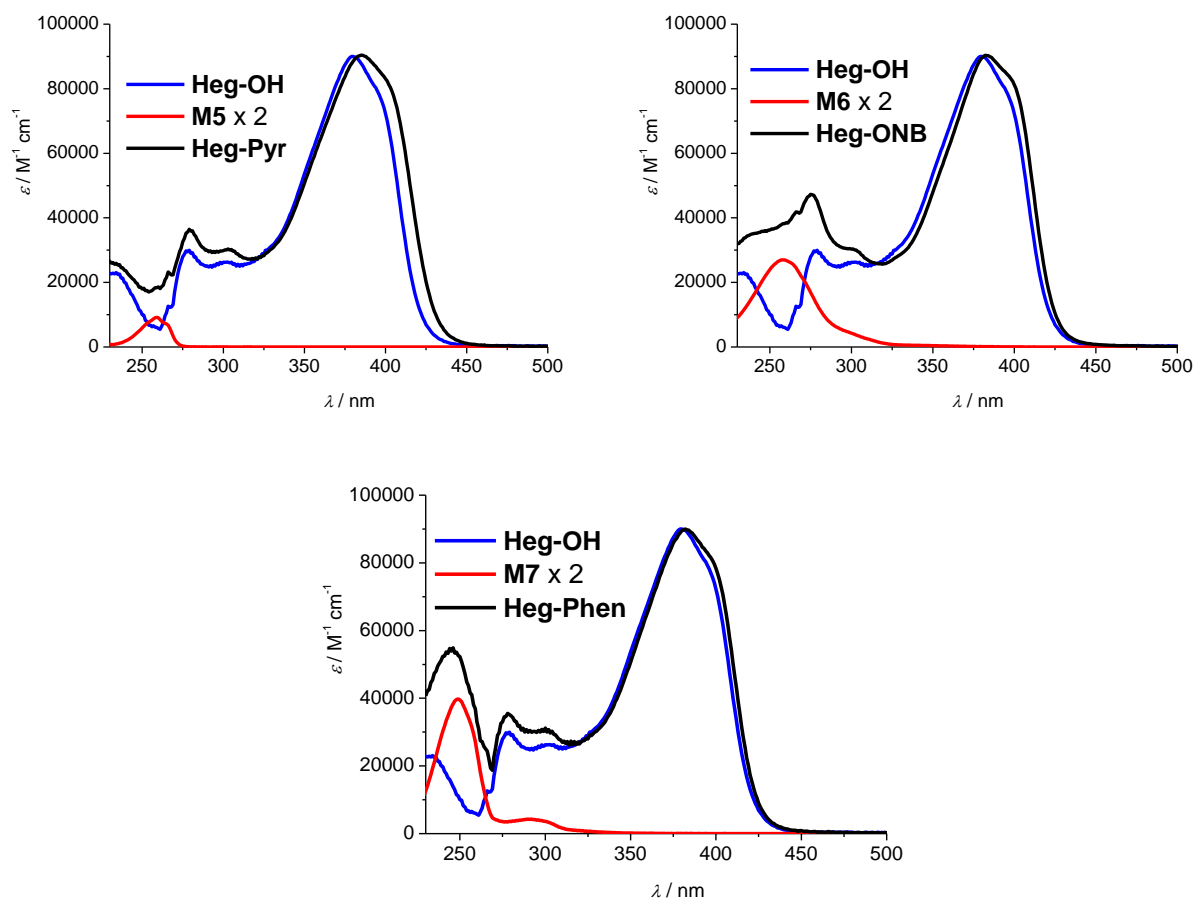
Figure 5.7. Absorption spectra of the dyads and models in MeOH solutions.

The spectra of the models **M5**, **M6** and **M7** are characterized by absorption bands under 320 nm and with extinction coefficients (ε) between 5 000 and 20 000 M^{-1} cm^{-1} in MeOH. The absorption spectra of the dyads maintain the fluorene features, displaying broad bands between 350 and 450 nm (ε about 100 000 M^{-1} cm^{-1}) (Figure 5.7). A minor bathochromic shift of the fluorene bands and a hypsochromic shift of the acceptors can be observed in the dyads, but overall their absorption spectra are well-reproduced by the addition of the absorption of the constituent models (Figure 5.7). This indicates a weak electronic coupling of the different moieties of the dyads in the ground state.
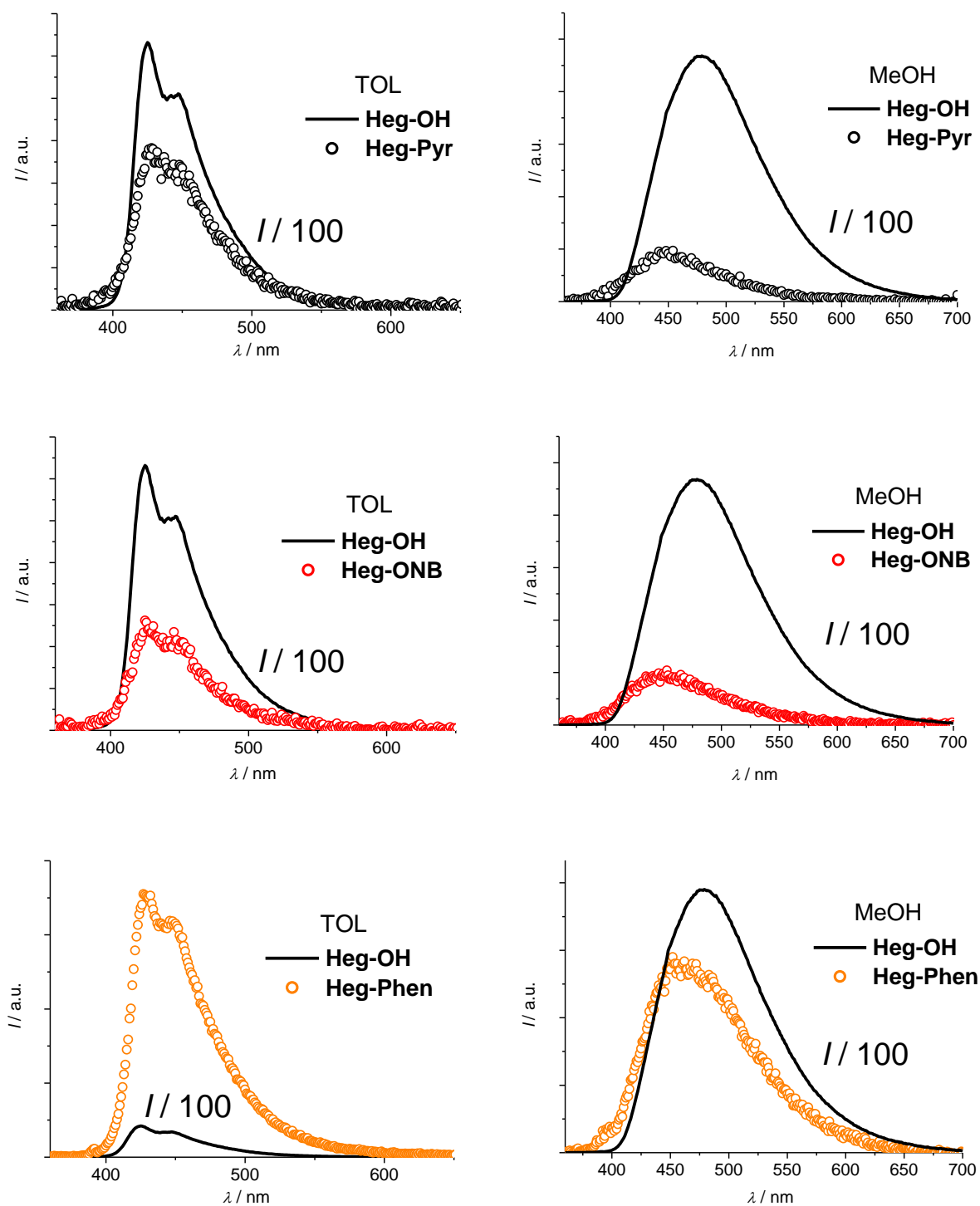
Figure 5.8. Luminescence spectra of model **Heg-OH** divided by the indicated value and of dyads in TOL and MeOH at room temperature. Excitation was at 350 nm and $A_{350\ nm} = 0.10$.

The models **M5**, **M6** and **M7** are non-emissive at room temperature after excitation on the respective bands, both in TOL and MeOH. On the contrary, selective excitation at 350 nm on the fluorene chromophore in optically matched model and dyads solutions returned the luminescence spectra collected in Figure 5.8. The fluorescence of model **Heg-OH** is structured in TOL and the

shape and band positions are maintained in the dyads. In MeOH the spectrum of model fluorene is structureless and bathochromically shifted by almost 50 nm with respect to the spectrum in apolar toluene. In MeOH, the fluorescence band appears slightly hypsochromically shifted in the dyads with respect to the model. Taken altogether, these data indicate the presence of charge transfer interaction in the excited state of the model **Heg-OH**, stabilized in polar MeOH but slightly destabilized in the dyads, with respect to the model in the same solvent. The fluorene model **Heg-OH** emits strongly, with $\phi_{fl} = 0.52$ in TOL and 0.48 in MeOH (Table 5.4). Its fluorescence is dramatically quenched in the dyads with respect to the model, more in MeOH than in TOL (Figure 5.8 and Table 5.4). The fluorene luminescence is quenched in TOL to 0.5% of the initial model fluorescence in **Heg-Pyr** and **Heg-ONB**, and to 8% in **Heg-Phen**. In MeOH the quenching in the first two dyads reduces the fluorescence to below 0.5% and in **Heg-Phen** to 0.6% of the original model fluorescence. Since an energy transfer process in the dyads from the fluorene to the acceptor is thermodynamically unfeasible (see energy levels on Table 5.4), the quenching in the dyads is an indication of an electron transfer process.

Time resolved luminescence experiments were performed by Time Correlated Single Photon Counting (TCSPC) technique with excitation at 373 nm and resolution of 0.3 ns. The lifetime of the model **Heg-OH** was measured as 0.75 ns in TOL and 1.30 ns in MeOH. The fluorene based chromophore in the dyads was too short- lived and a picosecond laser ($\lambda_{ex} = 355$ nm) with Streak Camera detection was necessary. The fluorescence lifetimes of fluorene moiety in MeOH in **Heg-Pyr**, **Heg-ONB** and **Heg-Phen** were 15 ps, 18 ps and 43 ps, respectively. In TOL, slightly higher lifetimes were measured for **Heg-Pyr** (24ps) and **Heg-ONB** (21 ps), whereas for **Heg-Phen** a longer bi-exponential decay (66 ps and 352 ps) was detected (Figure 5.9 and Table 5.4), with a 50% contribution by each lifetime. The presence of two different lifetimes with an almost equivalent contribution in TOL solutions is indicative of the presence of two different populations of fluorene excited state with a similar weight, which do not equilibrate during the lifetime of the state. This might well correspond to two conformers with similar energy in the donor-acceptor structure, whose formation is favored in TOL solutions. In MeOH there is a single population as testified by the monoexponential decay (Figure 5.9).

Table 5.4. Photophysical parameters of the investigated compounds at room temperature and 77 K.

	Excited state	295 K			77 K		
		λ_{max}/nm	ϕ_{fl}[a]	τ/ns	λ_{max}/nm	τ/ns [b]	E/eV [d]
				TOL			
Heg-OH	^{1}Heg-OH	425; 447	0.52	0.75[b]	422; 448; 482	0.76	2.94
	^{3}Heg-OH				511; 548	72×10^6; 224×10^6	2.43
Heg-Pyr	^{1}Heg-Pyr	426; 449	0.003	0.024[c]	442; 471 [e]	0.50 [e]	2.90 [e]
	^{3}Heg-Pyr				574; 620	300×10^6	2.16
Heg-ONB	^{1}Heg-ONB	425; 451	0.002	0.021[c]	428; 454	0.30	2.90
	^{3}Heg-ONB				570; 611	348×10^6	2.17
Heg-Phen	^{1}Heg-Phen	426; 448	0.04	0.066 ; 0.352[c]	426; 450	0.70	2.91
	^{3}Heg-Phen				567; 611	360×10^6	2.18
M7	^{1}M7	-	-	-	-	-	-
	^{3}M7				409; 438; 471; 504	48×10^6; 124×10^6	3.03
				MeOH			
Heg-OH	^{1}Heg-OH	478	0.48	1.30[b]	428; 446	0.92	2.89
	^{3}Heg-OH				548, 590	349×10^6	2.26
Heg-Pyr	^{1}Heg-Pyr	451	0.001	0.015[c]	434; 460	0.79	2.86
	^{3}Heg-Pyr				572; 613	318×10^6	2.16
Heg-ONB	^{1}Heg-ONB	452	0.001	0.018[c]	430	0.30	2.88
	^{3}Heg-ONB				-[f]	-[f]	-[f]
Heg-Phen	^{1}Heg-Phen	462	0.003	0.043[c]	426; 449	0.77	2.91
	^{3}Heg-Phen				567; 613	274×10^6	2.18
M7	^{1}M7	-	-	-	-	-	-
	^{3}M7				411; 440; 471	55×10^6; 235×10^6	3.01

[a] Fluorescence quantum yield. [b] Lifetime by TCSPC (resolution 0.3 ns). [c] Lifetime by Streak Camera (resolution 10 ps). [d] Energy levels of the excited state from luminescence maxima at 77 K. [e] Emission from an aggregate; the monomer singlet excited state is expected to have an energy of ca. 2.90 eV, similar to that of fluorene in the other dyads. [f] Not observed.
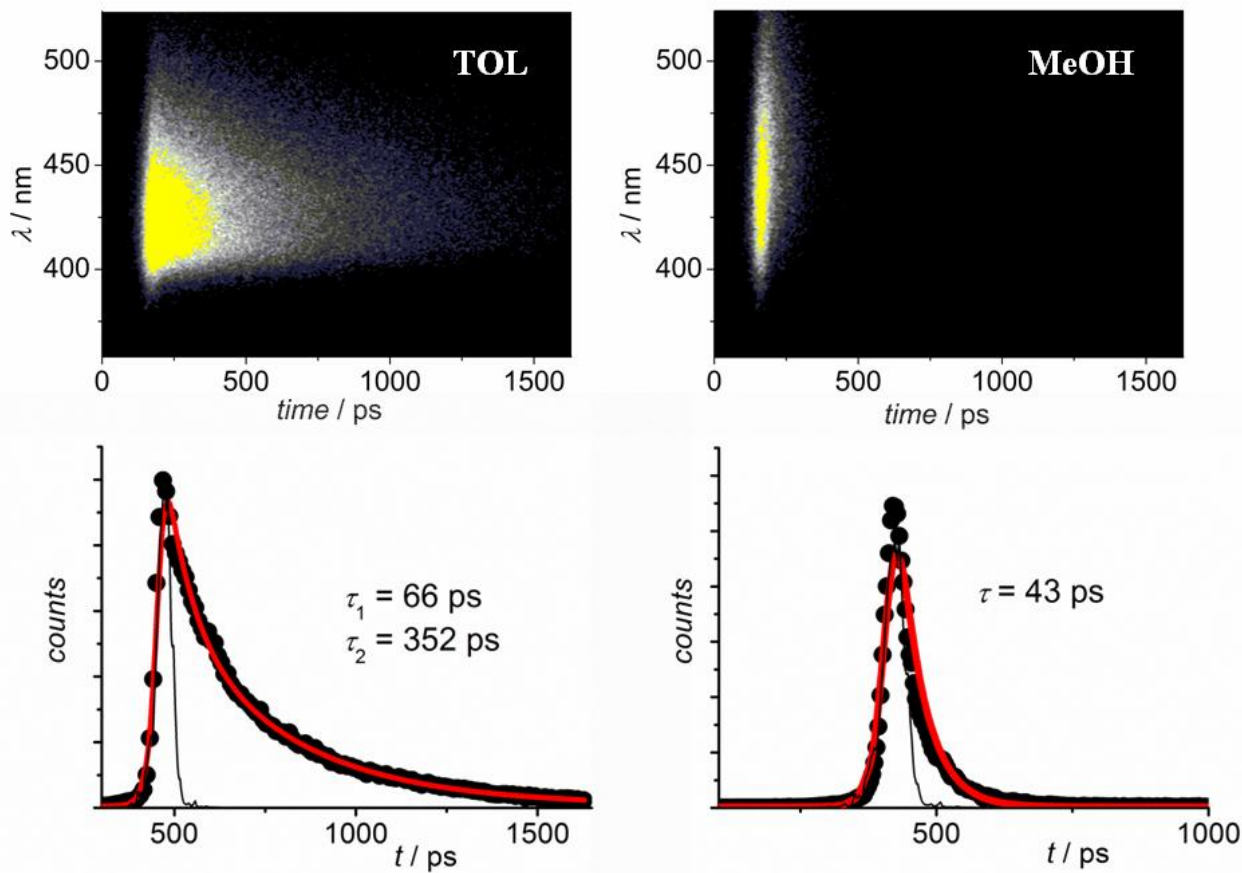
Figure 5.9. Streak camera images of **Heg-Phen** in TOL and MeOH .The time profiles data at 435 nm in TOL and 450 nm in MeOH are displayed with the fitting and the flash profile.

Luminescence experiments were run at 77 K in rigid glasses and the fluorescence spectra of the samples registered upon excitation at 370 nm in TOL are reported in Figure 5.10. Luminescence data at 77 K have only a qualitative meaning, as the conditions of the sample and the geometry of excitation (glass of irreproducible quality in cylindrical tube within a quartz Dewar filled with liquid nitrogen) do not allow for a direct comparison of signals from optically matched samples. However, it is quite evident that in TOL the electron donor fluorescence is still quenched in **Heg-ONB**, whereas in **Heg-Pyr** and **Heg-Phen** an intense fluorescence from fluorene moiety is detected. The fluorescence of **Heg-Pyr** is remarkably broader and bathochromically shifted compared to the others dyads and we assign it to an aggregate. Similar data were obtained in MeOH glass (data not shown). A more conclusive confirmation on the quenching of the fluorene chromophore luminescence at 77 K comes from lifetime determinations. Following excitation at 373 nm by a TCSPC apparatus, lifetimes of 0.50 ns, 0.30 ns, and 0.70 ns were measured for **Heg-Pyr**, **Heg-ONB**, and **Heg-Phen** in TOL against a model lifetime of 0.76 (Table 5.4). In MeOH a model

lifetime lower than at room temperature is measured, 0.92 ns against 1.30 ns. The reason of this behavior is unclear, but it might be ascribable to an emitting state different from that at room temperature. However the luminescence lifetime in the dyads in MeOH is 0.79, 0.30, and 0.77 ns for **Heg-Pyr**, **Heg-ONB**, and **Heg-Phen** respectively. This indicates that only in **Heg-ONB** the quenching process due to electron transfer is still effective. In the dyads **Heg-Pyr** and **Heg-Phen**, the reduction in lifetime is modest and it is difficult to state whether the small variation represents a real quenching or a change of the fluorene moiety lifetime, induced by a change in radiative/non-radiative decays of the excited state in the dyads. A decreased or even suppressed quenching by electron transfer in glassy solutions is well known and is often used as an evidence of the identification of the quenching process, i.e. electron- against energy-transfer. In fact, the rigidification of the solvent prevents its re-polarization around a polar state formed upon electron transfer and destabilizes (i.e. raise the energy) the charge separated states. This in general, except for highly exergonic reactions at room temperature, is sufficient to decrease the driving force for charge separation to an extent that it is not anymore feasible.

Luminescence experiments at 77 K are also useful to establish the existence of emitting triplets. In order to do so, luminescence was detected with a phosphorimeter, which allowed detecting delayed luminescence spectra. This technique not only allowed to detect a weak phosphorescence from **Heg-OH** with bands around 510 and 550 nm, but also to observe a rather strong phosphorescence with bands at about 570 and 615 nm in all dyads in TOL (Figure 5.10). Almost identical results, not shown here, were obtained for MeOH solutions of **Heg-Pyr** and **Heg-Phen**, but not in **Heg-ONB**, where no triplet phosphorescence was detected. We identify the emitting species as a fluorene based triplet, bathochromically shifted in the dyads with respect to the one seen in **Heg-OH** for the different substituents present and the slight charge-transfer character of the excited state in the arrays. The fluorene based triplet, ^{3}Heg-Pyr, ^{3}Heg-ONB and ^{3}Heg-Phen can be formed in the dyads at 77 K as a decay product of the unquenched corresponding singlet excited state. We can infer from the moderate fluorescence lifetime reduction to be a relatively large amount, except for the case of **Heg-ONB** in MeOH. However, formation of triplet as a consequence of the charge separated state (CS) recombination cannot be excluded. Upon excitation at 300 nm in TOL and 270 nm in MeOH of the acceptors, an intense structured phosphorescence was detected for acceptor **M7**, with bands around 410, 440 and 468 nm in both solvents, Figure 5.10. The phosphorescence lifetimes for all compounds are in general around 250 – 350 ms (Table 5.4). In some cases they display a non-exponential decay, suggesting the involvement of aggregates in the glass.
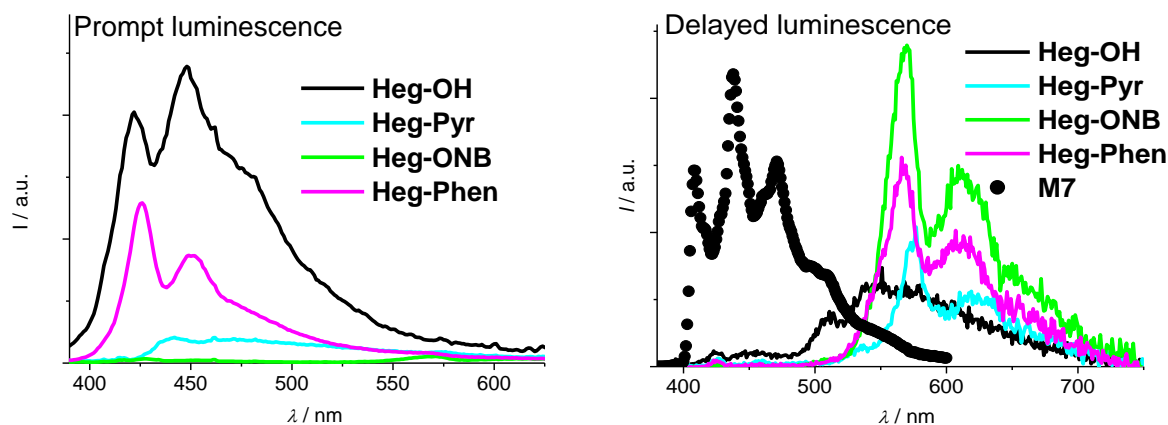
Figure 5.10. Prompt and delayed (1 ms delay, 4 ms gate) luminescence spectra of models **Heg-OH** and **M7** and dyads in TOL glass at 77 K. Excitation was at 370 nm.

In order to detect the absorbing transients, as products of the electron transfer process, transient absorption experiments with picosecond resolution (λ_{ex} = 355 nm) were performed. Fluorene model **Heg-OH** and the dyads were examined in TOL and MeOH. Solutions of the model **Heg-OH** in TOL displays a structured band (with maxima at 680 nm and 740 nm and τ = 0.7 ns) whereas the same sample in MeOH has a single broad maximum at 675 nm (τ = 1.2 ns) (Figure 5.11). Based on the reasonably good agreement with the corresponding fluorescence lifetime, 0.75 and 1.30 ns the species can be positively ascribed to the singlet excited state of the fluorene chromophore.
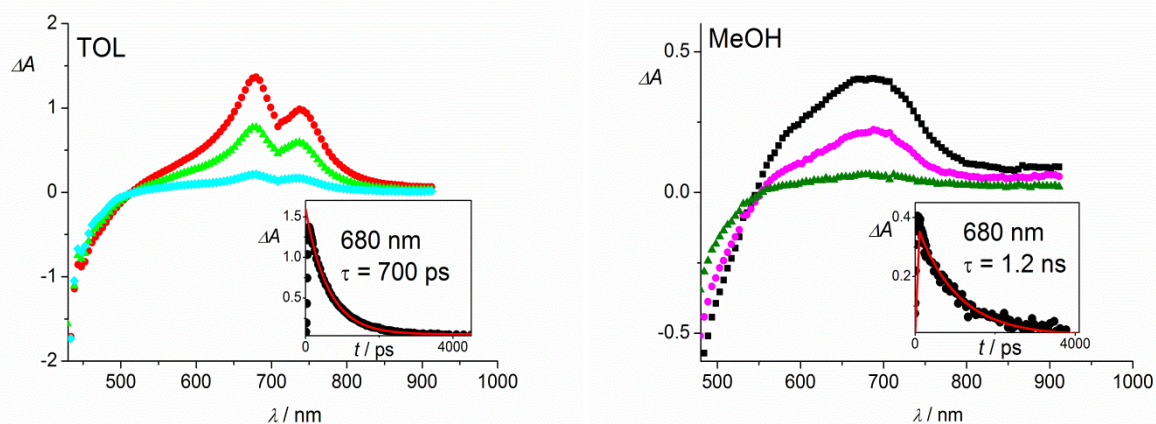
Figure 5.11. Left-TOL: Transient absorption spectra of **Heg-OH** detected after end of pulse (red), 450 ps (green) and 1400 ps (cyan). Right-MeOH: Transient absorption spectra of **Heg-OH** detected after end of pulse (black), 500 ps (magenta) and 1800 ps (olive). In the inset, the time profiles at the selected wavelengths with the corresponding fitting.
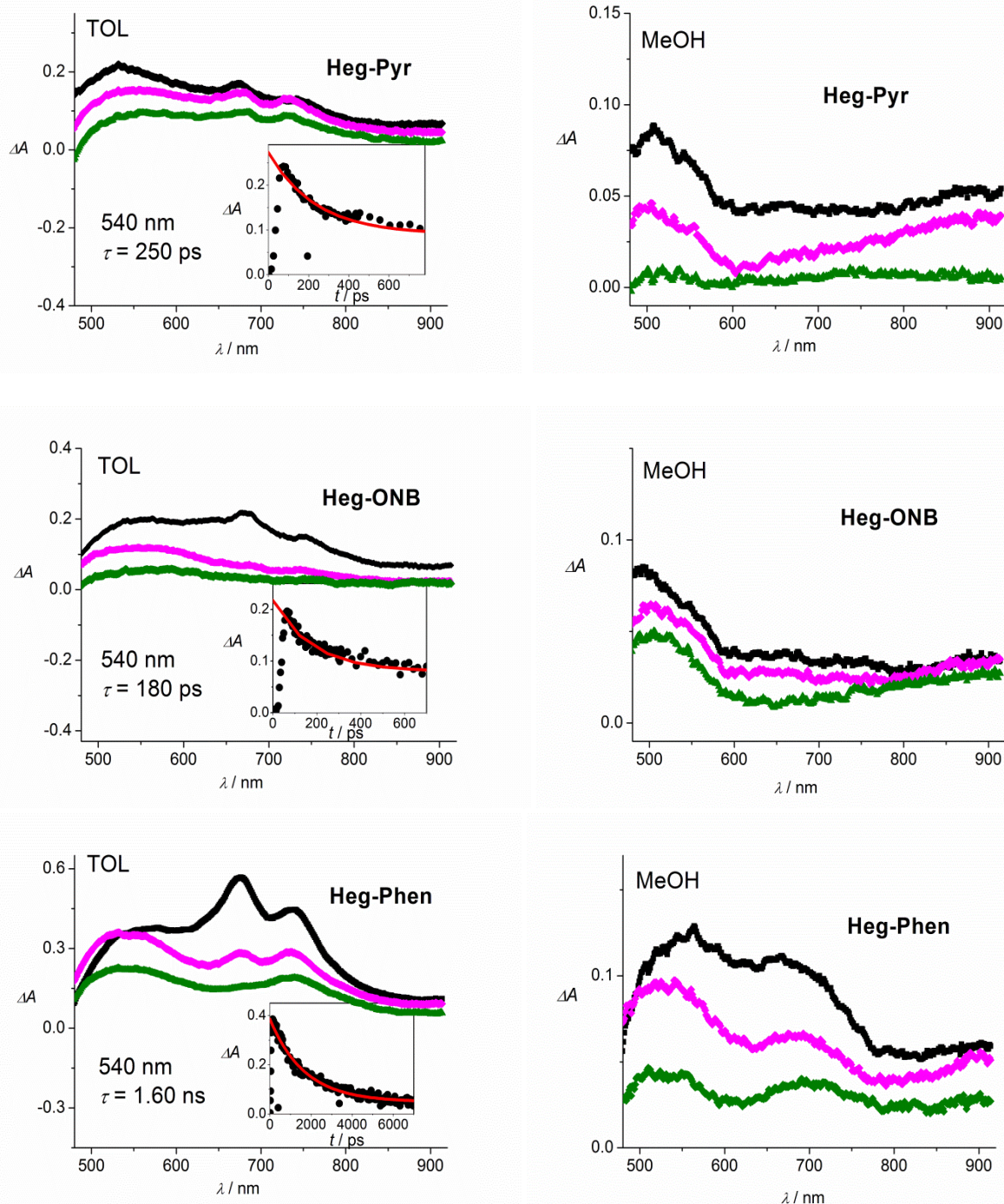
Figure 5.12. Transient absorption spectra of arrays detected after 35 ps pulse (355 nm, 3 mJ pulse) at various delay times. TOL: end of pulse (black), 275 ps (magenta) and 1 ns (green) with the fitted time profiles at 540 nm in the insets. MeOH: end of pulse (black), 100 ps (magenta) and 140 ps (green).

The fluorene singlet excited state ^{1}Heg-OH, was present during the pulse but rapidly decayed to produce a positive band between 500 and 600 nm (Figure 5.12). Consistent with the literature data reporting an absorption between 580 and 700 nm for fluorene cation, depending on the substitution type,[25] we ascribe this band to the cation of the fluorene chromophore. This is a confirmation of the occurrence of electron transfer with production of the charge separated state

formed upon LUMO-LUMO electron transfer from excited fluorene to the acceptor. The corresponding reduced radicals of the acceptor units, M5[-] and M6[-] (for M5[-] at 410 nm,[26] for M6[-] at 435 and 465 nm[27]) are not detected since their absorption bands are out of the spectral range of detection of the pump and probe apparatus. Only M7[-] has an absorption band at 580 nm,[28] but overlays the fluorene cation band. In TOL the cation band disappears with lifetimes of 0.25, 0.18 and 1.6 ns for Heg[+]-Pyr[-], Heg[+]-ONB[-] and Heg[+]-Phen[-], respectively. One can also notice the persistence of some free fluorene chromophore in the solution of **Heg-Pyr**, (Figure 5.12) very likely coming from a slight degradation of the solution under the high energy laser irradiation. In MeOH solutions the spectra of the fluorene cation can be observed (Figure 5.12), but their decays (not shown here) are faster than in TOL: ca. 30 ps for Heg[+]-Pyr[-] and Heg[+]-ONB[-] and ca. 60 ps for Heg[+]-Phen[-].
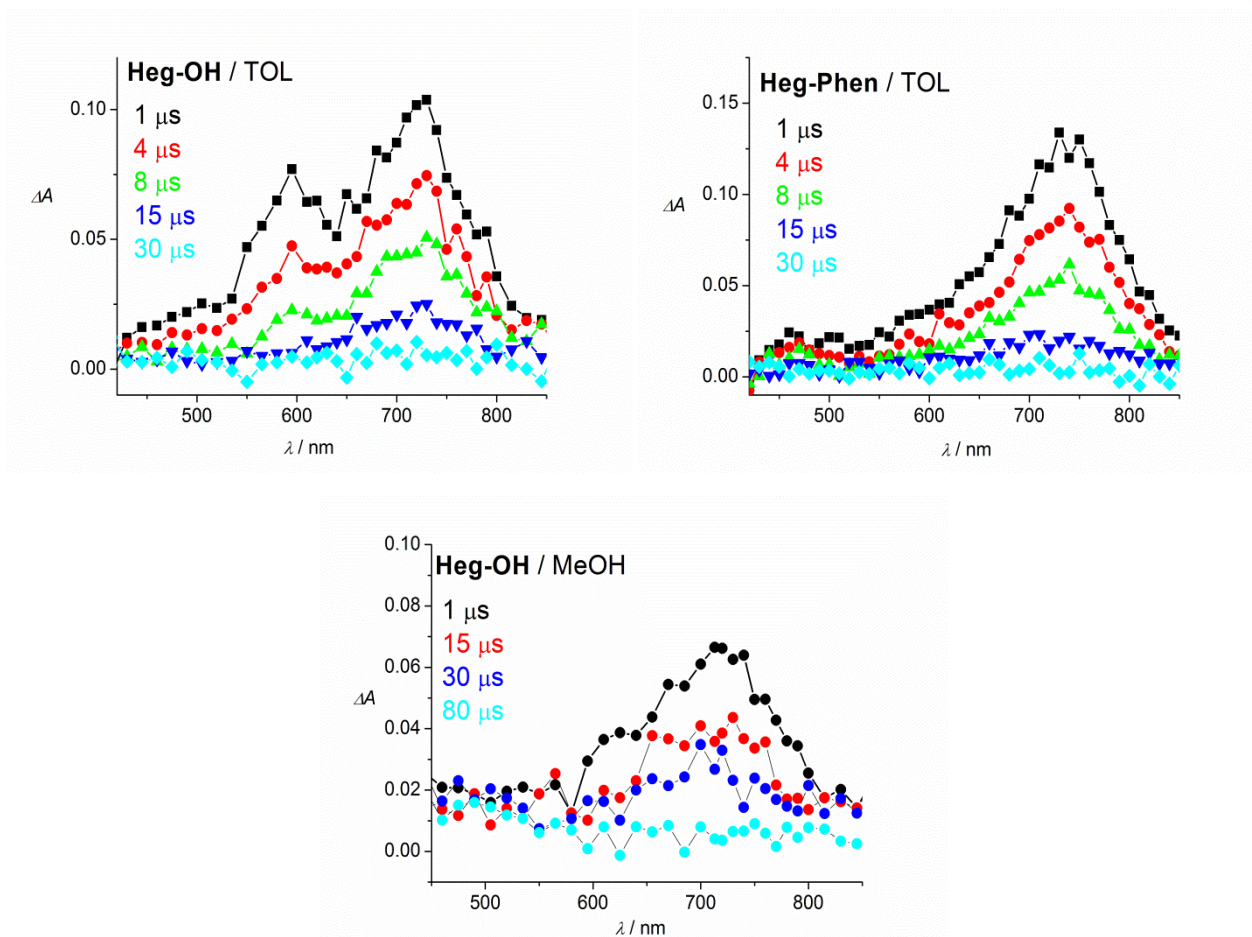
Figure 5.13. Transient absorption spectra of **Heg-OH** in TOL and MeOH and **Heg-Phen** in TOL after laser excitation (18 ns pulse, 355 nm, 3 mJ/pulse).

The poor accumulation of charge separated state which decayed during the pulse (35 ps FWHM) and the lifetime close to the resolution limit prevented a more precise determination. As already noticed for the luminescence quenching, i.e. the charge separation reaction, also charge

recombination is faster in the polar MeOH compared to TOL, and this can be explained by the thermodynamics of the processes (see below).

Transient absorption determinations in the microsecond range were performed in order to obtain information on triplet excited states. Optically matched (A_{355} = 0.8) air free solutions of the arrays and model **Heg-OH** in TOL and MeOH solutions were examined by flash-photolysis after excitation at 355 nm. The end of pulse absorption spectrum of model (Figure 5.13) in TOL is characterized by two bands at 600 and 730 nm, with lifetime of 8 μs.[29] In MeOH the main band is at 720 nm and the 600 nm band is less pronounced. The lifetime is longer than in TOL, 28 μs. The presence of oxygen quenches the species with a rate of 4×10^9 M^{-1} s^{-1} in both solvents, in agreement with a triplet assignment. The data indicates a lower triplet yield for the MeOH solution, ca. 40 % lower than in TOL assuming a similar molar absorption coefficient. Being the fluorescence quantum yield in the two solvents similar (ca. 50%, see Table 5.4) this points to the presence of more efficient processes competitive to intersystem crossing in MeOH solution.

After excitation at 355 nm, **Heg-Pyr** did not display any transient absorption signal both in TOL and MeOH. In the same conditions, **Heg-ONB** displayed a very weak transient absorption band maximizing around 600 nm in TOL with a lifetime of 4 μs, which was absent in MeOH solutions (data not shown). The species reacts with oxygen with a rate of the order of 10^{10} M^{-1} s^{-1}, however we are unable to assign the band at the moment and a more a detailed study would be necessary to ascribe it.

No signal is detected in MeOH solution of **Heg-Phen**. On the contrary, in TOL the end of pulse spectrum of Heg-Phen is very intense, with a strong band maximizing at 730 nm, Figure 5.13, similar to that detected in the model **Heg-OH** but with a much weaker shoulder at 600 nm. The species reacts with oxygen with a rate of 4×10^9 M^{-1} s^{-1}, confirming its identification as a fluorene centered triplet, ^{3}Heg-Phen. One might notice that, provided that the molar absorption coefficient of ^{3}Heg-OH is similar to that of ^{3}Heg-Phen, the yield of triplet in the dyad is more than expected. The quenching of the singlet excited state by electron transfer in **Heg-Phen** competes in fact with intersystem crossing, and the resulting triplet should be reduced to 28%, according to the singlet lifetime reduction (Table 5.4) . This is not the case here and the extra triplet might be produced by recombination of the charge separated state.

Excitation of the acceptors **M5**, **M6** and **M7** at 266 nm in MeOH solutions was also performed, but only for **M7** a transient signal was observed (Figure 5.14). We identified the triplet absorption of the phenacyl group around 330 nm, which decays with a lifetime of 20 μs, in agreement with former reports.[28, 30] A longer lived transient species with an intense maximum overlaying the one of triplet at 330 nm and a weaker band at 500 nm was also detected. Based on

literature data, the species is ascribable to an intermediate formed upon proton transfer reactions and this might be the case here, in protic MeOH.[30] The experiment on TOL solution of M7 was not possible since the 266 nm is absorbed by the solvent.
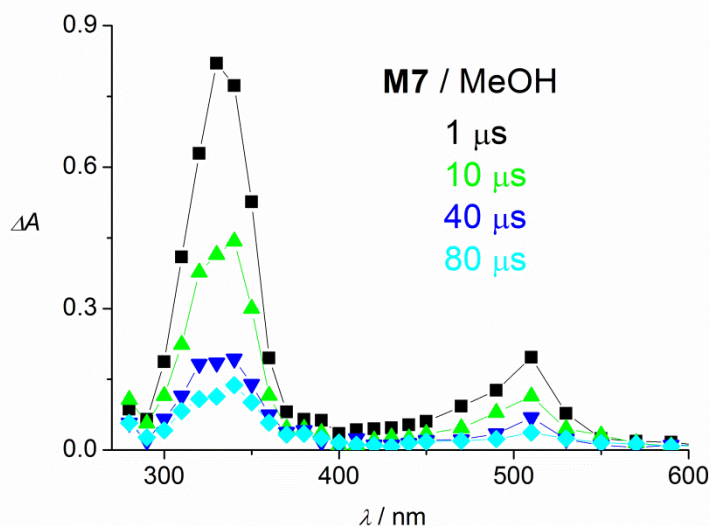
Figure 5.14. Transient absorption spectra of **M7** in MeOH solutions at various delays after laser excitation (18 ns pulse, 266 nm, 3 mJ/pulse).

Photoinduced processes. Schematic energy level diagrams for the three dyads are illustrated in Figure 5.15. The energy levels of the excited states are derived by the luminescence data obtained at 77 K (Table 5.4) and they are 2.90 eV for the singlet and 2.13 eV for the triplet localized on the fluorene unit of the dyads. Another triplet localized on the acceptor **M7** at above 3 eV is not relevant to the present discussion since it is higher that the relaxed excited state of excited fluorene. The electrochemistry data (Table 5.5) provide the parameters necessary for the determination of the energy levels of the charge separated (CS) state.

The CS state resulting from electron transfer from fluorene electron donor toward each of the electron acceptors in the dyads is calculated rather crudely in MeOH, simply from the addition of the energy necessary to oxidize the donor and to reduce the acceptor in the dyads (Table 5.5). This leads in the polar solvent to a CS state energy of 2.04 eV in **Heg-Pyr**, 1.88 eV for **Heg-ONB** and 2.56 eV for **Heg-Phen**. The determination of the CS energy levels in TOL solutions by applying the Weller equation,[31] largely overestimate the level of the charge separated state in apolar media,[32] especially when excited states with a charge transfer character as the present ones, are involved.[33] The formula is furthermore strongly dependent on geometric molecular parameters, liable to large errors in a flexible structure.[31] Therefore, we feel more appropriate to discuss the results on a qualitative basis, assuming for the CS state level in TOL a destabilization, with respect

to MeOH of ca. 0.3 eV. This is a very simplified view, but sufficient for the qualitative discussion of the results.

Table 5.5. Electrochemistry data vs. ferrocenium/ferrocene in tetrahydrofuran (THF) measured in the group of Harry Anderson.

Compound	Reduction potential / V	Oxidation potential / V
HegOH		+0.36
M5	-1.76	
M6	-1.47	
M7	-2.18	
HegPyr	-1.71	+0.33
HegONB	-1.51	+0.37
HegPhen	-2.20	+0.36

From the lifetime of the donor fluorescence quenching in the dyads (Table 5.4) rate constants corresponding to electron transfer process *1*, *charge separation*, can be determined from the relation

$$k = (1/\tau) - (1/\tau_0) \tag{5.1}$$

where τ and τ_0 stand for the lifetime of the fluorene moiety in the dyad and in the model respectively.

In MeOH the rates of charge separation are 6.6×10^{10} s^{-1} for **Heg-Pyr**, 5.5×10^{10} s^{-1} for **Heg-ONB**, 2.2×10^{10} s^{-1} for **Heg-Phen**. These are all very high rates, justified by a driving force for charge separation in MeOH of 0.86 eV for **Heg-Pyr**, 1.02 eV in **Heg-ONB** and of 0.34 eV in **Heg-Phen**. We can observe that whereas for larger driving forces there is almost no dependence on the ΔG (activationless regime)[34] some slight slowing down is noticed in the case of **Heg-Phen** characterized by the lower driving force, with $\Delta G_{CS} = $ -0.34 eV. In TOL the calculated rates are 4.0×10^{10} s^{-1} for **Heg-Pyr**, 4.6×10^{10} s^{-1} for **Heg-ONB**, 1.4×10^{10} s^{-1} and 1.5×10^9 s^{-1} for the two conformers populations of **Heg-Phen**. In apolar solvent, where all driving forces are reduced by a value of ca. 0.3 eV, we can still notice an activationless regime for **Heg-Pyr**, and **Heg-ONB**, $\Delta G_{CS} = $ -0.56 and -0.72 eV respectively, while in **Heg-Phen**, the less exergonic reaction ($\Delta G_{CS} = $ -0.04 eV) the rate is decreased remarkably. The above behavior is typical of the so called "normal Marcus region". [34]

On the contrary, a "Marcus inverted region" behavior, consisting in the decrease of the reaction rate with the increase of the driving force, can be noticed in the *charge recombination* (CR) reaction *2*. In MeOH the rates of *2* are poorly defined: **Heg-Pyr**, and **Heg-ONB** have lifetimes of the order of the instrumental resolution (30 ps in the absorption mode) and a rate of ca. 3.3×10^{10} s^{-1} can be calculated for both. Only **Heg-Phen** has a recombination rate lifetime longer, of the order of 60 ps which allows to calculate a rate of 1.6×10^{10} s^{-1}. The trend is however indicative of a reduction of the recombination reaction by increasing the driving force, 2.04 eV for **Heg-Pyr**, 1.88 eV for **Heg-ONB** and 2.56 eV for **Heg-Phen**, in agreement with the "Marcus inverted" behavior. This is more evident in TOL solutions, where rates of 4.0×10^9 s^{-1}, 5.5×10^9 s^{-1} and 6.2×10^8 s^{-1} can be measured. Whereas in the first two dyads the recombination is to the ground state, with a ΔG_{CR}= -2.34 eV and -2.18 eV, in the case of **Heg-Phen** the remarkably high ΔG_{CR} = -2.86 decreases the back electron transfer reaction to an extent that the recombination to triplet, step *3*, thermodynamically feasible, becomes competitive. This is evident from the triplet yield in this dyad, approximately 1.3 times higher than the one in the model, Figure 5.13. This is made possible by the fact that, whereas in the model the triplet yield is, at most, 0.48 (i.e. $1-\phi_{fl}$) in the dyad the new path of triplet formation occurring through the CS state (formed with a 70% yield from the singlet excited state), is more efficient. The occurrence of recombination of the CS state to a lower triplet rather than to the ground state has been reported previously not only for heavy metal containing arrays,[35] but also for systems based on purely organic chromophores. In one case it has also been observed in a very similar donor-acceptor dyad based on anthracene and on chromophore **M7**.[28]

What is however surprising in the excited state dynamics of the present dyads, is the fast rate of both the forward and the back electron transfer. The latter are orders of magnitude faster that those reported for closely related systems based on similar photoinduced electron-transfer releasable protective groups. Lifetimes of the charge separated states of the order of 10^{-7} s in acetonitrile have been in fact reported for these systems, characterized by similar thermodynamic parameters.[28] In absence of other explanations, we ascribe the poor performances of the present systems in term of lifetime of charge separation, to the flexibility of the dyad. This can allow, in spite of the large *through bond* distance, a close *through space* approach of the donor and acceptor reacting partners. A further development of the system will have to take this point in due consideration.
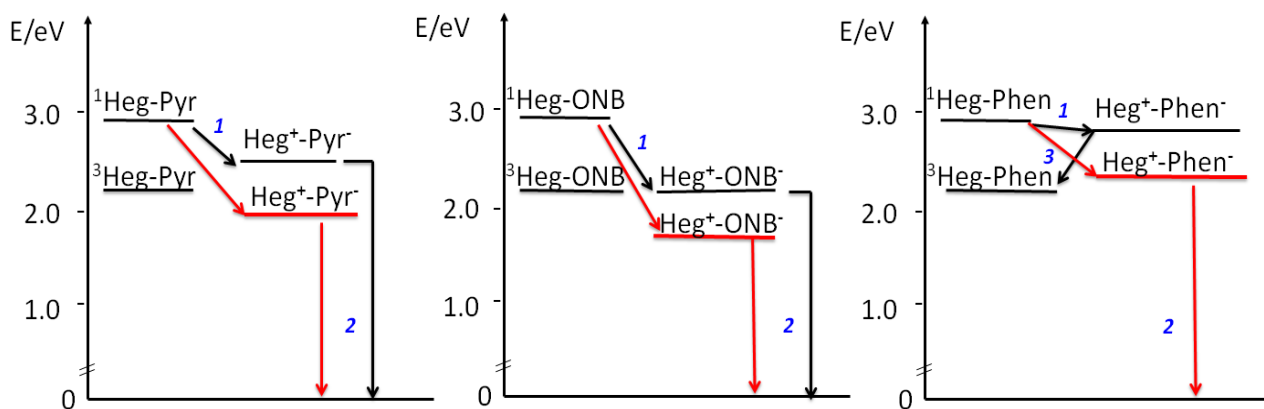
Figure 5.15. Schematic energy level diagrams for **HegPyr**, **HegONB** and **HegPhen** in TOL (black) and MeOH (red).

Two photon absorption. 2PA data on these compounds were not available at the submission of the present thesis.

5.2.3. Conclusions

We have solved the electron transfer dynamics in a series of model dyads designed for the photo-induced release of biologically active molecules upon 2PA. The process is activated by electron transfer from the relaxed lowest excited state of the donor, a fluorene derivative. Several acceptors, characterized by different redox properties, have been used to assemble the dyads. Photoinduced release of the active component is competitive with the recombination of the charge separated state formed upon electron transfer, therefore high yield and long lifetime of this state are desirable. Polar solvents, which mimic physiological conditions, are found to increase the yield of charge separation but also their recombination rate. Between the examined acceptors the best performances is shown by the worst (in terms of difficulty to be reduced) electron acceptor, **M7**; the corresponding dyad has a driving force for charge separation of ca. 0.05 eV and for charge recombination of almost 2.9 eV (TOL). In the **Heg-Phen** dyad, a still efficient charge separation reaction, (70%) coexists with a slow recombination. In fact, the high negative value of ΔG_{CR} prevents a fast recombination to the ground state and increases the lifetime of the charge separated state to an extent that recombination to triplet excited state of the donor is favored. Overall, very

likely as a result of the structural flexibility of the dyads, charge recombination in this series is fast and consequently the potential for the current dyads to promote molecular uncaging is poor. In the design of further systems the flexibility issue needs to be addressed in order to improve the performances.

5.3. References

[1]   a) H. B. Sun, S. Matsuo, H. Misawa, *Appl. Phys. Lett.* **1999**, *74*, 786-788; b) J. Serbin, M. Gu, *Adv. Mater.* **2006**, *18*, 221-224.

[2]   a) D. A. Parthenopoulos, P. M. Rentzepis, *Science* **1989**, *245*, 843-845; b) B. H. Cumpston, S. P. Ananthavel, S. Barlow, D. L. Dyer, J. E. Ehrlich, L. L. Erskine, A. A. Heikal, S. M. Kuebler, I. Y. S. Lee, D. McCord-Maughon, J. Q. Qin, H. Rockel, M. Rumi, X. L. Wu, S. R. Marder, J. W. Perry, *Nature* **1999**, *398*, 51-54; c) S. Krivec, N. Matsko, V. Satzinger, N. Pucher, N. Galler, T. Koch, V. Schmidt, W. Grogger, R. Liska, H. C. Lichtenegger, *Adv. Funct. Mater.* **2010**, *20*, 811-819.

[3]   a) V. Melissinaki, A. A. Gill, I. Ortega, M. Vamvakaki, A. Ranella, J. W. Haycock, C. Fotakis, M. Farsari, F. Claeyssens, *Biofabrication* **2011**, *3*; b) J. Torgersen, A. Ovsianikov, V. Mironov, N. Pucher, X. Qin, Z. Li, K. Cicha, T. Machacek, R. Liska, V. Jantsch, J. Stampfl, *J.Biomed. Opt.* **2012**, *17*; c) M. T. Raimondi, S. M. Eaton, M. Lagana, V. Aprile, M. M. Nava, G. Cerullo, R. Osellame, *Acta Biomater.* **2013**, *9*, 4579-4584.

[4]   M. Gu, *Presented at CLEO/Europe-IQEC* **2013**.

[5]   a) K. D. Belfield, X. B. Ren, E. W. Van Stryland, D. J. Hagan, V. Dubikovsky, E. J. Miesak, *J. Am. Chem. Soc.* **2000**, *122*, 1217-1218; b) M. Farsari, G. Filippidis, K. Sambani, T. S. Drakakis, C. Fotakis, *J. Photochem. Photobiol. A* **2006**, *181*, 132-135.

[6]   J.-F. Xing, W.-Q. Chen, X.-Z. Dong, T. Tanaka, X.-Y. Fang, X.-M. Duan, S. Kawata, *J. Photochem. Photobiol. A* **2007**, *189*, 398-404.

[7]   a) D. P. Specht, P. A. Martic, S. Farid, *Tetrahedron* **1982**, *38*, 1203-1211; b) J. Xue, Y. Zhao, H. Wu, F. Wu, *J. Photochem. Photobiol. A* **2008**, *195*, 261-266; c) M. Tasior, D. T. Gryko, D. J. Pielachinska, A. Zanelli, L. Flamigni, *Chem. Asian J.* **2010**, *5*, 130-140; d) J. Xue, Y. Zhao, F. Wu, D.-C. Fang, *J. Phys. Chem. A* **2010**, *114*, 5171-5179.

[8]   a) T. Urano, H. Nagasaka, S. Shimizu, H. Ito, M. Shimizu, S. Takahara, T. Yamaoka, *Bull. Chem. Soc. Jpn.* **1997**, *70*, 1659-1664; b) T. Urano, E. Hino, H. Ito, M. Shimizu, T. Yamaoka, *Polym. Adv. Technol.* **1998**, *9*, 825-830; c) J. P. Fouassier, X. Allonas, J. Lalevee, M. Visconti, *J.Polym. Sci. A* **2000**, *38*, 4531-4541; d) X. Allonas, J. P. Fouassier, M. Kaji, M. Miyasaka, T. Hidaka, *Polymer* **2001**, *42*, 7627-7634; e) H. Salmi, H. Tar, A. Ibrahim, C. Ley, X. Allonas, *Eur. Polym. J.* **2013**, *49*, 2275-2279.

[9]   a) X. Li, Y. Zhao, T. Wang, M. Shi, F. Wu, *Dyes Pigm.* **2007**, *74*, 108-112; b) X. Li, Y. Zhao, J. Wu, M. Shi, F. Wu, *J. Photochem. Photobiol. A* **2007**, *190*, 22-28.

[10]   Z. Li, N. Pucher, K. Cicha, J. Torgersen, S. C. Ligon, A. Ajami, W. Husinsky, A. Rosspeintner, E. Vauthey, S. Naumov, T. Scherzer, J. Stampfl, R. Liska, *Macromolecules* **2013**, *46*, 352-361.

[11]   For biexponential decays, the radiative rate constant $k_{rad} = \phi_{fl}/\tau$ is calculated for the major component.

[12]   R. Nazir, P. Danilevicius, A. I. Ciuciu, M. Chatzinikolaidou, D. Gray, L. Flamigni, M. Farsari, D. T. Gryko, *Chem. Mater.* **2014**, *submitted*.

[13]   a) M. P. Van Ryssen, N. Avlonitis, R. Giniatullin, C. McDougall, J. L. Carr, M. N. Stanton-Humphreys, E. L. A. Borgstroem, C. T. A. Brown, D. Fayuk, A. Surin, M. Niittykoski, L. Khiroug, S. J. Conway, *Org. Biomolec. Chem.* **2009**, *7*, 4695-4707; b) A. Deiters, *ChemBioChem* **2010**, *11*, 47-53.

[14]   A. Silanskas, M. Foss, W. Wende, C. Urbanke, A. Lagunavicius, A. Pingoud, V. Siksnys, *Biochemistry (Mosc).* **2011**, *50*, 2800-2807.

[15]   G. Marriott, *Biochemistry (Mosc).* **1994**, *33*, 9092-9097.

[16]   J. A. Sanchez, J. Vergara, *Am. J. Physiol.* **1994**, *266*, C1291-C1300.

[17]   J. Noguchi, A. Nagaoka, S. Watanabe, G. C. R. Ellis-Davies, K. Kitamura, M. Kano, M. Matsuzaki, H. Kasai, *J. Physiol. London* **2011**, *589*, 2447-2457.

[18]   A. Banerjee, D. E. Falvey, *J. Org. Chem.* **1997**, *62*, 6245-6251.

[19]   J. A. Neville, E. Welch, D. J. Leffell, *Nat. Clin. Pract. Oncol.* **2007**, *4*, 462-469.

[20]   D. Ormrod, B. Jarvis, *Am. J. Clin. Dermatol.* **2000**, *1*, 133-139; discussion 140-131.

[21]   C. Sundararajan, D. E. Falvey, *J. Am. Chem. Soc.* **2005**, *127*, 8000-8001.

[22]   C. G. Bochet, *J. Chem. Soc., Perkin Trans. 1* **2002**, *(2)*, 125–142.

[23]   M. Matsuzaki, T. Hayama, H. Kasai, G. C. R. Ellis-Davies, *Nat. Chem. Biol.* **2010**, *6*, 255-257.

[24]   a) L. Donato, A. Mourot, C. M. Davenport, C. Herbivo, D. Warther, J. Leonard, F. Bolze, J.-F. Nicoud, R. H. Kramer, M. Goeldner, A. Specht, *Angew. Chem. Int. Ed.* **2012**, *51*, 1840-1843; b) A. Specht, F. Bolze, L. Donato, C. Herbivo, S. Charon, D. Warther, S. Gug, J.-F. Nicoud, M. Goeldner, *Photochem. Photobiol. Sci.* **2012**, *11*, 578-586.

[25]   a) M. O. Delcourt, M. J. Rossi, *J. Phys. Chem.* **1982**, *86*, 3233-3239; b) R. A. McClelland, N. Mathivanan, S. Steenken, *J. Am. Chem.Soc.* **1990**, *112*, 4857-4861; c) N. Takeda, S. Asaoka, J. R. Miller, *J. Am. Chem.Soc.* **2006**, *128*, 16073-16082.

[26]   C. Sundararajan, D. E. Falvey, *J. Org. Chem.* **2004**, *69*, 5547-5554.

[27]   R. E. Sioda, W. Kemula, *J. Electroanal. Chem.* **1971**, *31*, 113-117.

[28]   K. Lee, D. E. Falvey, *J. Am. Chem. Soc.* **2000**, *122*, 9361-9366.

[29]   The band around 600 nm is sligtly shorter lived (5.5μs) than the band at 720 nm (8.0 μs). This can be the result of the presence of a minor contribution to this band in the 550-620 nm range, of a shorter lived product. We are however unable to identify such species.

[30]   A. Banerjee, D. E. Falvey, *J. Am. Chem. Soc.* **1998**, *120*, 2965-2966.

[31]   A. Weller, *Z. Phys. Chem,. (Muenchen Ger.)* **1982**, *133*, 93– 98.

[32]   a) N. Mataga, H. Chosrowjan, S. Taniguchi, Y. Shibata, N. Yoshida, A. Osuka, T. Kikuzawa, T. Okada, *J. Phys. Chem. A* **2002**, *106*, 12191-12201; b) M. Tasior, D. T. Gryko, M. Cembor, J. S. Jaworski, B. Ventura, L. Flamigni, *New J. Chem.* **2007**, *31*, 247 –259.

[33]   a) S. R. Greenfield, W. A. Svec, D. Gosztola, M. R. Wasielewski, *J. Am. Chem. Soc.* **1996**, *118*, 6767–6777; b) L. Flamigni, B. Ventura, C.-C. You, C. Hippius, F. Würthner, *J.Phys. Chem. C* **2007**, *111*, 622-630.

[34]   R. A. Marcus, *Angew. Chem. Int. Ed. Engl.* **1993**, *32*, 1111 –1121 and references therein.

[35]   I. M. Dixon, J.-P. Collin, J.-P. Sauvage, L. Flamigni, *Inorg. Chem.* **2001**, *40*, 5507-5517.

6. Experimental section

6.1. Electronic absorption spectra

The experiments were carried out on solutions contained in quartz cuvettes (from 10 mm to 1 mm optical path) at room temperature. The absorption spectra were recorded with a Perkin-Elmer Lambda 9 or with Perkin-Elmer Lambda 650 spectrophotometer. The molar absorption coefficient values were determined by applying the Lambert-Beer law; the experimental error is estimated to be $\pm$ 10 % and the precision on the wavelengths values was $\pm$ 2 nm.

6.2. Electronic emission spectra

The luminescence spectra were registered with a Spex Fluorolog II spectrofluorimeter equipped with a Hamamatsu R928 photomultiplier (PMT) or with an Edinburgh FSP920 fluorimeter equipped with a R928P Hamamatsu PMT. All the spectra were corrected for the photomultiplier response, unless otherwise specified. The experiments at room temperature made use of solutions placed in quartz cuvettes (10 mm optical path). Absolute luminescence quantum yields of the samples, ϕ_s, were evaluated against a standard with known emission quantum yield, ϕ_r, by comparing the areas under the corrected spectra using the equation: $\phi_s/\phi_r = A_r n^2_s \, (area)_s \, / \, A_s n^2_r \, (area)_r$, where A is the absorbance, n is the refractive index of the solvent employed and s and r stand for sample and reference, respectively. A values $<$ 0.15 were used. The standard used was air-equilibrated quinine sulphate in 1N H_2SO_4 with an emission quantum yield $\phi_{fl} = 0.546$[1] or an air-equilibrated coumarin 153 in ethanol with the emission quantum yield $\phi_{fl} = 0.544$.[2] Experiments at 77 K made use of capillary quartz tubes dipped in a home-made quartz Dewar filled with liquid nitrogen. Phosphorescence spectra, corrected for the PMT response, were registered upon excitation with a microsecond Xenon flash lamp μF920H with the Edinburgh FSP920 fluorimeter. The estimated errors were $\pm$ 2 nm for the wavelength maxima and $\pm$ 10 % for the emission quantum yields.

6.3. Luminescence lifetimes measurements

Lifetime measurements in the nanosecond time range at room temperature and at 77 K were performed by IBH Time Correlated Single Photon Counting apparatus. The excitation was made by

NanoLED diodes with different excitation wavelengths. The flash of the diode excites the sample and a sensitive photomultiplier (PMT), placed in right angle with respect to incident light, receives the emitted photons. Simultaneous with the excitation (*start*), the TAC (time to amplitude converter) starts generating a tension direct proportional with the time, until the PMT receives the first photon (*end*). The value of the tension is registered, and the TAC takes the initial position (*zero*) for the new measurement. Even any photon arrives at PMT, after a constant time (typical for the instrument) TAC comes anyway to the *zero* position. In practice, this allows for the conversion of the time in a proportional tension, easier to elaborate. The signals are registered on a multichannel analyzer, which divides the time in a certain number of channels. In this way, by measuring the time delay between the arrival of the photon at PMT (*end*) and the *start* of the incident photon, and distributing it on different channels, the emission decay *versus* time is reconstructed. The decay has an exponential value, and the probability that a single photon is emitted by the sample is statistically connected in time with the excited state concentration. The data were elaborated by *DAS6 Analysis* software, capable of calculating single or multiple decays.

Phosphorescence lifetimes were registered upon excitation with a microsecond Xenon flash lamp μF920H with Edinburgh FSP920 fluorimeter equipped with a R928P Hamamatsu PMT and elaborated by the corresponding software.

For picosecond time-resolved luminescence, Streak Camera Hamamatsu C1587 equipped with a fast unit M1952 (2 ps resolution) was used after excitation with a Nd-YAG laser (Continuum PY62/10, 35 ps pulse, energy < 1 mJ). The third (355 nm) or fourth (266 nm) harmonic were used for the excitation of the samples. A small part of the laser beam is captured by the PIN diode head (Hamamatsu C1083), whereas the other part is focused on 0.1 cm^2 on the sample. The necessary time adjustments of the trigger signal are performed by a delay unit, Hamamatsu C1097. The transmitted light from the sample is collected at 90° and focused into the entrance slit of a spectrograph (HR 250 Jobin-Yvon) equipped with a 300 grooves/mm. Neutral density or cut-off filters can be used if necessary. The light, horizontally dispersed by the spectrograph, enters the slit (20 μm) of the Streak camera. The result is an image produced by photoelectrons on the phosphorous screen, which contains spectral, temporal and intensity information. Acquisition and processing of the data are performed by a cooled charge-coupled device (CCD) camera (Hamamatsu C3140) and related software running on the computer. The image consists of 1280 time points by 1024 wavelength points (ca. 190 nm). Time decays were acquired on Streak horizontal profiles ± 10 nm wide around the specified wavelength. Deconvolution with the instrumental profile was carried out for all decays with $\tau < 0.5$ ns by a program provided by

Hamamatsu (HPD-TA version 6.4). The overall time resolution of the system is estimated to be 10 ps.

6.4. Transient absorption measurements

Transient absorbance in the picosecond range made use of a pump and probe system based on a Nd-YAG laser (Continuum PY62/10, 35 ps pulse). With two amplification stages it is capable of delivering pulses up to 120 mJ / pulse (1064 nm) at 10 Hz with 35 ps full width at half-maximum (fwhm). The third (355 nm) harmonics with energy of ca. 3 mJ/pulse were used to excite the samples with absorbance around 0.5 in 0.5 cm cell. The residual 1064 nm was focused on a cell containing a mixture of D_2O/D_3PO_4 to produce a white light continuum, used as analyzing light. The optical delay stage (Ealing Electro-optics) of the excitation beam is computer-controlled and provides a variable delay time (0-3.3 ns) between the excitation and the analyzing beam. The emission is transmitted by optical fibers to a spectrograph (Spectrapro 275, ARC) and it is detected by a detected by a CCD on which two separate portions are used to detect the incident light (I_0) and a part of the sample's transmitted light (I) as function of delay time and the obtained differential absorbance is given by the following equation:

$$\Delta A(t) = \log \frac{I_0(t)}{I(t)}$$

The kinetic analysis was made at a specific wavelength by applying standard iterative procedures.

Transient absorbance to detect triplet properties (nanosecond and microsecond range) was performed on air free solutions if not otherwise specified. To this aim, solutions contained in homemade, 10 mm optical path cuvettes, were bubbled with argon for 15-20 minutes and sealed. Quenching rates by oxygen k_q were derived from: $k_q = (1/\tau - 1/\tau_0) / [O_2]$, where τ_0 and τ are the lifetimes of the triplet in air free and air equilibrated solutions, respectively and $[O_2]$ is the concentration of oxygen in air equilibrated solutions. The apparatus used was based on a Nd:YAG laser (JK Lasers) delivering pulses of 18 ns.

The third harmonic (355 nm) or the fourth harmonic (266 nm) was used for excitation. Absorbance of the solutions at the exciting wavelength was around 1 and the energy used was 3 mJ/pulse for the determination of the spectra and ca. 0.8 mJ/pulse for lifetime measurements, in

order to prevent undesired second order triplet-triplet annihilation reactions. The analyzing light was perpendicular to the exciting laser beam and probed the first 0.2 cm of the sample cell. The light transmitted by the sample was detected by a Hamamatsu R936 photomultiplier. A Tektronix R7912 transient digitizer or a digital oscilloscope in conjunction with a computer was used to acquire and process the signals by standard iterative methods.

6.4. References

[1] D. F. Eaton, *Pure Appl. Chem.* **1988**, *60*, 1107 –1114.
[2] K. Rurack, M. Spieles, *Anal. Chem.* **2011,** *83*, 1232-1242.

Acknowledgements

There are many people to whom I would like to express my gratitude at the end of this PhD. My first thought and gratefulness are toward my principal supervisor, Dr. Lucia Flamigni, particularly for the infinite tolerance during these three years. My thesis would not have been possible without her close guidance, insightful discussions and priceless scientific advices. I am also extremely indebted to my university supervisor, Prof. Paola Ceroni, for the permanent support and availability, and for the amazing chance of studying at Bologna University.

I take this opportunity to sincerely acknowledge Dr. Barbara Ventura and Dr. Andrea Barbieri for their support and assistance, their helpful suggestions and not last, their friendship. I kindly thank Maria Pia for her warm and friendly heart and for her irreplaceable encouragements in the toughest days. I am sincerely grateful to all the colleagues from ISOF 4, researchers and students, which altogether represented my surrogate family in the past three years. I was always aware of the fact that I could ask them freely at any time for advices or opinions regarding laboratory issues and not only.

My gratitude is also extended to the synthetic partners. The groups of Prof. Dr. Daniel T. Gryko, Dr. Mireille Blanchard-Desce, Dr. Harry Anderson and Dr. Heinz Langhals provided us promptly the compounds for investigation, smoothing the way of obtaining quantitative and qualitative results. A particular thought to the first two collaborators and their students Dikhi, Rashid, Eduardo and Imanol, who all welcomed me as a friend during my secondments. Thank you all for transferring me a part of your synthetic knowledge and for making the place an attractive one to stay. To Roman and Kamil I am grateful for the interesting samples offered and for the mutual help and friendship during our collaboration.

I will forever be thankful to TOPBIO members, PIs, ESRs and ERs, for the unique opportunity of professional and personal development they offered me. I am grateful for all the meaningful debates and demanding questions which helped me simply to progress. Thank you, Victoria and Karolina, for being such wonderful friends! I am confident that our friendship will resist over the years.

A special acknowledgement goes to Marie Curie actions, which made possible this PhD to happen. It was a period of hard work, happiness and sadness, but overall the best period of my life. Its fingerprint will always be on my personal and my carrier evolution.

Last but not least, I would like to thank my future husband Sorin, for his irreplaceable and inexhaustible support during my studies. My gratefulness goes also to my family and friends, for their sincere encouragements and help in the successful completion of this project.